COVALENT BONDING EFFECTS IN DIFFRACTION FROM AMORPHOUS SOLIDS

by

Bryn John Stenhouse

Thesis submitted for the degree of Doctor of Philosophy of the University of London

Blackett Laboratory
Imperial College of Science and Technology
London, S.W.7

September 1977

To my parents

for their constant support and encouragement

ABSTRACT

This thesis is concerned with the structure and the electron density distribution in amorphous semiconductors, particular attention being focussed on the interpretation of X-ray and electron scattering experiments. The main investigation is of amorphous silicon (α-Si) but extensive work on amorphous carbon (α-C) and vitreous silica (α-SiO_2) is also reported.

Two basic assumptions are made about the electron density distribution in α-Si and α-C :

(a) The total density can be written as a sum of the densities in the individual Si-Si or C-C bonds.

(b) The density in a single covalent bond can be constructed from the method of linear combination of atomic orbitals (LCAO).

To calculate the electron and X-ray scattering a third, less basic but essential assumption for further progress is made, namely

(c) The bond density can be written as a sum of three spherical distributions, two identical distributions centred on the nuclei and a third centred at the mid-point of the bond.

For α-Si, with these assumptions a knowledge of the nuclear-nuclear, nuclear-bond centre and bond centre-bond centre correlations enables the X-ray and electron scattering to be calculated. The correlation functions have been determined from several well known structural models of the amorphous state, both random networks and models based on ordered units being employed.

Similar analysis is performed on α-C. Here the structure is difficult to characterize and detailed calculations are reported concerning the dependence of the diffraction patterns on the type of structure used.

For α-SiO_2 ionic bonding has to be considered and the relative effects

of ionic and covalent bonds on the X-ray diffraction intensities are investigated.

It is concluded that covalent bonding significantly affects the X-ray and electron diffraction intensities in both α-Si and α-C. For α-Si, random networks containing odd-membered rings are to be preferred to models based on ordered units for a representation of the structure.

ACKNOWLEDGEMENTS

The work presented in this thesis was carried out at Imperial College under the supervision of Professor N. H. March and with the financial support of the Science Research Council.

I am extremely grateful to Professor March for his generous and enthusiastic guidance and for arousing my interest in amorphous solids.

I have benefitted greatly from close collaboration with Dr. P. J. Grout throughout the past two years, and with Dr. J. Wenzel for the work described in Chapter 3.

I am indebted to Dr. R. J. Bell for introducing me to Continuous Random Networks, to him and Dr. P. H. Gaskell for kindly providing me with their model coordinates.

My thanks go to the Solid State physics group at Imperial College for providing such a friendly atmosphere in which to study.

Finally, I am grateful to Ms. Deanne Eastwood for typing this thesis.

CONTENTS

CHAPTER ONE

INTRODUCTION

The concept of the chemical bond was first proposed (Lewis, 1916) soon after the discovery of the electron and can be defined as follows (Pauling, 1960 a) :

"There is a chemical bond between two atoms or groups of atoms if the forces acting between them are such as to lead to the formation of an aggregate with sufficient stability to make it convenient for the chemist to consider it as an independent molecular species".

The type of chemical bond that will principally concern us in this thesis is the covalent bond which involves the sharing of a pair of electrons by the two bonded atoms. The ionic bond, which will be discussed briefly in Chapter 5, results from the coulomb attraction of the excess electric charges on oppositely charged ions.

The chemical bond has proved a powerful tool for understanding the electrical properties of many materials (Pauling, 1960) and in particular those of carbon and silicon. Both carbon and silicon have four valence electrons per atom. Carbon forms two crystalline structures, diamond and graphite, silicon only one, that of diamond. In the chemical bond picture all four valence electrons in diamond are localized in covalent bonds between nearest neighbour atoms. The insulating properties of diamond are thus explained in terms of the localized nature of the valence electrons. For graphite in the chemical bond picture, only three valence electrons per carbon atom are localized in covalent bonds, the remaining unbonded electron being loosely bound and thus available for conduction. Silicon crystallises in the diamond structure and thus all four valence electrons are localized in covalent bonds. The distinction between the insulating and semiconducting properties of

diamond and silicon, respectively, is explained simply in terms of the degree of localization of the bonded electrons.

Many observable 'bond properties', for example the fact that the Si-Si equilibrium distance (the bond length) varies only slightly with different environments, are easily explained in terms of this localized picture. For the crystal as a whole, the chemical bond picture leads to a total electron density as being built up from such localized bond densities.

In a full quantum mechanical treatment of crystalline silicon, say, one must consider the valence electrons as moving through a periodic lattice of positive ions. The distinction between insulating and conducting properties can then be explained in terms of the forbidden energy gaps arising from the modification of the electron energies by diffraction. Solving Schrodinger's equation for the electrons must lead to electron wavefunctions and a ground state electron density $\rho(\underset{\sim}{r})$ that extends throughout the entire crystal. It is a fact, very relevant to this thesis, that there exists no unique way of dividing up the delocalized density $\rho(\underset{\sim}{r})$ into localized contributions in accord with the chemical bond picture. The forbidden energy gap arising from the delocalized approach is, in the chemist's picture, approximately equal to the energy required to remove an electron from a localized bond.

In this thesis we shall be investigating disordered solids, that is, solids which, due to their method of preparation, have no crystalline structure. Much of the current interest in these solids stems from a desire to know how well one can characterize the amorphous state and which factors one needs to take into account in order to do so. Since an amorphous solid is a metastable state, usually obtained under forced conditions (for example by rapid cooling) to prevent crystallization

taking place, the answers to these questions are believed to be statistical in nature. For our work we shall make no distinction between non-crystalline solids such as α-Si formed, for example, from the vapour and true glassy solids such as vitreous silica (α-Si O_2) formed by cooling the melt. The important point here is that liquid silicon is a metal with a resistance that increases with temperature whereas molten silica is a semiconductor. For our work, the important properties common to these solids are a lack of long range order in the atomic arrangements and the possession of an electron density describable in terms of covalent bonding.

For the disordered state, then, no long range lattice periodicity exists and the effectiveness of band theory, the delocalized approach, is correspondingly reduced. The chemist's localized bond picture is, however, still powerful. For silicon, for example, the only restriction imposed by this approach is that each Si atom should have four bonds and this can be satisfied equally well with either a regular network, as in the crystal, or by an irregular one as in the amorphous case. For α-Si the electrons are thus still pictured as localized and the semiconducting properties are again easily explained. The observation of well defined forbidden energy gaps in α-Si (Donovan et al, 1969) lends strong support to this localized picture.

Diffraction experiments based on Bragg's condition relating the crystalline lattice spacings to the diffracting wavelength have been a major tool for probing the solid state. For amorphous solids short range order is retained and diffraction experiments still give us useful information about the local atomic environment. X-rays are scattered by electrons and therefore X-ray cross sections are related to electron correlation functions. Electrons are scattered by all charges present

and so electron scattering cross sections are related to both nuclear and electronic correlations. Thus both X-rays and electrons will be affected by the form of the electron density $\rho(\underset{\sim}{r})$ in the amorphous state. An interpretation of these effects in terms of a localized bond picture will be a major objective of this thesis.

In Chapter 2 we give a short review of X-ray, electron and neutron diffraction theory with particular reference to amorphous covalently bonded solids.

In Chapter 3 we apply the equations developed in Chapter 2 to α-Si and demonstrate how the formalism of diffraction from spherical charge distributions can be extended to take account of directional bonding and that, with this model of the covalent bond, we can account for the experimentally observed X-ray and electron diffraction intensities from α-Si.

In Chapter 4 we perform similar calculations for α-C. More detailed structural modelling is involved and because of the two types of crystalline carbon it is necessary to consider two types of covalent bond, namely those due to sp^2 and sp^3 hybridization. Again, we are able to account for the experimentally observed X-ray and electron diffraction intensities in terms of the covalent bond model. We also show how the fraction of partially ordered material in a sample of α-C can be included in a structural model as a simple parameter.

In Chapter 5 we discuss two component systems and give X-ray and neutron diffraction calculations for a model of vitreous silica. The effects of covalent versus ionic bonding, with regard to diffraction intensities, are investigated.

Some of the work presented in this thesis has also appeared in the following :

B. Stenhouse, P.J. Grout and N.H. March :

Scattering Intensities and Model Partial Structure factors in Vitreous Silica and Amorphous Silicon, Physics Letters 57A, 1976, 99-101

B. Stenhouse, P. J. Grout, N.H. March and J. Wenzel :

Chemical Bonding Effects on the Diffraction Intensities in Amorphous Silicon and Carbon. Philosophical Magazine 36, 1977, 129-147

B. J. Stenhouse and P. J. Grout :

Diffraction Intensities and the Structure of Amorphous Carbon :

Journal of Non-Crystalline Solids (in the press).

CHAPTER TWO

DIFFRACTION FORMALISM

2.1 Introduction

We shall now give a brief review of the main ingredients of X-ray, electron and neutron diffraction from an array of atoms. The purpose of this review is first to obtain the quantities that are used extensively in the work described in later chapters, and second to emphasize the assumptions made in their derivation that influence our approach to the problem of diffraction from covalently bonded amorphous solids.

We restrict the discussion below to coherent elastic scattering. For a fuller, more general discussion of diffraction methods see, for example, Bacon (1962), Leadbetter and Wright (1972), Wright (1974).

2.2 X-ray diffraction

X-rays are scattered by electrons and it will be sufficient for our purposes to take the amplitude of radiation scattered in a particular direction by a single electron as our scattering unit (often referred to as the electron unit). If we define $\underset{\sim}{k}_i$ as a vector with magnitude $2\pi/\lambda$, where λ is the incident wavelength, in the direction of the incident beam and $\underset{\sim}{k}_d$ the wave vector of the scattered radiation, then, since we are considering elastic scattering we have

$$|\underset{\sim}{k}_i| = |\underset{\sim}{k}_d| \qquad 2.1$$

We define the scattering vector $\underset{\sim}{k}$ as

$$\underset{\sim}{k} = \underset{\sim}{k}_d - \underset{\sim}{k}_i$$

$$= 4\pi \sin\theta/\lambda \qquad 2.2$$

where 2θ is the scattering angle.

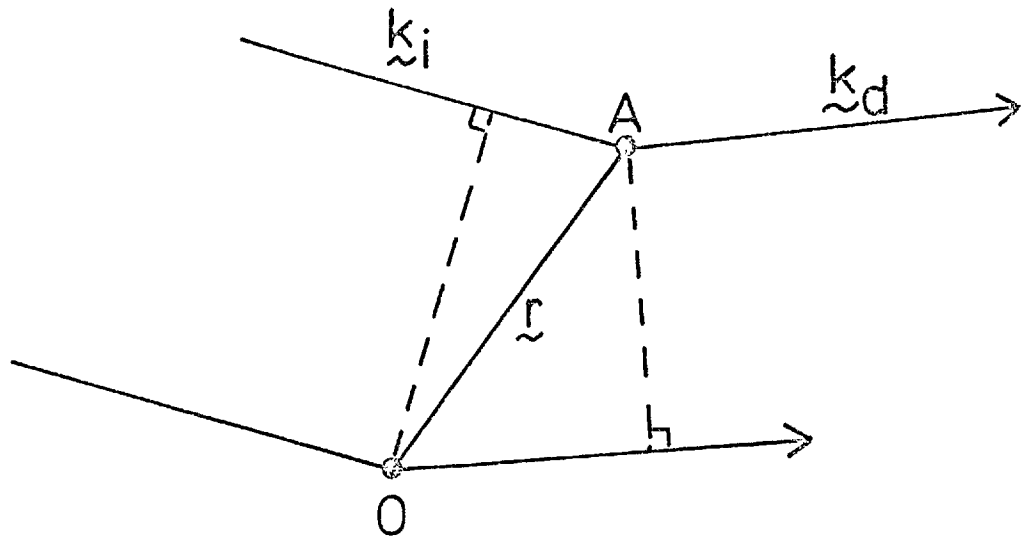

Figure 2.1 : X-ray scattering from two electrons at O and A, separated by vector $\underset{\sim}{r}$.

Referring to figure 2.1, the phase difference between radiation scattered by electrons at A and O is

$$(\underset{\sim}{k}_d - \underset{\sim}{k}_i).\underset{\sim}{r} = \underset{\sim}{k}.\underset{\sim}{r} \qquad 2.3$$

and the contribution to the amplitude of the scattered beam will be $\exp(i\underset{\sim}{k}.\underset{\sim}{r})$. Thus the amplitude $Y(k)$ of the beam scattered in the direction defined by $\underset{\sim}{k}_d$ by N electrons is given by

$$Y(\underset{\sim}{k}) = \sum_{s=1}^{N} \exp(i\underset{\sim}{k}.\underset{\sim}{r}) \qquad 2.4a$$

and for a continuous electron density

$$Y(\underset{\sim}{k}) = \int_{\underset{\sim}{r}} \rho(\underset{\sim}{r}) \exp(i\underset{\sim}{k}.\underset{\sim}{r})\, d\underset{\sim}{r} \qquad 2.4b$$

Now, if we consider an array of atoms, referred to hereinafter as 'the system', and we write the total electron density in the system $\rho(\underset{\sim}{r})$ as a sum of the electron distributions around each nucleus

$$\rho(\underset{\sim}{r}) = \sum_m \sigma_m(\underset{\sim}{r} - \underset{\sim}{r}_m) \qquad 2.5a$$

then we obtain

$$Y(\underset{\sim}{k}) = \sum_m e^{i\underset{\sim}{k}.\underset{\sim}{r}_m} f_m(\underset{\sim}{k}) \qquad 2.6$$

where

$$f_m(\underset{\sim}{k}) = \int_{\underset{\sim}{r}} \sigma_m(\underset{\sim}{r}) \exp(i\underset{\sim}{k}.\underset{\sim}{r})\, d\underset{\sim}{r} \qquad 2.7a$$

is the form factor for the electron distribution around nucleus m. The diffracted intensity $I(\underset{\sim}{k})$ is given by

$$I(\underset{\sim}{k}) = |Y(\underset{\sim}{k})|^2$$

$$= \sum_{m,n} f_m(\underset{\sim}{k})\, f_n(\underset{\sim}{k}) \exp\left(i\,\underset{\sim}{k}.(\underset{\sim}{r}_n - \underset{\sim}{r}_m)\right)$$

$$= \sum_{m,n} f_m(\underset{\sim}{k})\, f_n(\underset{\sim}{k}) \exp(i k r_{nm} \cos\alpha) \qquad 2.8$$

where

$$r_{nm} = |\underset{\sim}{r}_n - \underset{\sim}{r}_m| \qquad 2.9$$

and

$$\cos\alpha = \underset{\sim}{k}.(\underset{\sim}{r}_n - \underset{\sim}{r}_m)/k r_{nm} \qquad 2.10$$

If we further assume that the total electron density $\rho(\underset{\sim}{r})$ of equation (2.5a) can be written as a sum of spherical distributions, i.e.

$$\rho(\underset{\sim}{r}) = \sum_m \sigma_m(|\underset{\sim}{r} - \underset{\sim}{r}_m|) \qquad 2.5b$$

with

$$f_m(k) = \int_0^\infty \sigma_m(r)\, 4\pi r^2 \frac{\sin kr}{kr}\, dr \qquad 2.7b$$

then we can average over α in equation (2.8) to obtain

$$I(k) = \sum_{nm} f_n(k) f_m(k) \frac{\sin k r_{nm}}{k r_{nm}} \qquad 2.11$$

Separating out terms with n = m this takes the form

$$I(k) = \sum_n f_n^2(k) + \sum_{\substack{n,m \\ n \neq m}} f_n(k) f_m(k) \frac{\sin k r_{nm}}{k r_{nm}} \qquad 2.12$$

For an amorphous material where we can define $\rho_{nm}(r)$ as the density of centres of type m at a distance r from a centre of type n, we have from equation (2.12)

$$I(k) = \sum_n f_n^2(k) + \sum_{n,m} f_n(k) f_m(k) \int_0^\infty \rho_{nm}(r) 4\pi r^2 \frac{\sin kr}{kr}\, dr \qquad 2.13$$

where, now, the summations over n and m are over atoms and atom types, respectively, in the system. Here, of course, we have assumed

that r, the radius of the amorphous sample is large ($r \to \infty$). If ρ_{om} is the mean density of centres of type m we can write equation (2.13) in the form

$$I(k) = \sum_n f_n^2(k) + \sum_{n,m} f_n(k) f_m(k) \int_0^\infty [\rho_{nm}(r) - \rho_{om}] 4\pi r^2 \frac{\sin kr}{kr} dr$$

$$+ \sum_{n,m} f_n(k) f_m(k) \int_0^\infty \rho_{om} 4\pi r^2 \frac{\sin kr}{kr} dr \qquad 2.14$$

The contribution from the last term on the right hand side of equation (2.14) is a delta function at k = 0 and will be neglected hereinafter. We now define the n-m radial distribution (or correlation) function such that $\rho_{om} g(r) 4\pi r^2 dr$ is the number of centres of type m a distance between r and r + dr from a typical n centre. Clearly from equation (2.14)

$$I(k) = \sum_n f_n^2(k) + \sum_{n,m} f_n(k) f_m(k) \rho_{om} \int_0^\infty [g_{nm}(r) - 1] 4\pi r^2 \frac{\sin kr}{kr} dr \qquad 2.15$$

For a homogeneous medium we can rewrite equation (2.15) in terms of the scattering from a basic scattering unit (as an example, for vitreous silica $Si O_2$, the unit would contain one silicon atom and two oxygens)

$$I(k) = N\left[\sum_i f_i^2(k) + \sum_{ij} \rho_{oj} f_i(k) f_j(k) \int_0^\infty [g_{ij}(r) - 1] 4\pi r^2 \frac{\sin kr}{kr} dr\right] \qquad 2.16$$

where the summations over i and j are over atoms and atom types, respectively, in the basic unit and N is the number of such units in the total system. Equation (2.16) is of the required form for calculating the X-ray diffraction intensities from a model of an amorphous solid. However, equation (2.11) will also be required when we are dealing with models that have a crystalline nature and where a continuous distribution $\rho_{ij}(r)$ is not a useful definition.

If we define the partial structure factors $S_{ij}(k)$ as

$$S_{ij}(k) = 1 + \rho_{oj} \int_0^\infty [g_{ij}(r) - 1] 4\pi r^2 \frac{\sin kr}{kr} dr \qquad 2.17a$$

then finally equation (2.16) takes the form

$$I(k) = N \sum_{ij} f_i(k) f_j(k) [S_{ij}(k) - \varepsilon_{ij}] \qquad 2.18$$

where

$$\varepsilon_{ij} = 0 \qquad i = j$$

$$= 1 \qquad i \neq j \qquad 2.19$$

This completes the formalism for the X-ray scattering from a superposition of spherical free atom-like charge densities. For a monatomic amorphous solid, such as α-Si or α-C, equation (2.18) reduces to

$$I(k) = N S(k) f^2(k) \qquad 2.20$$

where f(k) is usually taken to be the free atom form factor and S(k) is defined solely in terms of the Si or C nuclear correlation function g(r)

$$S(k) = 1 + \rho_{on} \int_0^\infty [g(r) - 1] 4\pi r^2 \frac{\sin kr}{kr} dr \qquad 2.17b$$

where the subscript n refers to nuclear type (Si or C). It is important to realize that for the covalently bonded amorphous solids equation (2.20) is an approximation. The approximation was introduced in equation (2.5b) where the total charge density was written as a sum of spherical distributions, one of which was assigned to each nucleus in the system. However, equation (2.20) has been used extensively in the literature, and for example for α-Si in fig. 2.2 we show $\rho_{on} 4\pi r^2 g(r)$ as obtained from X-ray diffraction (Richter and Breitling, 1958) using equation (2.20), where g(r) is given by the inverse transform of equation (2.17 b).

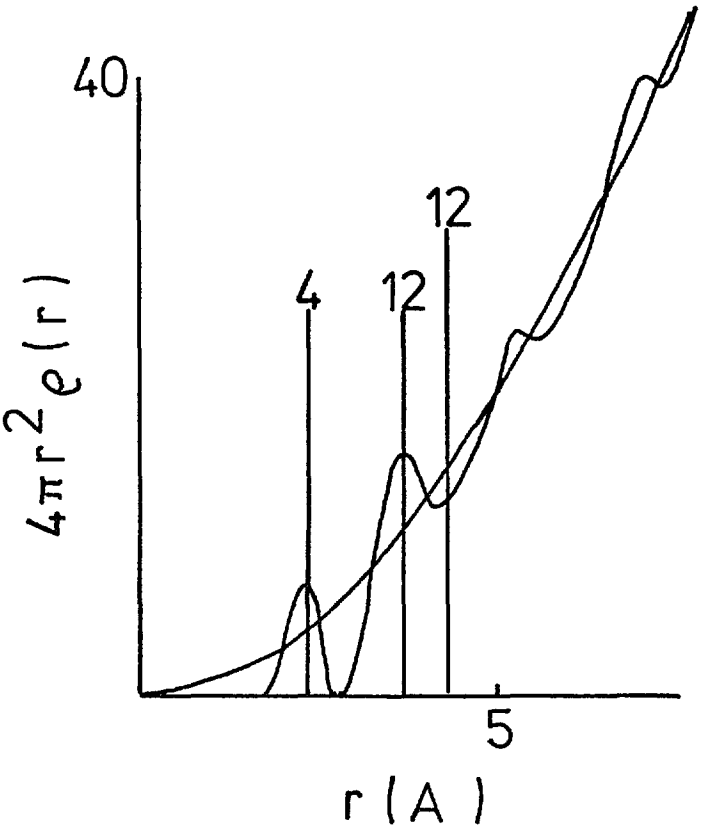

Figure 2.2 : Pair distribution function for α-Si as determined by X-ray diffraction (Richter and Breitling, 1958) together with the mean density and the number and positions of neighbours in the corresponding diamond lattice.

$$g(r) = 1 + \frac{1}{2\pi^2 \rho_{on} r} \int_0^\infty [S(k)-1] k \sin kr \, dr \qquad 2.17c$$

Our interest in the effects produced by a neglect of covalent bonding stems from considerations of the crystalline case. For example, for the diamond lattice, a spherical atom densities model predicts zero intensity for the (222) reflection. This so called "forbidden" reflection is, however, observed experimentally. For the crystal there is, of course, no need to assume a spherical atom density model since the form of the angularity due to bonding is, in principle, exactly known. For an amorphous solid, however, this is not the case. The curve $\rho_{on} 4\pi r^2 g(r)$ in fig. 2.2 has broad first and second peaks, indicating variations of bond length and, more importantly, of the tetrahedral bond angle. Thus for the amorphous state we have no a priori method for modelling the angularity of $f_i(k)$ in equation (2.8) and hence we make the assumption contained in equation (2.5b). For α - Ge the X-ray diffraction intensity is dominated by scattering from the core electrons and for this case the spherical atom densities model is a good approximation. Our investigations will, therefore, concentrate on α -Si and α -C where the ratio of core/valence electrons is lower.

2.3 Electron Diffraction

For high energy electron diffraction the analysis is similar to that for X-rays, the essential difference being that the electrons are scattered by the potential they feel. This potential is related, by Poissons equation, to the total charge (nuclei + electrons)

$$q(\underset{\sim}{r}) = Z - \sigma(\underset{\sim}{r}) \qquad 2.21$$

where z is the nuclear charge. Then, for electrons, the form factor $f_i(k)$ in equation (2.18) is replaced by $f_i^e(k)$, say, given by

$$f_i^e(k) = [Z_i - f_i(k)]/k^2$$

where the factor k^{-2} arises from the r^{-1} behaviour of the Coulomb potential. Since generally $Z_i \geq \varrho_i(r)$ the units for electron scattering as defined here are often referred to as proton units. Since electron scattering involves the electron density $\varrho(\underset{\sim}{r})$, the comments made for X rays with regard to equation (2.20) are also relevant here.

2.4 Neutron Diffraction

For neutron diffraction the scattering centre is the nucleus which for our purposes can be considered as a hard sphere. The k dependent form factors of X-ray and electron diffraction are replaced by a constant, b_i, the neutron scattering length for nucleus i which, unlike $f_i(k)$ and $f_i^e(k)$ can only be deduced empirically from experiment. Neutron diffraction is thus unaffected by the electron density distribution (and by the assumption of equation (2.5b)) and leads to unambiguous structural information.

However, for α-Si, the neutron experiment has not been carried out. The problem is that, for a neutron experiment, one needs a large sample ($\sim$ 1 cm^3) and the preparation of such a specimen of α-Si is very slow, although essentially not difficult. Also, the sample, if prepared, would be highly prone to oxidation and would need to be obtained under high vacuum.

For α-C we do have some neutron data (Mildner and Carpenter, 1975). However, as we shall see in Chapter 4, every α-C sample presents us with a new structural problem, and for most samples a neutron diffraction experiment has not been performed.

Thus for both α-Si and α-C a correct interpretation of X-ray and electron diffraction takes on added importance. We shall begin by discussing α-Si in Chapter 3.

CHAPTER THREE

AMORPHOUS SILICON

3.1 Introduction

Amorphous silicon (α-Si) is a typical non-crystalline solid possessing approximate short range order, similar to that found in the crystal, but having a complete lack of long range order. Attempts to model the structure have traditionally been based on two apparently conflicting ideas. These are to describe α-Si either by means of a microcrystallite model or by means of a continuous random network (CRN) model.

In the microcrystallite picture one assumes that the local atomic environment, in the amorphous state, is exactly crystal-like, but that long range order is removed by the crystals having a size of only a few angstroms, the complete amorphous sample consisting of an ensemble of such microcrystallites with random orientation.

The CRN concept was originally proposed (Zachariasen 1932, 1935) as a structural model for vitreous silica, α-Si O_2. As applied to α-Si, the concept takes the following form. Each Si atom is linked to four others with a bond length of $L \pm \Delta L$ and a bond angle (see figure 3.1) of $\Theta \pm \Delta\Theta$ where L and Θ are the bond length and bond angle in the crystal and ΔL and $\Delta\Theta$ are termed the bond length and bond angle distortions. The relative orientation of adjacent tetrahedral units (neighbouring Si_4 units will be referred to as tetrahedral units, despite the variations in bond angle) is varied randomly, subject only to the condition that the network is continuously connected.

These definitions are sufficiently broad for us to apply them to a wide range of structures. For example, we have not specified how individual mircocrystals are linked together and there is obviously much freedom as to how one joins a network

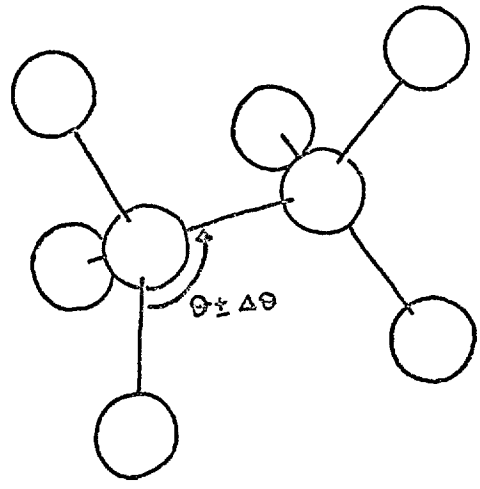

Figure 3.1 : Adjoining silicon tetrahedra.

together in a random way.

In Chapter 2 we saw how, given the coordinates of the atoms in a monatomic amorphous solid, we could calculate the X-ray and electron diffraction intensities in terms of the nuclear-nuclear structure factor S(k) and a spherical atom form factor - equation (2.20). However, this required the assumption that we could write the electron density in the amorphous state as a superposition of spherical atom charge densities. Our first step for testing whether a neglect of covalent bonding has significant effects on the X-ray and electron diffraction intensities in α-Si must be to compare the theoretical intensities as given by equation (2.20) with those observed in experiment.

If we take the neutral atomic form factor to define $f_i(k)$ (equation 2.7b) then all we require is the nuclear-nuclear structure factor S(k) and for this we need a model of the amorphous structure. For the purpose of explaining which model structures we shall use to obtain S(k) it is convenient to begin by reviewing the development of the microcrystallite and CRN pictures.

As we discussed in Chapter 2, from our point of view α-Ge is not as interesting as α-Si because for α-Ge the ratio of core/valence is large and we do not expect the effects of covalent bonding to be evident in the diffraction intensities. However, the structure of α-Ge is expected to be essentially the same as for α-Si and, where relevant, we shall take experimental evidence from α-Ge as pertaining to α-Si.

3.2 Development of the microcrystallite and CRN models

The radial distribution function (RDF) for α-Si, g(r) as defined by equations (2.17c) and (2.20),was first obtained from X-ray diffraction (Richter and Breitling, 1958). The main difference between the RDF for α-Si and that for crystalline Si is

the absence, in the amorphous case, of a sharp third neighbour peak. This can be seen in figure 2.2, where we show $4\pi r^2 \rho(r)$ for α-Si as determined from experiment (Richter and Breitling, 1958), together with the contribution from the mean density ($4\pi r^2 \rho_{on}$) and the number and positions of neighbours in the corresponding diamond lattice. Thus the experimental curve would seem to be consistent with a structural picture of small, randomly oriented, crystallites based on the diamond structure.

This idea was investigated (Moss and Graczyk, 1969) with calculations of the reduced intensity function F(k) given by

$$F(k) = k[S(k)-1] \qquad 3.1$$

where S(k) is defined by equation (2.17b), for several microcrystallite models based on the diamond cubic structure. No correlation between different microcrystals was included and it was demonstrated quite conclusively that this simple microcrystallite picture could not be consistent with the experimental data. The function that was used in the calculations, F(k), is, of course, derived from the experimental intensity assuming equation (2.20) to be correct. As we have previously stressed, we do not believe this to be the case for α-Si. However, the effects observed by Moss and Graczyk were for all k and could not have been due to assumptions about the electron density distribution.

The structure of α-Si was subsequently interpreted on the basis of the CRN model; the lack of a third neighbour peak in the experimental RDF being consistent with the free rotation of neighbouring tetrahedral units about their common bond. Indeed, such a structure was shown (Polk, 1972) to give an RDF in reasonable agreement with experiment for α-Si (Moss and Graczyk, 1969).

One important set of parameters for a CRN model are the ring statistics. A

P-fold ring can be defined as a closed path in the network which passes once and only once through P different Si atoms and along P Si-Si bonds. The crystalline diamond structure is composed entirely of six-membered rings whilst the wurtzite structure contains both four and six-membered rings. Because of the free rotation of neighbouring tetrahedra, in the CRN, it is possible to construct an amorphous structure containing only even or odd membered rings or a mixture of both. The P-fold ring statistic is then the average number of P fold rings per atom in the network.

The possible existence in the amorphous state of a network topology differing greatly from that in the crystal is interesting when one considers that very different methods for preparing α-Si appear to lead to the same structure. α-Si can be prepared by sputtering, evaporation, electrodeposition, decomposition in glow discharge and ion implantation. In the last case the amorphous film is obtained by the progressive destruction of order in a perfect crystalline lattice. Yet it has been demonstrated (Smith et al, 1971, Moss et al, 1971) that ion implanted Si is not just severely damaged crystalline Si and that the structure is similar to that of vapour deposited α-Si.

The Polk model, that gave quite good agreement with the experimental RDF for α-Si, contained a mixture of odd and even membered rings and was, therefore, topologically, quite different from the diamond structure; (more details of the model can be found in Table 3.1 where an essentially identical structure, the Steinhardt model, is shown as model VII). Clearly, then, it was of interest to investigate whether or not very different CRN models could give similar agreement with the same experimental RDF; the important point being that the structural information embodied in g(r) is average information obtained from the sample as a

whole. Thus comparisons between theoretical and experimental curves could not be expected to distinguish between individual network topologies but could be expected to reflect the different model rings statistics.

A 201 atom CRN model containing a large number of odd membered rings (Steinhardt et al, 1974), hereinafter referred to as the Steinhardt model, and a 238 atom CRN model composed entirely of even membered rings (Connell and Temkin, 1974) were built soon afterwards. Both gave fits to the RDF of α-Ge (Temkin et al, 1973) that were qualitatively similar to that given by the Polk model for α-Si. However it was noted by Connell and Temkin that an average of the RDFs for the 238 and 201 atom models gave a better fit than was given by either model individually. The Connell-Temkin (CT) model was thus gradually restructured (Beeman and Bobbs, 1975) to generate a series of models containing varying numbers of five and seven fold rings. Six models, including the original, were so generated and, as had been hoped, it was found that greatly improved agreement between model and experimental RDF could be obtained for a model having ring statistics that lay between those of the Steinhardt and CT models. The ring statistics for the six modifications of the CT model are shown in Table 3.1 - models I to VI, together with those for the Steinhardt model which, because of its ring statistics (as previously stated these are essentially the same as those of the Polk model), fits roughly into Table 3.1 as model VII. The average bond angle distortion $\overline{\Delta\theta}$ (see figure 3.1), for each model, is also given. The improved agreement, referred to above, was obtained for model V, the agreement improving down the table towards model V and then worsening for models VI and VII.

Obviously, this method needs to be repeated using several different models as the starting point. Then, given optimum fits to the experimental RDF, obtained from a number of distinct initial structures, one would hope to see some convergence

Table 3.1 : Model Structural Parameters

Model		Rings/Atom			Average bond angle distortion
(a)*	(b)+	5	6	7	$\overline{\Delta\theta}$
I	CT 1	0.00	2.43	0.00	9.1
II		0.59	2.27	0.16	10.2
III	CT 2	0.16	2.09	0.31	10.6
IV		0.20	1.96	0.47	10.8
V	CT 3	0.34	1.51	0.81	11.6
VI		0.40	1.29	1.01	13.3
VII	Steinhardt	0.43	0.89	0.99	6.8

* Notation of Beeman and Bobbs, 1975

\+ Notation used in this work

towards an ideal amorphous structure and discover the correct statistics for a complete description of the amorphous state.

Independently of these developments of the CRN model, the microcrystallite model was rather surprisingly (in view of the diffraction evidence referred to above) revived by evidence from high resolution electron microscopy experiments.

For α-Ge and α-Si using the dark field configuration, uniformly bright, patches about 15 Å across were observed in the image (Rudee 1972, Chaudhari et al, 1972, Rudee and Howie, 1972), indicative of more structural order than is present in a random network model. The bright patches were assumed to arise from crystalline regions of approximately the average patch dimensions (15 Å) (Rudee, 1972, Rudee and Howie, 1972) or from coherently diffracting regions of a random network (Chaudhari et al, 1972). Later results (Howie et al, 1973, Chaudhari et al, 1973) indicated that the bright patches were only about 5 Å across. Calculations (Chaudhari and Graczyk, 1974) for a computer built CRN model (Henderson and Herman, 1972) containing 64 atoms (the HH model) and for a 519 atom modified Polk model (Polk and Bourdeaux, 1973) indicated that a CRN can be consistent only with the latter measurement (5 Å). However, it was pointed out (Moss and Adler, 1973) that the irregular spots in dark field could be due to density fluctuations which limit the CRN size to small regions separated by voids. This view is supported by evidence from glassy chalcogenides (Chaudhari et al 1972b) where bright spots are also observed in dark field but which vanish above the glass transition temperature.

More convincing evidence for the microcrystallite picture, for α-Ge, came from tilted bright field configuration electron microscopy experiments (Rudee and Howie, 1972, Howie et al, 1973) where lattice fringes were observed

corresponding to a spacing of about 3.3 Å similar to the spacing of the (111) planes in the diamond or wurtzite structures.

The ability of a CRN (or any other type of model) to produce fringes can be seen by looking at the projected atom density for different orientations of the model. One orientation of the 64 atom HH model was found (Chaudhari et al, 1974) for which atoms in the projected atom density aligned to form planes with a regular spacing corresponding approximately to the (111) planes in the crystal. However, for the 519 atom modified Polk model, the preferred orientation gave much less well defined planes (Chaudhari and Graczyk, 1974) and the picture was not convincing. Indeed, it has been remarked (Cochran, 1974) that the chances of a CRN structure being sufficiently crystal-like in projection to produce recognizable fringes, are very low, the HH model being atypical in this respect. A major objection to the HH model, for the above calculations, is its small size. The model contains too few atoms in comparison to those in a film of 50-100 Å thickness which are expected to participate in the imaging process in the electron microscope.

Consequently, attention has recently returned to the problem of whether a modified microcrystallite picture can be consistent with the available diffraction data, further calculations (Howie et al, 1973, Weinstein and Davies, 1973) for simple microcrystalline models based on diamond and wurtzite structures having given in general poor agreement with experiment.

Of course, one possible reason for the disappointing results obtained by these calculations was the assumption that the microcrystals had random orientation with no account being taken of the correlation between atoms in different crystalline regions. In other words, no specification was given of how the microcrystals were linked together, whether directly or via some intervening matrix

region. For a microcrystallite model the importance of this matrix region or connective tissue was recognized very early on (Warren, 1937) and recently restated (Gaskell, 1975) where it is pointed out that, for an ordered unit of the size indicated by electron microscopy (5 Å - 15 Å) as many atoms would be bonded to atoms within the matrix region as would be bonded to atoms within the microcrystallites.

Consequently, an attempt to improve on the simple microcrystallite picture was made (Gaskell, 1975) with the construction of a continuous network that was based on ordered units; the model being constructed by the packing of ordered tetrahedral units, having the diamond structure and joined by eclipsed bonds across the (111) faces; (referring to figure 3.1, the bonds are 'eclipsed' when adjoining tetrahedral units have identical orientation). The polytetrahedral (PT) cluster so formed was not strain free (it is not possible to fill space by packing tetrahedra), the average strain per bond increasing approximately linearly as more tetrahedral units were added. This network strain resulted in bond lengths and angles within the cluster taking on a range of values. Hence, nearest and next nearest neighbour distributions were broadened as the cluster size increased, there arising an optimum cluster size at which the distribution broadening accorded with that seen in the experimental RDF for α-Ge (Temkin et al, 1973).

Thus to a certain extent the model correlates the microcrystallite and CRN descriptions of the amorphous state. The model has been shown to be consistent with the electron microscopy experiments described above (the 15 Å result for the dark field experiments) and the model RDF gives better agreement with experiment than has been given by any previous ordered units model (although still not as good as that shown by most CRN structures).

To summarize this section; although the majority of evidence is in favour of the CRN model, containing odd membered rings, there is still some controversy (since as we have stated, g(r) does not define a unique structure) as to whether a slightly more ordered model could explain all the experimental evidence.

Consequently, we shall present diffraction calculations for both types (microcrystallite and CRN) of model. Firstly, the Steinhardt and modified CT models as described above, and secondly, the ordered units PT model of Gaskell containing 720 atoms. We shall only give results for three of the CT models (hereinafter relabelled and referred to as models CT 1, 2 and 3 as indicated in Table 3.1), which is sufficient to show the trends apparent as one moves down the table.

3.3. Model Structure Factors

As was mentioned in the Introduction, to calculate the X-ray and electron diffraction intensities for α-Si, in the spherical atom densities approximation, we require the nuclear-nuclear structure factor S(k) and hence the radial distribution function g(r) (see equations 2.20 and 2.17c).

For a model calculation it is convenient to introduce (Bell and Dean, 1972) a pair histogram $R_{A-B}(r)$ with interval δr such that $R_{A-B}(r)\delta r$ gives the number of B sites lying in the range r to r + dr from a typical A site. Formally we have

$$R_{A-B}(r) = \underset{i}{\text{Average}} \sum_j S\left(\text{distance } A_i B_j \,|\, r, \delta r\right) \qquad 3.2$$

where

$$S(x \,|\, y, \delta y) = \frac{1}{\delta y} \quad \text{if } y < x \leq y + \delta y \qquad 3.3$$

$$= 0 \text{ otherwise}$$

Here A_i and B_j represent the positions of the i and j^{th} atoms of types A and B

respectively. In dealing with a model which contains only a finite number of atoms it is necessary to define these distributions as histograms with a finite interval. In the limit of an infinitely large model the interval $\delta y \to 0$, the histogram becomes a curve and $S(x \mid y, \delta y)$ tends to a delta function. For α-Si, the relationship between the pair distribution function $R_{Si-Si}(r)$ and the radial distribution function g(r) is

$$g(r) = R_{Si-Si}(r) / 4\pi r^2 \rho_{on} \qquad 3.4$$

where ρ_{on} is the mean number density of Si nuclei in the model. Hence we can obtain S(k) from equation (2.17b). Of course, we are trying to predict, using a model, a quantity that is representative of a bulk sample of α-Si. Thus $R_{AB}(r)$ from equation (3.2) must be corrected for finite model size and this can be achieved in the following way (Germer and White, 1941).

We suppose that a sphere S of diameter D is inscribed within a model of infinite extent and that the RDF of this model is to be calculated by using the positions of only those atoms which are inside S. We consider an atom in S a distance d from its centre and calculate the number of atoms, also within S, a distance r to r + dr from it. We can write this as the fraction of the total number of atoms in the model in this distance range. This fraction is given by

$$\begin{aligned} \varepsilon(r,d) &= 1 && r+d \le \tfrac{D}{2} \\ &= \left(\left(\tfrac{D}{2}\right)^2 - (r-d)^2\right)/4rd && r+d > \tfrac{D}{2} \\ &= 0 && r-d \ge D/2 \end{aligned} \qquad 3.5$$

If S contains a large (> 150, Beeman and Bobbs, 1975) number of atoms, then we can average ε (r, d) over S to obtain

$$\mathcal{E}(r) = 1 - \frac{3}{2}\frac{r}{D} + \frac{1}{2}\left(\frac{r}{D}\right)^3 \qquad r < D$$

$$= 0 \qquad r > D \qquad 3.6$$

Thus, for a roughly spherical model of diameter D, the corrected function $R_{A-B}(r)$ is related to the model function $R_{AB}(r)$, say, by

$$R_{A-B}(r) = R_{AB}(r) / \mathcal{E}(r) \qquad 3.7$$

Of course 'infinity' for the high r limit of equation (2.17b) is still limited by the model size since equation (3.7) diverges for r = D.

S(k) calculated from equation (2.17b) is shown (curve 1 in each case) in figures 3.2, 3.3, 3.4 for models CT 1, 2, 3 respectively, figure 3.5 for the Steinhardt model and figure 3.6 for the PT model. S(k) as shown for the PT model is that calculated for a central core of the model containing 214 atoms. Calculations for the complete 720 atom structure led to peak splittings in the low k region of S(k). This can be seen in figure 3.7 where S(k) is shown as calculated including 214 atoms (curve 1) and 720 atoms (curve 2). The appearance of the peak splittings as more atoms are included indicates the presence of long range crystal-like correlations which are, of course, not expected to be present in a truly amorphous structure. A similar effect has been noted (Weinstein and Davies, 1973) for several simple microcrystallite models of α-Ge. Hereinafter we shall present results only for the central core of the PT model containing 214 atoms.

The curves of S(k) immediately give us, apart from a factor b_{Si}^2 (see § 2.4), the neutron diffraction intensity to be expected from each model which will be of interest should the neutron experiment be carried out. However, we turn our attention now to the X-ray and electron diffraction intensities from

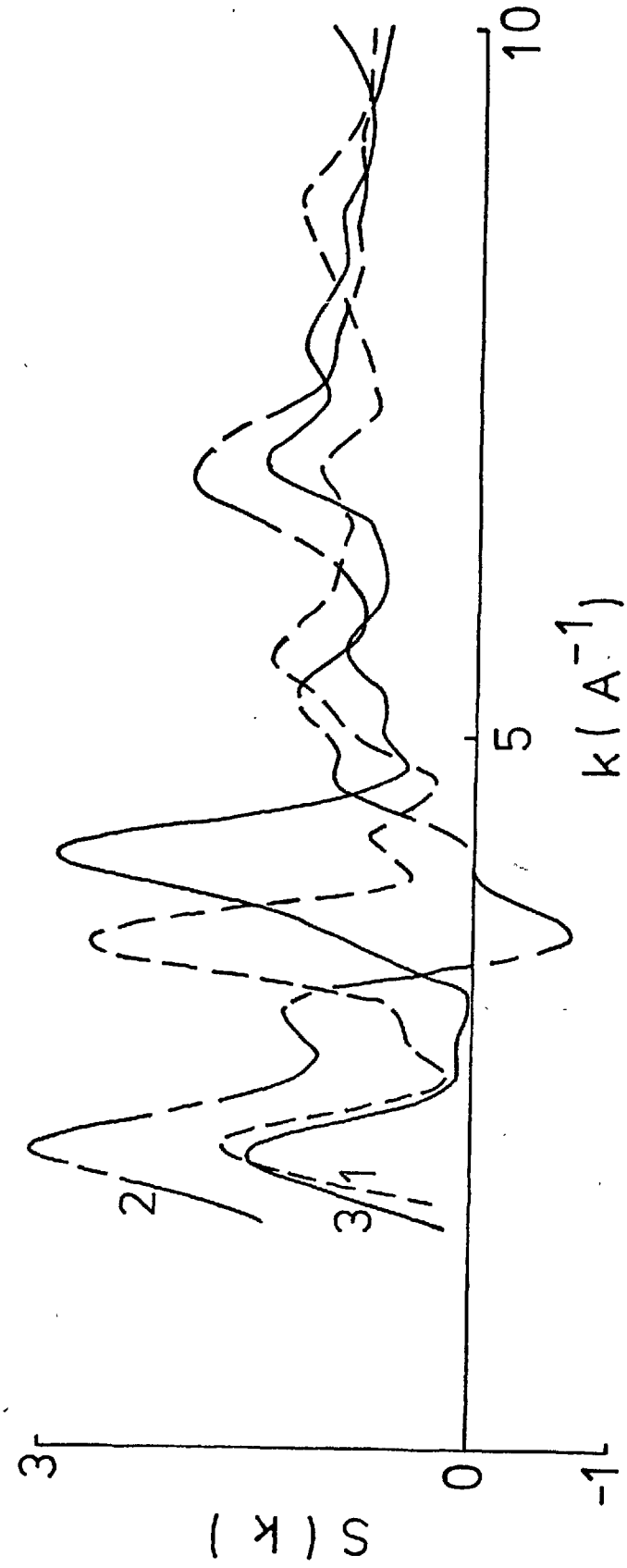

Figure 3.2 : The partial structure factors for the C T 1 model.

1. S (k)
2. S_{nb} (k)
3. S_{bb} (k)

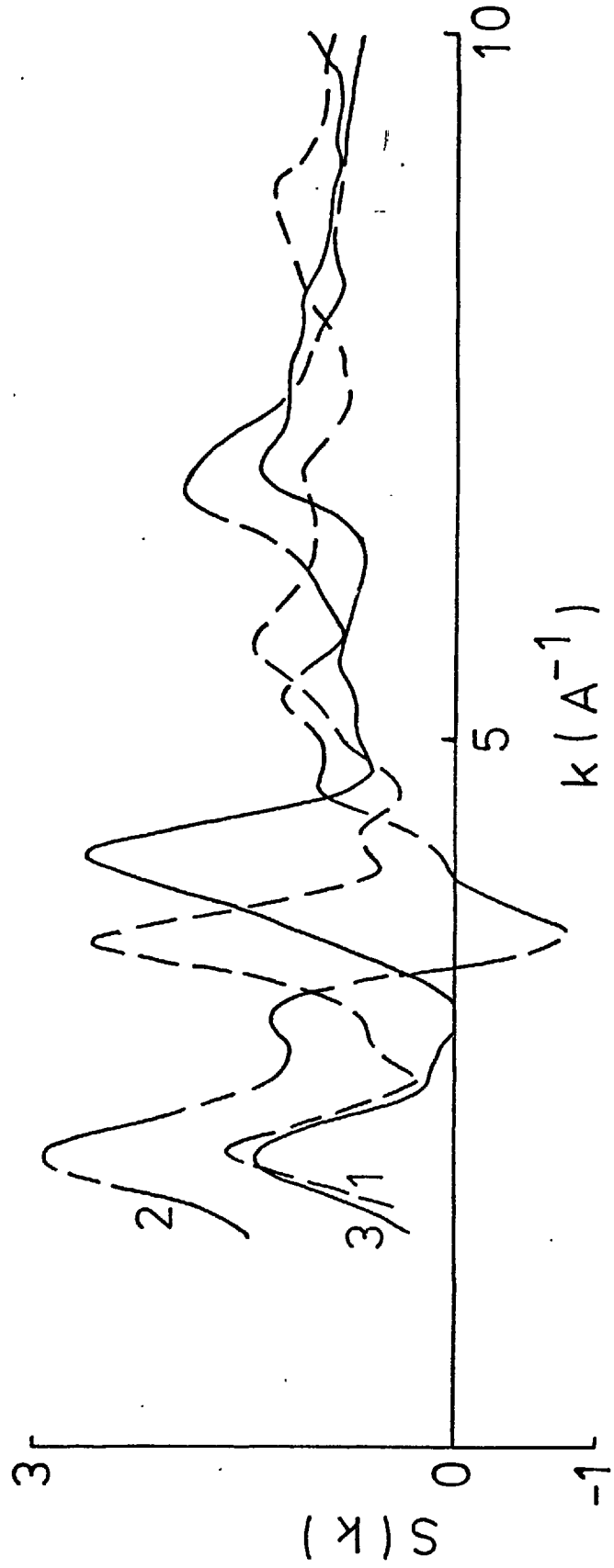

Figure 3.3 : The partial structure factors for the C T 2 model

1. S (k)
2. S_{nb} (k)
3. S_{bb} (k)

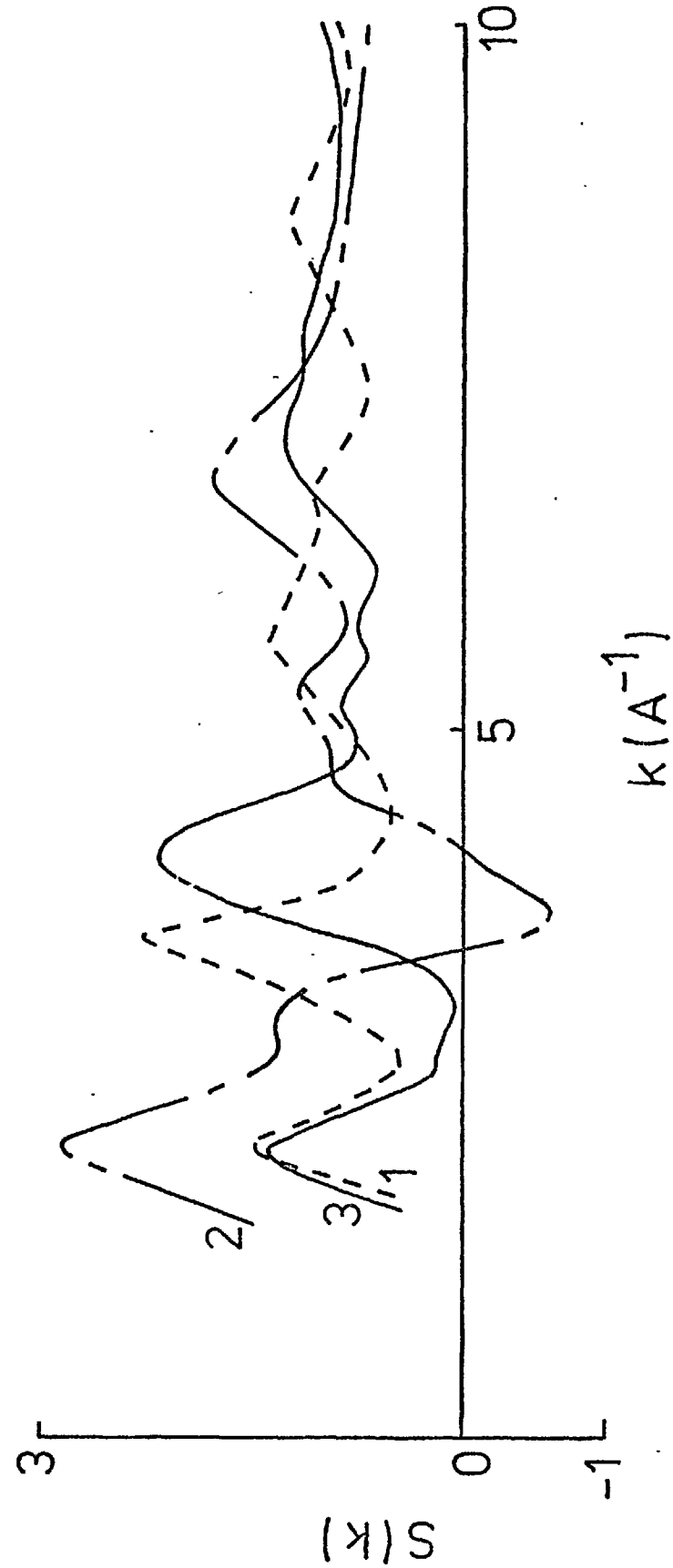

Figure 3.4 : The partial structure factors for the C T 3 model.

1. S (k)
2. S_{nb} (k)
3. S_{bb} (k)

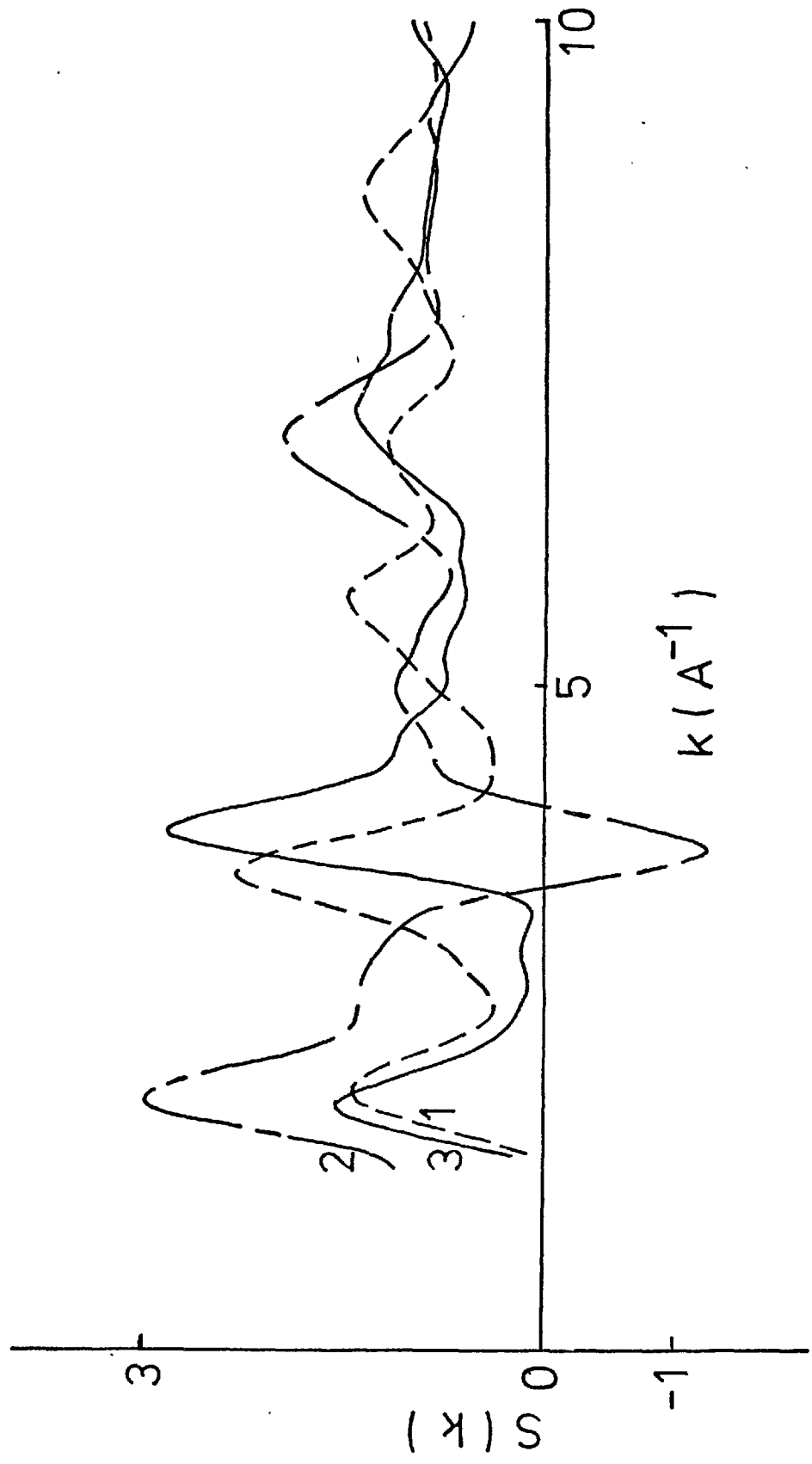

Figure 3.5 : The partial structure factors for the Steinhardt model.

1. S(k)
2. S_{nb} (k)
3. S_{bb} (k)

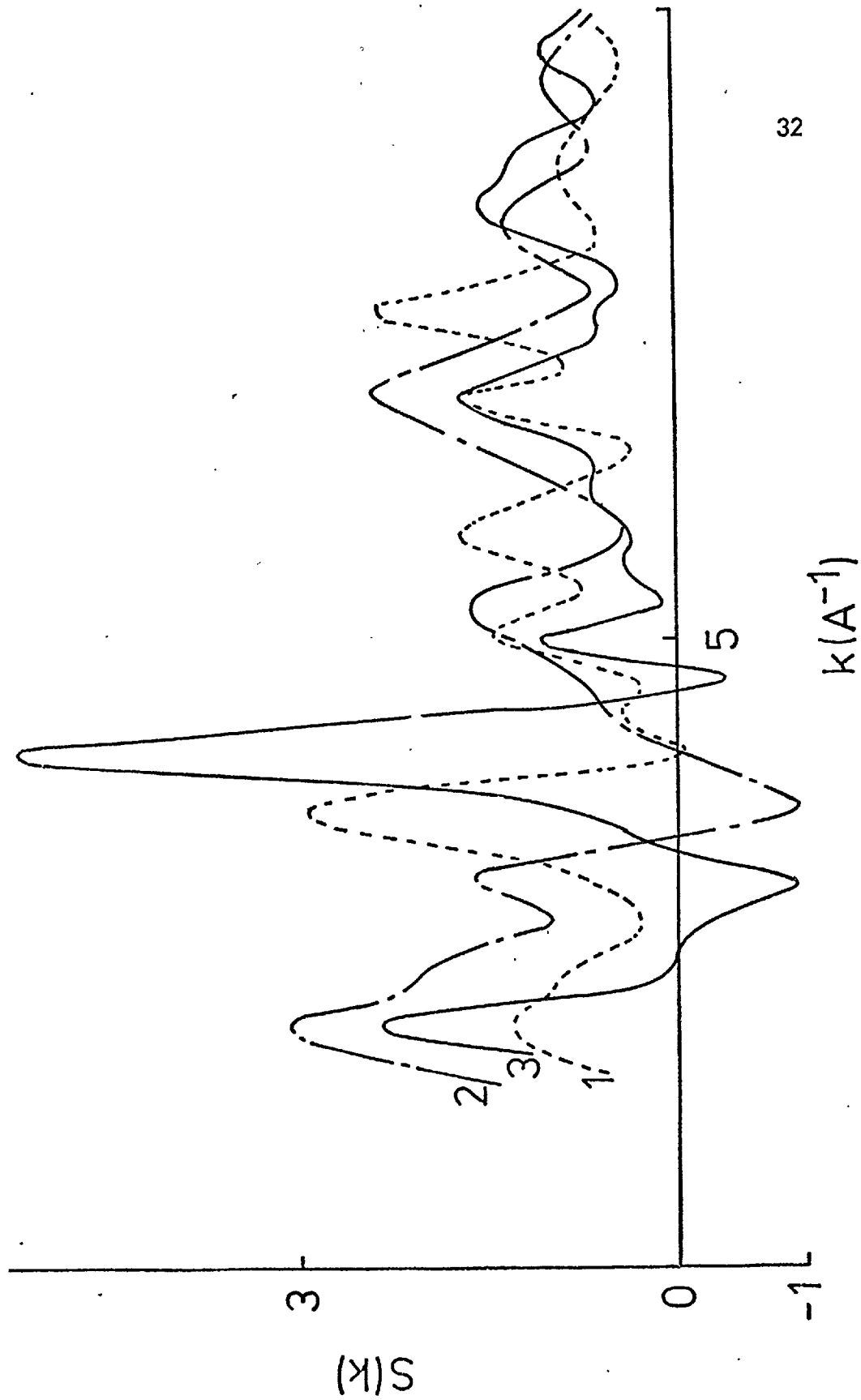

Figure 3.6 : The partial structure factors for the P T model.

1. S (k)
2. S_{nb} (k)
3. S_{bb} (k)

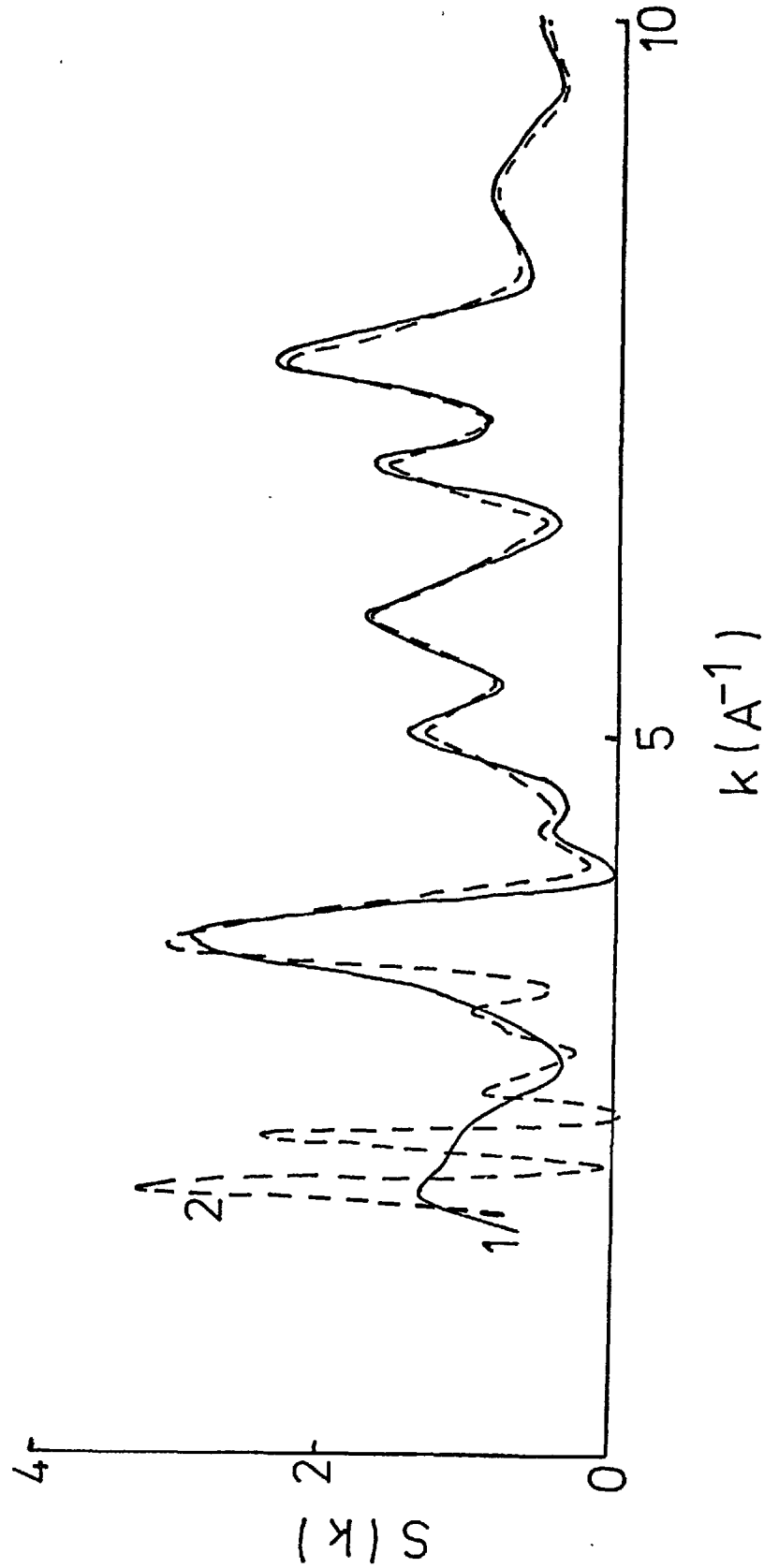

Figure 3.7 : Structure factor S (k) for the P T model.

1. 214 atoms
2. 720 atoms

α-Si, where we do have experimental data.

3.4. X-ray and Electron Diffraction using atomic form factors

We define $S^x(k)$ and $S^e(k)$ as the structure factors derived from the experimental X-ray (Richter and Breitling, 1958) and electron (Moss and Graczyk, 1969) diffraction intensities respectively. These are shown in figure 3.8 $S^x(k)$ in curve 1 and $S^e(k)$ in curve 2. It can be seen that the curves are in disagreement at low k over the height of the first peak, but in quite good agreement at high k ($> 4A^{-1}$). These curves can also be compared with the calculated model structure factor S(k) curves of figures 3.2 to 3.6. No model curve agrees with either experimental curve for all k. Agreement is good for the CT3 model in the region $k > 4A^{-1}$ and for direct comparison with the experimental data this curve is shown as curve 3 in figure 3.8.

For the CT3 and PT models we have also calculated the X-ray and electron diffraction intensities according to equations 2.20 and 2.22, with the atomic form factor as above. Thus, in figure 3.9, curve 1 we show the X-ray data (Richter and Breitling, 1958) together with the X-ray curves for the CT3 model (curve 2) and the PT model (curve 3) and in figure 3.10, curve 1, we show the electron data (Moss and Graczyk, 1969) together with the calculated model curves (labelled 2 and 3 as above). In figures 3.9 and 3.10, because of the damping effect of the atomic form factor for the high k region, much of the structural information that was evident in the comparisons of the S(k) functions is lost. Obviously, the intensity curves will only reflect the same features that we saw in the S(k) curves, and the main point that we wish to make here is that for X-rays, both model calculations have the relative heights of the first two peaks reversed with respect to experiment.

The good agreement shown for $k > 4A^{-1}$ between S(k) for the CT3 model and the experimental S(k) functions, coupled with the disagreement between $S^e(k)$

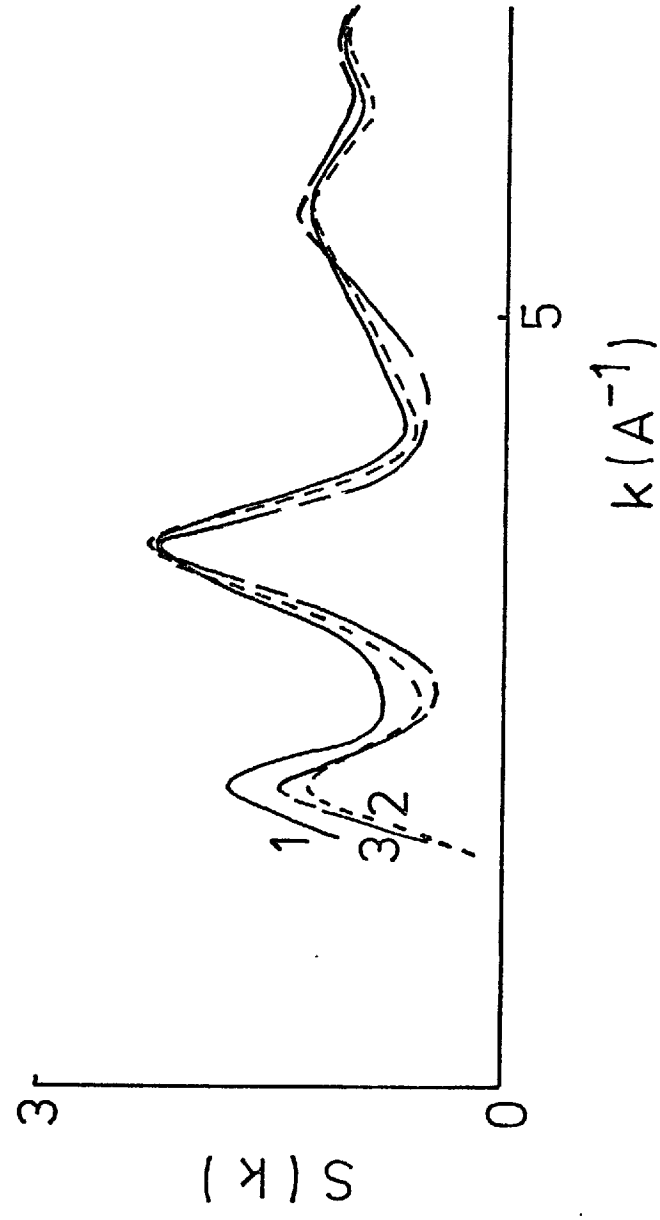

Figure 3.8 : Experimental and model structure factors.

1. S^x (k)
2. S^e (k)
3. S (k) for the CT3 model

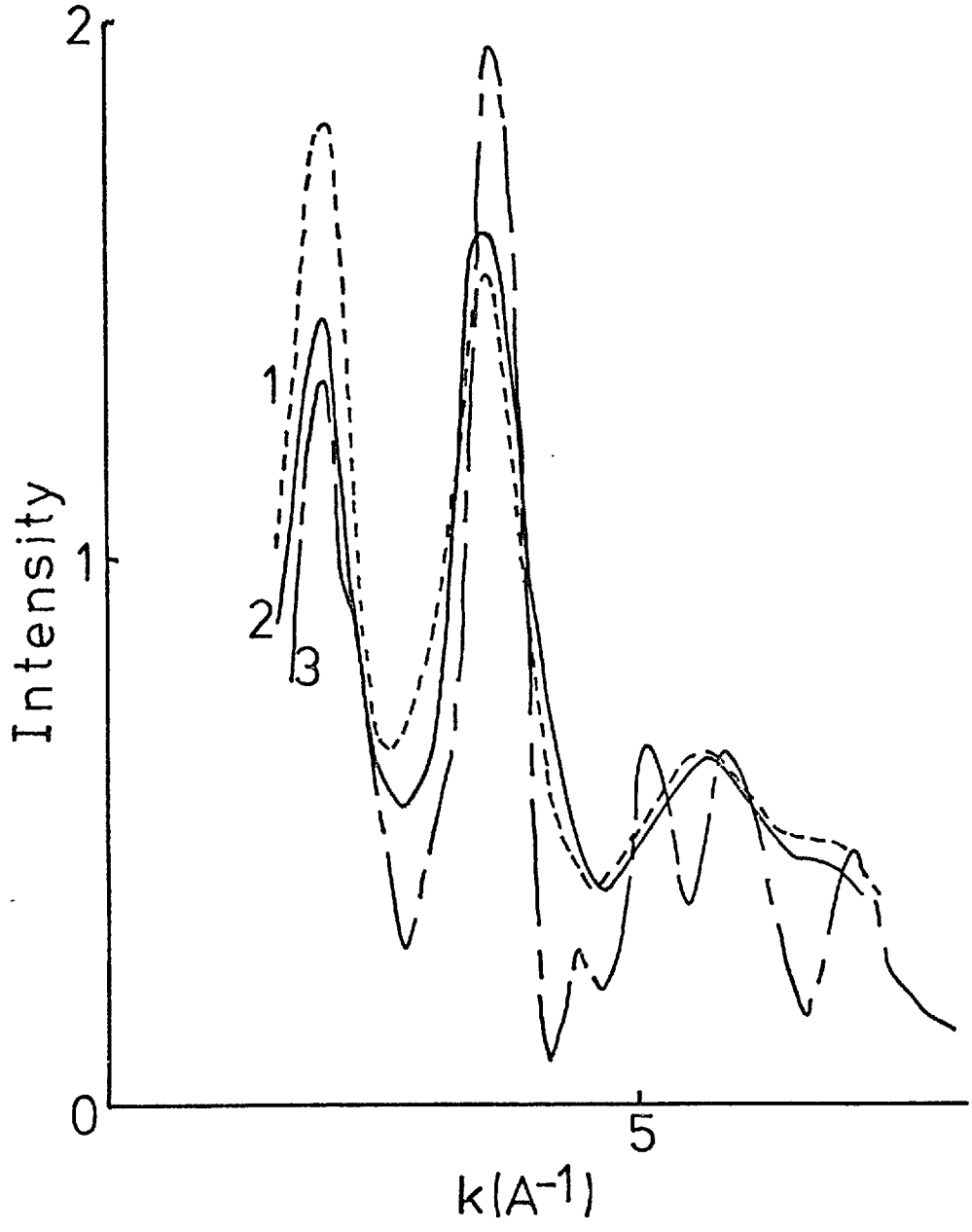

Figure 3.9 : The X-ray intensity for silicon using neutral atomic form factors.

1. Experiment
2. CT3 model
3. PT model

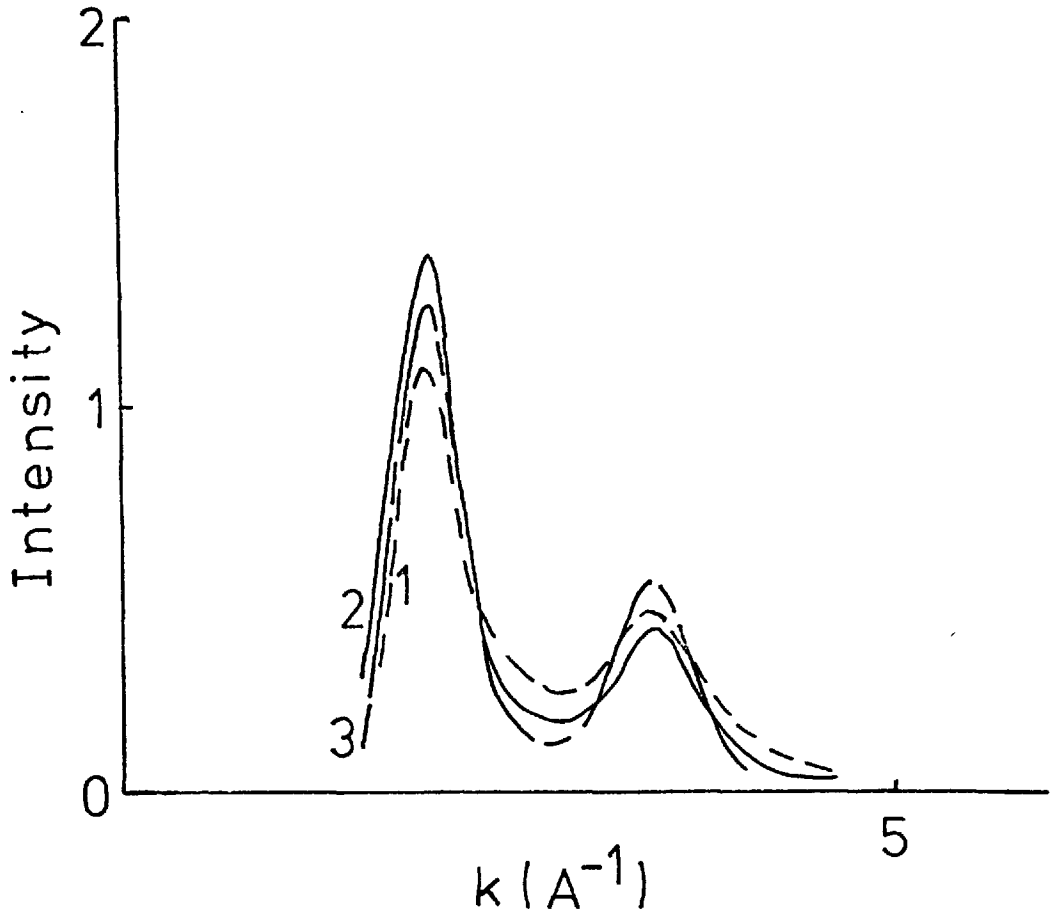

Figure 3.10 : The electron intensity for silicon using atomic form factors.

1. Experiment
2. The CT3 model
3. The PT model

and $S^{x}(k)$ below $4A^{-1}$, suggests that the effects at the first peak are not purely structural and must therefore be partly due to the atomic form factor. This is our second indication (the first being the "forbidden" reflection in the crystalline case as discussed in Chapter 2) that the superposition of free atom-like charge densities may be a bad model with regard to calculating X-ray and electron diffraction intensities from α-Si. Of course one experiment could be correctly simulated for all k by a model calculation in which we make a suitable modification of the atomic form factor in the low k region. However, this cannot be done consistently for both X-ray and electron diffraction since one obtains a different form factor in each case.

A consistent treatment of the electron density in α-Si is important because the structure factors and total intensities represent good tests of proposed model structures and discrepancies at any k between theory and experiment could be interpreted as structural facets of a model. Structural information obtained from the structure factor S(k) or the reduced intensity function F(k) (equation 3.1) is unambiguous for large k where the scattering is from the highly localized core states. For this region comparisons between theory and experiment for the S(k) and F(k) curves are to be preferred to those for the full intensity.

But S(k) and F(k) are basically functions derived from the measured intensity using the atomic form factor and thus for the low k region, to study the effects of covalent bonding, we shall need to look at the total intensity I(k). First of all, however, we require a realistic model of the electron density distribution in α-Si. In Chapter 1 of this thesis we gave some of the reasons for our believing in a localized approach to modelling the total electron density $\rho(\underset{\sim}{r})$. Our objective in the next section will be to obtain such a model for the electron density in a single covalent bond. We begin this important section of our work with a discussion

of some recent arguments directly in support of localized bond densities.

3.5 Arguments in support of localized bond densities

As discussed in Chapter 1, for crystalline Si one can clearly generate an exact electron density $\rho(\underset{\sim}{r})$ using Bloch waves calculated by the well established band theory methods. However, this delocalized approach is not a suitable starting point to discuss the disordered case in which one does not have lattice periodicity.

Despite the many electron aspect of the problem it is well known that the ground state electron density $\rho(\underset{\sim}{r})$ can be constructed from a one body potential $V(\underset{\sim}{r})$ (Hohenberg and Kohn, 1964). However, this potential depends on the exchange and correlation energy $E_{xc}[\rho]$ as a functional of the charge density ρ through

$$V(\underset{\sim}{r}) = V_{HARTREE} + \frac{\delta E_{xc}[\rho]}{\delta \rho} \qquad 3.8$$

where $V_{Hartree}$ is calculated for the exact electron density, and unless good physical arguments exist for constructing the second term as the right hand side of equation (3.8) this approach would not be fruitful. When the electron density $\rho(\underset{\sim}{r})$ is slowly varying good arguments (Hohenberg and Kohn, 1964) exist for setting up the exchange and correlation contribution to the one-body potential, but in general this is not so such a prescription failing when one has a rapidly varying $\rho(\underset{\sim}{r})$ with atomic like density gradients.

Nevertheless, given the existence of such a one body potential, a localized orbital approach (Anderson, 1968 and 1969) has been developed (Bullett, 1974, 1975 and 1976) for the covalently bonded semiconductors. Anderson models $V(\underset{\sim}{r})$ by a superposition of localized potentials centred on the nuclei $\underset{\sim}{R}_\alpha$

$$V(\underset{\sim}{r}) = \sum_\alpha V_\alpha(\underset{\sim}{r} - \underset{\sim}{R}_\alpha) \qquad 3.9$$

and then uses pseudopotential ideas to calculate localized orbitals for a covalent system (essentially an interpretation of the Huckel method for organic molecules).

Bullett has applied this approach to diamond, graphite and silicon, and in so doing gives some justification to the method we use here for constructing a localized bond charge distribution. Bullett considers a localized bond orbital between two isolated atoms A and B ϕ°_{ab}, say, which one would expect to satisfy some bond Schrodinger equation of the form

$$H_{ab} \, | \phi^{\circ}_{ab} \rangle = \varepsilon^{\circ} \, | \phi^{\circ}_{ab} \rangle \qquad 3.10$$

But in the solid state, of course, an electron in the bond feels the perturbing effect of all the other atoms which Bullett writes as

$$V_{ab} = H - H_{ab} \qquad 3.11$$

where H is the total one electron Hamiltonian. By projecting out a term in bond orbitals on other sites

$$[H_{ab} + V_{ab} - \Sigma | \phi_{cd} \rangle \langle \phi_{cd} | V'_{cd}] | \phi_{ab} \rangle = \varepsilon_{ab} | \phi_{ab} \rangle \qquad 3.12$$

where V_{cd} is the effect of atoms C and D, he was able to show that most of this perturbing potential is screened out. The important result for our work is that the self consistent solutions of equation (3.12) are well represented by the normalized sum of Pauling type hybridized orbitals on each atom. The valence bond structures obtained using only these functions and a simple model for V_{α} of equation (3.9) were found to contain the broad features of experiment with regard to bulk moduli, bond lengths and bond energies, and also explains the non-existence of the graphitic structure for silicon. In view of the inherent difficulties in

calculating $E_{xc}[\rho]$, and hence the one body potential $V(\underset{\sim}{r})$, in the covalent semiconductors it is interesting that a many electron approach (Herbert, 1974) again concludes with the validity of the localized bond concept. Herbert's work, essentially extracting a localized bond picture from band theory, also predicts the absence of states in the energy gap in α-Si and thus explains the experimentally observed sharp band edges (Donovan et al, 1969).

Thus, assuming that we can build the charge density in the amorphous state by superposing localized distributions we shall take, to be specific, the linear combination of atomic orbitals (LCAO) description of a covalent bond (although any other description could readily be incorporated within the theoretical framework set out below). We shall construct the LCAO electron density for a single bond in the crystal and then assume that this density can be carried over, intact, to the amorphous state. In fact, Raman spectra calculations (Meek, 1977) have indicated that this may not be the case, but that any differences between the amorphous and crystalline densities will be small. (The alteration of the charge density in the bonding region appears to be a necessary consequence of the presence of odd-membered rings in the structure).

In the chemist's picture the covalent bond in Si is due to sp^3 hybridization. Using orthogonalized Slater orbitals this hybrid, for Si, takes the form

$$\phi_{\pm}(\underset{\sim}{r}) = \frac{1}{2}\left\{\psi_{3s}(r) \pm \sqrt{3}\,\psi_{3p}(\underset{\sim}{r})\right\} \qquad 3.13$$

where the notation used is as in figure 3.11 and

$$\psi_{3s}(r) = Ar^2\exp(-\mu_1 r) - B r\exp(-\mu_2 r) - C\exp(-\mu_3 r)$$

$$\psi_{3p}(\underset{\sim}{r}) = D x r\exp(-\mu_1 r) - E x\exp(-\mu_2 r) \qquad 3.14$$

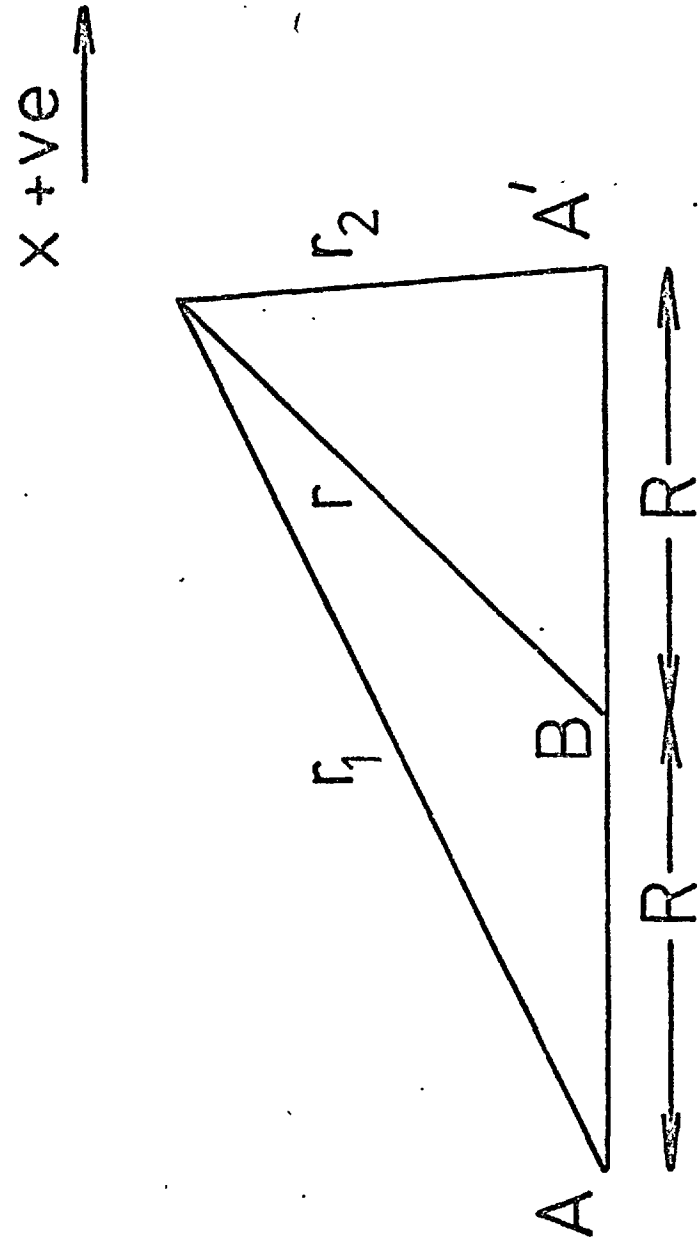

Figure 3.11 : The geometry used in constructing the bond orbitals.

where the constants have the values shown in Table 3.2. The wavefunctions are normalized, the unit of length being half the Si-Si bond length, which is also given in Table 3.2.

Then we form a molecular orbital for the bond by a linear combination of sp^3 orbitals centred on the two Si nuclei participating in the bond

$$\psi(\underset{\sim}{r}) = [\phi_+(\underset{\sim}{r}_1) + \phi_-(\underset{\sim}{r}_2)]/(1+S)^{1/2} \qquad 3.15$$

where S is the overlap integral given by

$$S = \int_{\underset{\sim}{r}} \phi_+(\underset{\sim}{r}_1)\,\phi_-(\underset{\sim}{r}_2)\,d\underset{\sim}{r} \qquad 3.16$$

and the charge density in the bond is given by

$$\rho(\underset{\sim}{r}) = |\psi(\underset{\sim}{r})|^2 \qquad 3.17$$

and evidently

$$\int_{\underset{\sim}{r}} \rho(\underset{\sim}{r})\,d\underset{\sim}{r} = 2 \text{ electrons} \qquad 3.18$$

The resulting bond charge density contours are shown in figure 3.12. Here we have added $\frac{1}{4}$ of the Si atom core electrons on each end of the bond to form the basic scattering unit for Si, this unit containing seven electrons in all.

In figure 3.13 we show the charge density contours formed from the superposition of free atoms model, again with $\frac{1}{4}$ of the silicon core electrons included on each atom. The marked difference between the superposition density and that of the LCAO density of figure 3.12 is the absence in figure 3.13 of the closed, almost spherical contours around the bond centre.

Thus the LCAO contours indicate that a better model of the covalent bonding in α-Si would include, in addition to the superposition of spherical charge clouds on each atom, a spherical charge distribution at the bond centre - the bond charge. This is an idea that has been exploited previously (Phillips, 1968). We want to

Table 3.2 : Constants for the Slater wavefunctions for silicon

Constant	Value [+]
μ_1	3.07
μ_2	10.933
μ_3	30.414
A	6.35
B	21.90
C	0.41
D	10.57
E	34.98

[+] The unit of length = 1.175 A, half the Si-Si bond length.

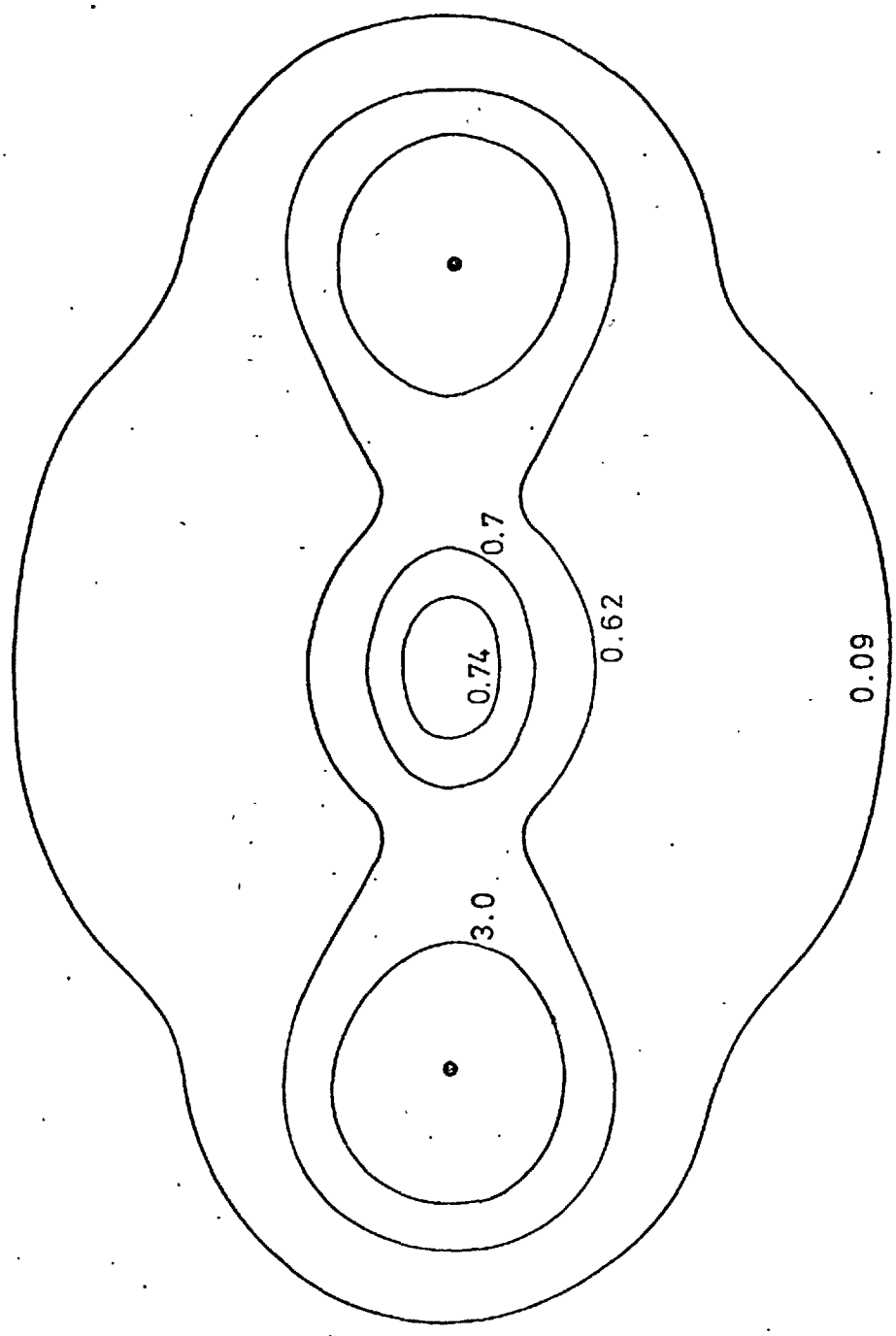

Figure 3.12 : Charge density contours for the LCAO description of a silicon-silicon covalent bond.

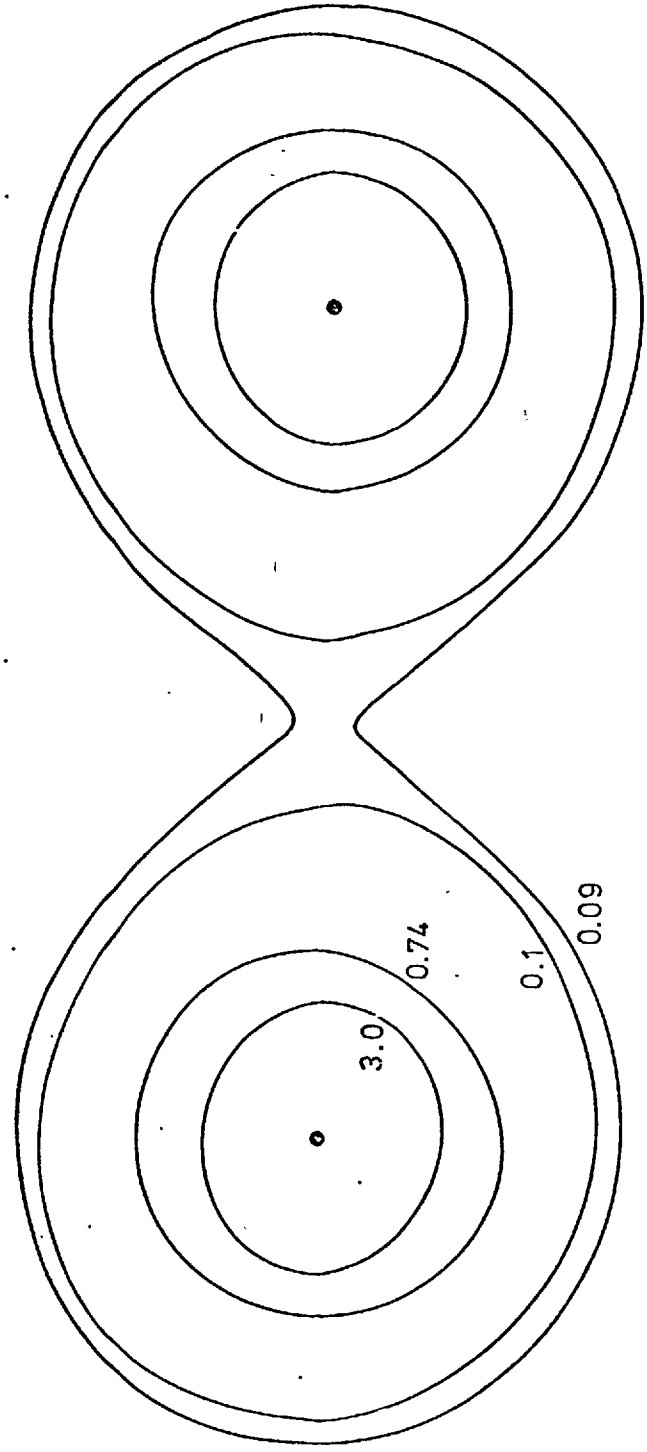

Figure 3. 13 : Charge density contours for the superposition of free atoms model.

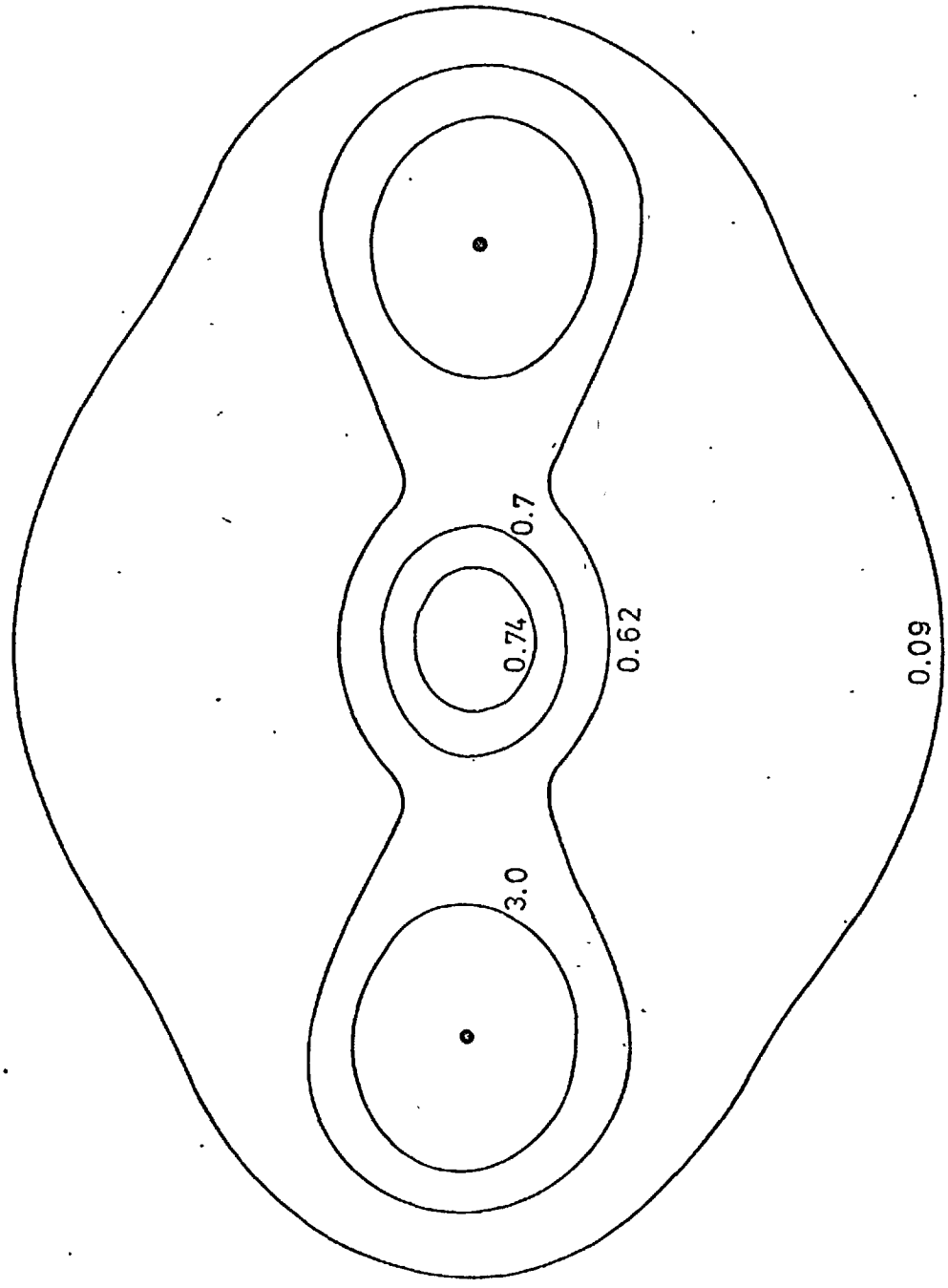

Figure 3.14 : Charge density contours for the three spherical distributions model of a covalent bond.

emphasize here that whereas Phillips was concerned with dielectric properties and lattice dynamics, and for his purposes was able to model the bond charge as a point charge, we are concerned with modelling diffraction intensities which require a spatial bond charge distribution.

3.6 Charge density in one bond

Having given a summary of the arguments for building the charge density from localized bonds we shall now discuss, explicitly, the way in which we have modelled the electron density in a single Si-Si bond. This charge density is defined by equations (3.13) to (3.17) and contains two electrons. The core electrons that are included in the basic scattering unit, as defined above, are, of course, already spherically symmetric about the Si atoms. Our problem is thus one of determining what proportion of the two valence electrons should be associated with the spherical charge distribution at the bond centre.

We represent the covalent bond density approximately as the sum of two identical spherical charge distributions $\rho_a(r)$ say, at the ends of the bond and a different spherical distribution $\rho_b(r)$ at the centre of the bond. Thus, again referring to figure 3.11, we have

$$\rho(\underset{\sim}{r}_1) \approx \rho_a(r_1) + \rho_b(|\underset{\sim}{r}_1 - \underset{\sim}{R}|) + \rho_a(|\underset{\sim}{r}_1 - 2\underset{\sim}{R}|) \qquad 3.19$$

Now the electron density $\rho(\underset{\sim}{r})$ can be expanded about A in Legendre Polynomials giving

$$\rho(\underset{\sim}{r}_1) = \sum_{n=0}^{\infty} \rho_n(r_1) P_n(\cos\theta_{\underset{\sim}{r}_1}) \qquad 3.20$$

where $\theta_{\underset{\sim}{r}_1}$ is the angle between vector $\underset{\sim}{r}_1$ and the internuclear axis vector $\underset{\sim}{R}$.

The bond form factor is given by

$$f(\underset{\sim}{k}) = \int_{\underset{\sim}{r}} \rho(\underset{\sim}{r}) \exp(i\underset{\sim}{k}.\underset{\sim}{r})\, d\underset{\sim}{r} \qquad 3.21$$

and combining equations (3.20) and (3.21) we have

$$f(\underset{\sim}{k}) = \sum_n i^n f_n(k) P_n(\cos\theta_{\underset{\sim}{k}}) \qquad 3.22$$

where

$$f_n(k) = \int_0^\infty \rho_n(r)\, 4\pi r^2 j_n(kr)\, dr \qquad 3.23$$

and $\theta_{\underset{\sim}{k}}$ is the angle between vectors $\underset{\sim}{k}$ and $\underset{\sim}{R}$. However, by combining equations (3.19) and (3.21) we obtain

$$f(\underset{\sim}{k}) \approx f_a(k)\{1 + \exp(2i\underset{\sim}{k}.\underset{\sim}{R})\} + f_b \exp(i\underset{\sim}{k}.\underset{\sim}{R}) \qquad 3.24$$

where

$$f_a(k) = \int_0^\infty \rho_a(r)\, 4\pi r^2 \frac{\sin kr}{kr}\, dr \qquad 3.25$$

with a similar relationship between $f_b(k)$ and $\rho_b(r)$. Then, using Bauer's expansion of a plane wave in terms of spherical waves

$$\exp(i\underset{\sim}{k}.\underset{\sim}{R}) = \sum_n i^n (2n+1) j_n(kR) P_n(\cos\theta_{\underset{\sim}{k}}) \qquad 3.26$$

and equating coefficients of $P_m(\cos\theta_{\underset{\sim}{k}})$ in equations (3.22) and (3.24) we obtain

$$f_o(k) = f_a(k)\left\{1 + \frac{\sin 2kR}{2kR}\right\} + f_b(k)\frac{\sin kR}{kR} \qquad 3.27$$

giving in particular at $k = 0$

$$f_o(0) = 2f_a(0) + f_b(0) = 2 \qquad 3.28$$

whilst for $n > 0$

$$f_n(k) = (2n+1)\{f_a(k) j_n(2kR) + f_b(k) j_n(kR)\} \qquad 3.29$$

Thus if we choose for $f_a(k)$ and $f_b(k)$ to simply reproduce lowest orders in the

harmonic expansion of equation (3.22) we obtain

$$f_a(k) = \frac{3 f_0(k) J_1(kR) - f_1(k) J_0(kR)}{3 J_1(kR)(1+J_0(2kR)) - 3 J_0(kR) J_1(2kR)} \qquad 3.30$$

and

$$f_b(k) = \frac{f_1(k)[1+J_0(2kR)] - 3 f_0(k) J_1(2kR)}{3 J_1(kR)[1+J_0(2kR)] - 3 J_0(kR) J_1(2kR)} \qquad 3.31$$

Clearly, different expressions for $f_a(k)$ and $f_b(k)$ could be obtained by pairing equation (3.27) with any of the n orders of equation (3.29). For each value of k our model has only two parameters, namely $f_a(k)$ and $f_b(k)$, and as soon as we include more than two terms in the expansion of equation (3.22) the problem is overdetermined.

However, if we assume a choice of $f_a(k)$ and $f_b(k)$ satisfying equation (3.27) we can write for all orders in equation (3.29)

$$f_n(k) = (2n+1)\left\{ f_a(k) J_n(2kR) + f_b(k) J_n(kR) \right\} + f_n^R(k) \qquad 3.32$$

where $f_n^R(k)$ is some remainder function representing that portion of $f_n(k)$ not reproduced by our choice of $f_a(k)$ and $f_b(k)$. If we now minimise $\sum_{n=1}^{N} |f_n|^2$ with respect to $f_a(k)$ or $f_b(k)$, where N is the number of terms that are included in equation (3.22) then we obtain a least squares fit to the first N terms of the expansion. Thus we require

$$\frac{\partial}{\partial f_b} \sum_{n}^{N} \left| f_n(k) - (2n+1)\left[\frac{f_0(k) - f_b(k) J_n(kR)}{1 + J_0(2kR)} \cdot J_n(2kR) + f_b(k) J_n(kR) \right] \right|^2 = 0 \qquad 3.33$$

for each value of k.

If we write

$$A_n(k) = \frac{(2n+1) f_0(k) J_n(2kR)}{1 + J_0(2kR)} \qquad 3.34$$

and

$$B_n(k) = (2n+1)\left[\frac{J_0(kR)J_n(2kR)}{1+J_0(2kR)} + J_n(kR)\right] \qquad 3.35$$

then we obtain

$$f_b(k) = \sum_{n=1}^{N} \frac{(f_n(k) - A_n(k))B_n(k)}{\sum_n^N B_n^2(k)} \qquad 3.36$$

and clearly $f_a(k)$ can be obtained from equations (3.27) and (3.36).

In figure 3.15 we show $f_b(k)$ as extracted using equation (3.36) for increasing values of N. Clearly for N = 1 we simply regain equation (3.31) and it can be seen that $f_b(k)$ obtained for this value of N ($f_b^1(k)$ in an obvious notation) is only slightly modified as we include higher orders and to graphical accuracy there is no difference between $f_b^3(k)$ and $f_b^4(k)$.

In figure 3.16 we show the form factors for our basic scattering unit containing 7 electrons; the bond charge form factor $f_b(k)$, curve 1, and the atom form factor $f_e(k)$, curve 2 where

$$f_e(k) = \frac{f_{core}(k)}{4} + f_a(k) \qquad 3.37$$

$f_a(k)$ and $f_b(k)$ are as calculated from equations (3.27) and (3.36) with N = 4 and $f_{core}(k)$ is the form factor for the Si core electrons.

One problem with our procedure for modelling the covalent bond is that using equations (3.27) and (3.36) the form factors $f_a(k)$ and $f_b(k)$ are difficult to extract accurately, for small k, since both numerator and denominator in equation (3.36) take on very small values. However, if we extrapolate the curves to k = 0, then $f_a(k)$ approaches a value of $f_a(0) \approx 0.15$ electrons and $f_b(k)$ a value $f_b(0) \approx 1.7$ electrons.

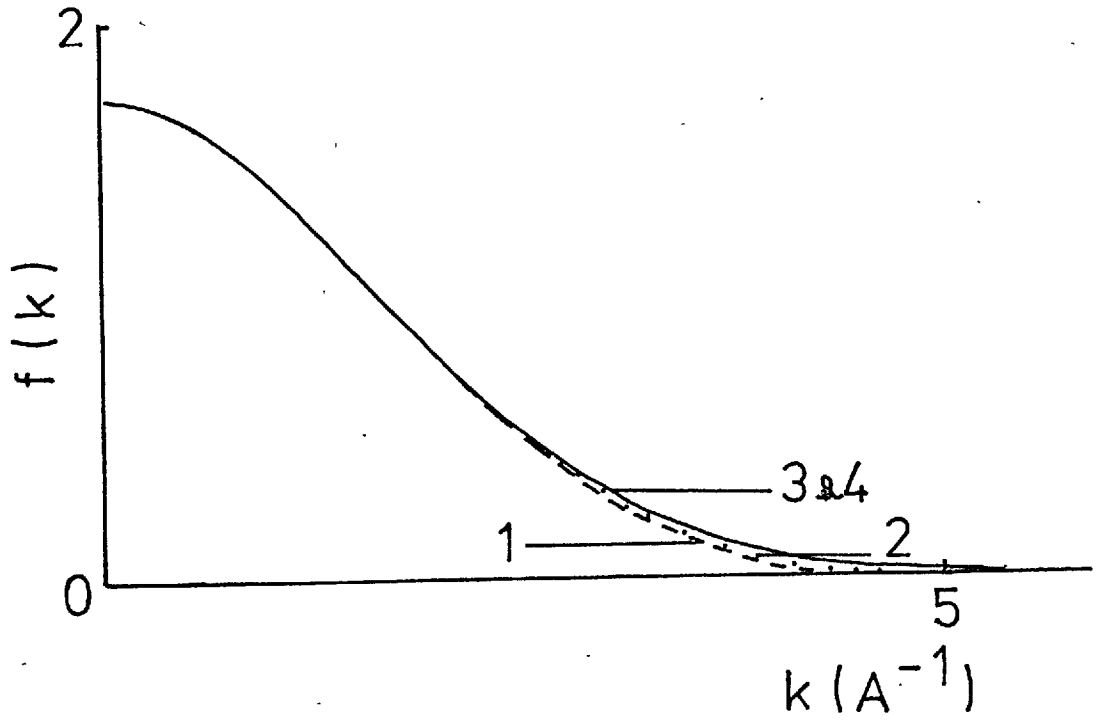

Figure 3.15 : The bond charge form factor f_b (k).

1. N = 1
2. N = 2
3. N = 3
4. N = 4

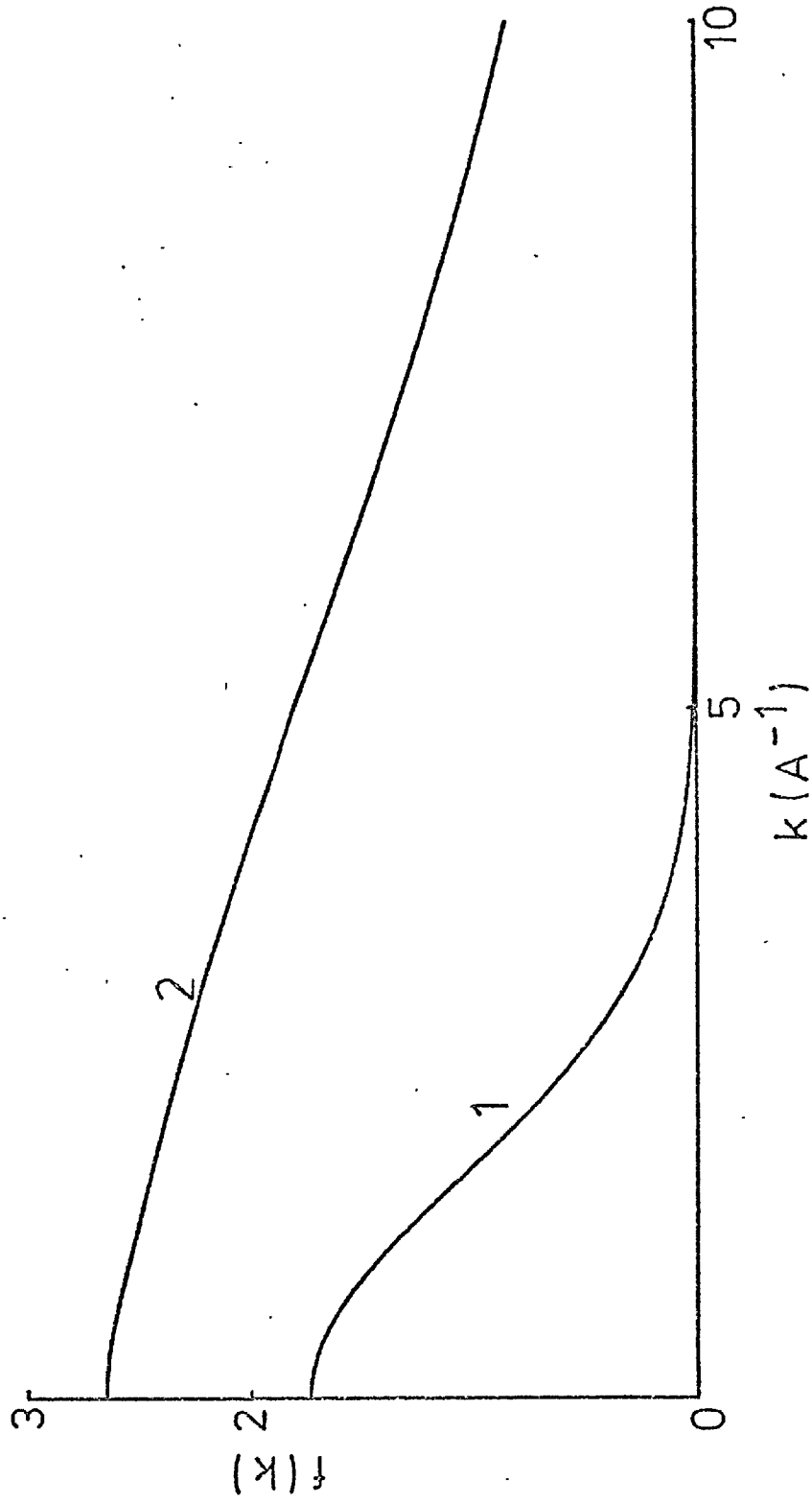

Figure 3.16 : The form factors for silicon.

1. f_b (k)
2. f_e (k)

Of course the complete LCAO bond density cannot be exactly represented as a sum of three spherical distributions and we have simply adopted one approximate way of doing so.

We can examine the problem in a slightly different way, by looking at the total bond density in r space. We have from equations (3.15) and (3.17) (where again the notation is given in figure 3.11)

$$\rho(\underset{\sim}{r}) = \frac{1}{(1+S)}\left(\phi_+^2(\underset{\sim}{r}_1) + \phi_-^2(\underset{\sim}{r}_2) + 2\phi_+(\underset{\sim}{r}_1)\phi_-(\underset{\sim}{r}_2)\right) \qquad 3.38$$

Immediately we see that the bond density consists of two one-centre terms, which we can associate with the two atoms at either end of the bond, and a two-centre term which we cannot associate uniquely with either atom. The overlap integral, S, of equation (3.16) has the value for Si of 0.77 and thus each one-centre term contains $1/(1+S) \approx 0.56$ electrons whilst the two-centre term contains $2S/(1+S) \approx 0.88$ electrons.

In figure 3.17, we show the charge density contours for the two-centre term and it can be seen that this makes a major contribution to the charge around the bond centre.

The one centre terms are not spherical about the atom sites since they contain explicitly (see equation 3.13)

$$\frac{\phi_\pm^2}{1+S}(\underset{\sim}{r}) = \frac{1}{4(1+S)}\left[\psi_{3s}^2(r) + 3\psi_{3p_x}^2(\underset{\sim}{r}) + 2\sqrt{3}\psi_{3s}(r)\psi_{3p_x}(\underset{\sim}{r})\right] \qquad 3.39$$

and clearly, due to the p orbital, the last two terms on the right hand side of equation (3.39) have a directional character. In figure 3.18 we show the charge density contours for these two terms. We have, of course, included the terms from both

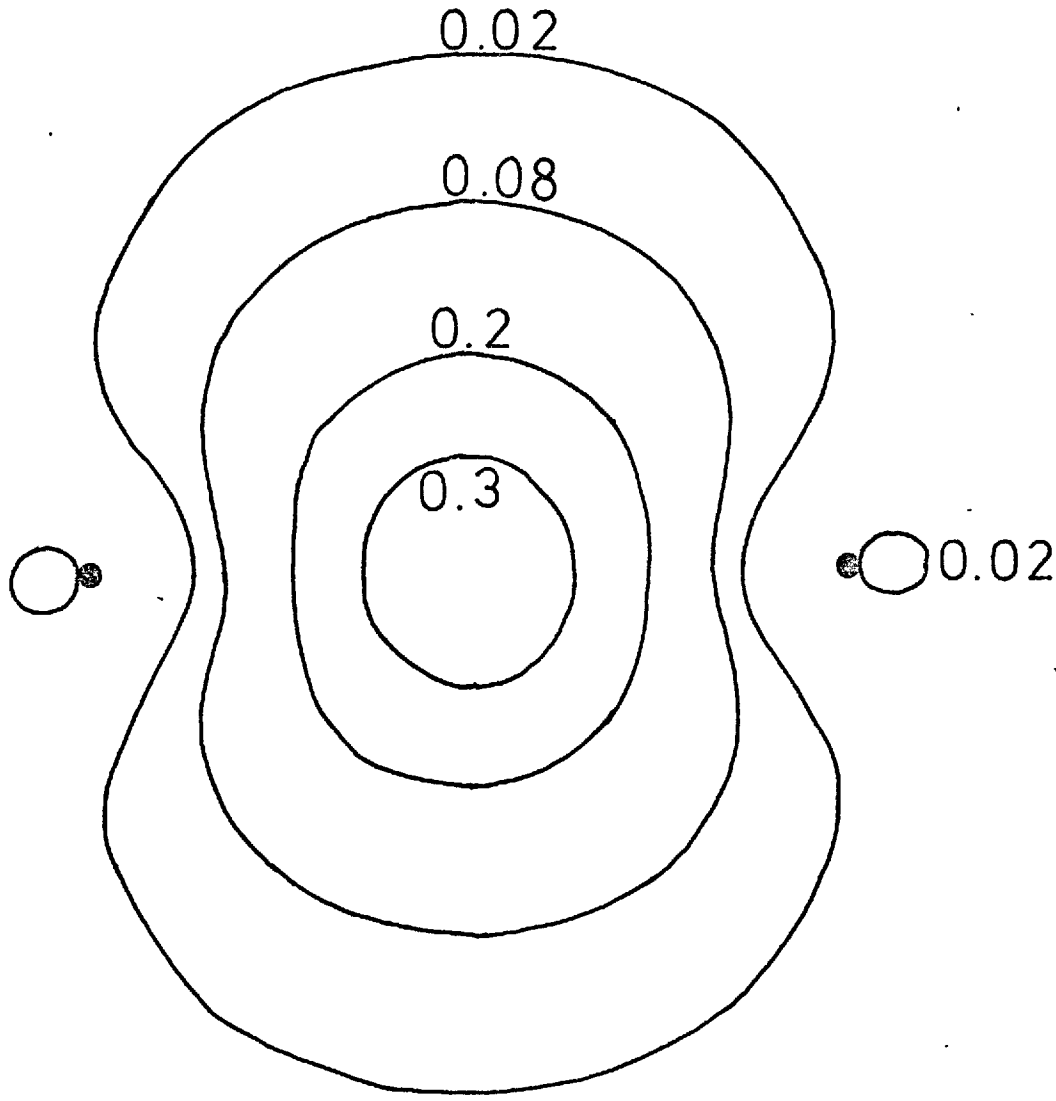

Figure 3.17 : Charge density contours for the two centre term in the LCAO covalent bond.

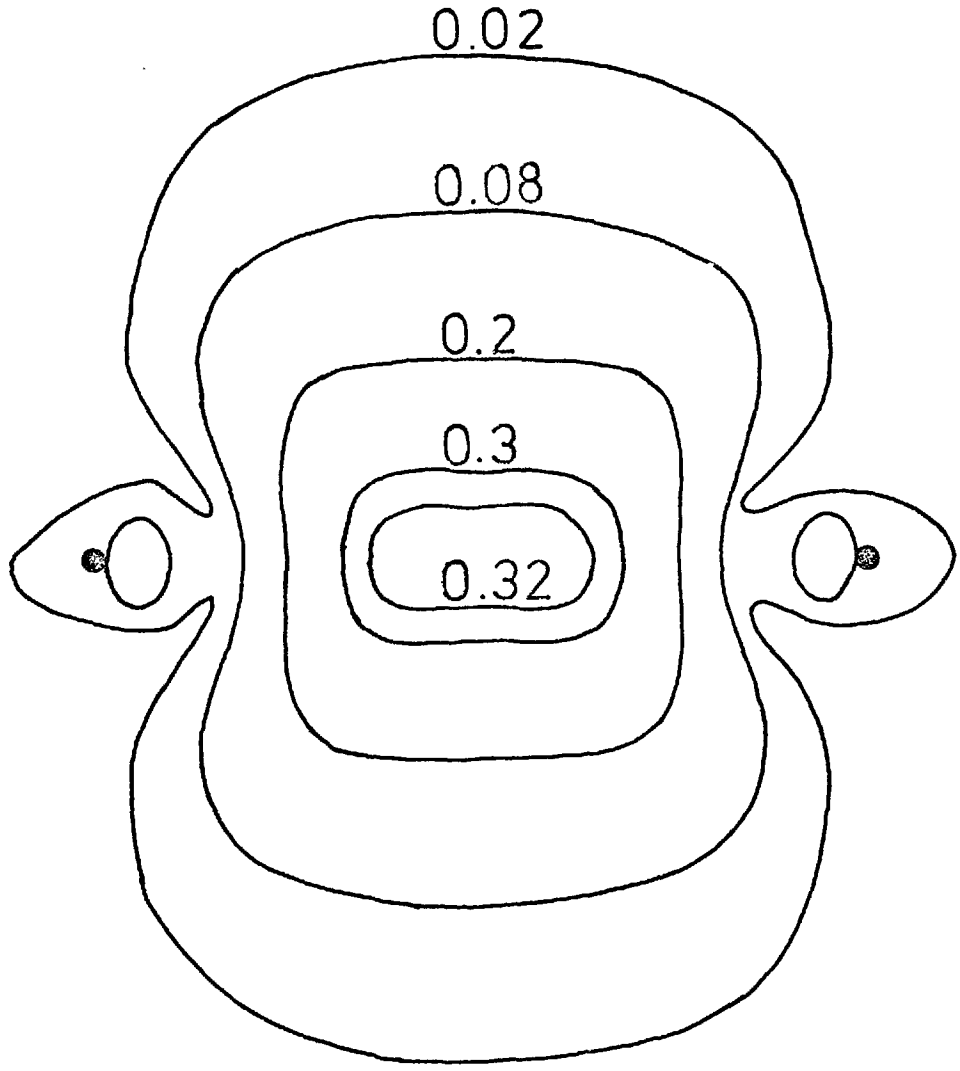

Figure 3.18 : Charge density contours for the directional one-centre terms in the LCAO covalent bond.

$\Phi_+^2(r_1)$ and $\Phi_-^2(r_2)$. It can be seen that there is a significant contribution to the charge in the bonding region.

The remaining contribution to equation (3.39) is the $\psi_{3S}^2(r)$ term which, clearly, is spherical around the atom site. The amount of charge in this spherical distribution is $1/4\,(1 + S) \approx 0.14$ electrons. This value is approximately that for $f_a(0)$ obtained by the extrapolation of $f_a(k)$ extracted from equations (3.27) and (3.36). It thus appears that the harmonic expansion procedure for obtaining $f_a(k)$ and $f_b(k)$ places all of the two valence electrons around the bond centre, except for the charge contained in the ψ_{3S}^2 terms at each end of the bond. However, this result appears to be in good accord with the picture presented by the charge density contours of figures 3.17 and 3.18.

We wish to stress that there is no unique way of extracting expressions for $f_a(k)$ and $f_b(k)$. To make progress we have adopted a method suggested by the LCAO contours for the Si covalent bond (figure 3.12). Because of this lack of uniqueness, the important point for calculating diffraction intensities, is to examine the corresponding bond charge density contours obtained from the superposition of three spherical distributions model. These are shown in figure 3.14 where, as before, we have added $\frac{1}{4}$ of the Si core electrons to each atom participating in the bond. There can be no doubt that our present modelling of the LCAO density, shown in figure 3.12, is a vast improvement on the superposition of spherical atom densities shown in figure 3.13. With the density contours of figure 3.14 plus the structural models discussed in § 3.2 we have a perfectly proper way of modelling the effects of chemical bonding on the X-ray diffraction and electron diffraction intensities.

3.7 Diffraction Intensities for crystalline Si

An important property that we must demand of our model of the electron density distribution is that it will correctly reproduce the X-ray intensities for the

crystalline state. Only then can we move on with confidence to consider the amorphous case. However, we emphasize at the outset that we do not, in any way, claim to compete in sophistication with other specifically crystalline studies (for example, that of Aldred and Hart, 1973).

We can define the X-ray diffraction intensity at the Bragg reflections according to

$$I_x(k) = |S(k)|^2 \qquad 3.40$$

where

$$S(k) = \int_{\underset{\sim}{r}} \sum_{\underset{\sim}{R}_{Atom}} \delta(\underset{\sim}{r} - \underset{\sim}{R}_{Atom}) \exp(i\underset{\sim}{k}.\underset{\sim}{r})\, d\underset{\sim}{r}\, . f_c(k)$$

$$+ \int_{\underset{\sim}{r}} \sum_{\underset{\sim}{R}_{\substack{Bond.\\CENTRE}}} \delta(\underset{\sim}{r} - \underset{\sim}{R}_{\substack{Bond.\\CENTRE}}) \exp(i\underset{\sim}{k}.\underset{\sim}{r})\, d\underset{\sim}{r}\, f_b(k) \qquad 3.41$$

and

$$f_c(k) = 4 f_a(k) + f_{core}(k) \qquad 3.42$$

$f_a(k)$ and $f_b(k)$ are defined by equations (3.27) and (3.36) and $f_{core}(k)$ is the form factor for the Si core electrons.

Here the intensity is normalized to one composition unit over which the summation is taken. The usual basic unit for the diamond lattice contains eight atoms and sixteen bond centres. The relation between $f_c(k)$ and $f_b(k)$ at some of the Bragg reflections are given in Table 3.3, from which it is clear that there is non-uniqueness in the choice of $f_c(k)$ and $f_b(k)$ at other than the (220) and (222) reflections. Nevertheless, as can be seen from table 3.3, the particular choice of $f_c(k)$ and $f_b(k)$ that we have adopted here, does indeed well represent the crystal data.

Table 3.3 : Some observed and calculated Bragg intensities for crystalline silicon

Reflection	$\lvert S(k) \rvert$	Calculated intensity	Observed * intensity
(111)	$4\sqrt{2}(f_c + \sqrt{2} f_b)$	60.66	60.81
(220)	$8 f_c$	68.08	67.84
(311)	$4\sqrt{2}(f_c - \sqrt{2} f_b)$	44.22	44.12
(222)	$16 f_b$	1.28	1.36

* McConnell and Sanger (1970)

Note : the (222) reflection is the so-called forbidden reflection.

The crystalline Bragg reflections provide the first test for our model of the charge density and the results are encouraging. They can also be used to give further indication of the value of $f_b(k)$ (and, of course, $f_a(k)$) as $k \to 0$ and to help clarify whether very different choices of the form factors $f_b(k)$ and $f_a(k)$ are possible.

We divide the normal atomic form factor into core and valence parts and introduce the parameter $\gamma : 0 \leq \gamma \leq 1$ representing that fraction of the 4 Si valence electrons that are located around the atom. Thus we write

$$f_c(k) = f_{core}(k) + \gamma f_{valence}(k) \qquad 3.43$$

The bond form factor as deduced from equation (3.36) is approximately gaussian in shape and therefore we can write

$$f_b(k) = (2 - 2\gamma) \exp(-\beta k^2) \qquad 3.44$$

so that the amount of charge in the bond charge distribution is $(2 - 2\gamma)$ electrons. The superposition of spherical atom-like densities model produces charge contours with a very low value at the bond centre (see figure 3.13), whereas the LCAO density of figure 3.12 has a high value at this point. Therefore we choose our bond charge density $\rho_b(r)$ to reproduce the bond centre value of the LCAO density ρ_0, say, and write

$$\rho_b(r) = \rho_0 \exp(-\alpha r^2) \qquad 3.45$$

The parameter β in equation (3.44) can now be written in terms of ρ_0 and γ since we have from equation (3.45)

$$f_b(k) = \int_0^\infty \rho_b(r)\, 4\pi r^2 \frac{\sin kr}{kr}\, dr \qquad 3.46$$

$$= \rho_0 \left(\frac{\pi}{\alpha}\right)^{3/2} \exp(-k^2/4\alpha) \qquad 3.47$$

and comparing equations (3.44) and (3.47) we have

$$2 - 2\gamma = \rho_o (\pi/\alpha)^{3/2} \qquad 3.48$$

and

$$\beta = 1/4\alpha \qquad 3.49$$

$$= [(2-2\gamma)/\rho_o]^{2/3}/4\pi \qquad 3.50$$

giving

$$f_b(k) = (2-2\gamma)\exp\left(-\frac{k^2}{4\pi}\left(\frac{2-2\gamma}{\rho_o}\right)^{2/3}\right) \qquad 3.51$$

Thus using the relations between $f_c(k)$ and $f_b(k)$ given in Table 3.3 we can now determine the crystalline Bragg reflections in terms of a single parameter γ (since ρ_o is known from the LCAO bond density $\rho(\underset{\sim}{r})$ of equation (3.17)). This parameter γ gives us a direct measure of the amount of charge located in the bond centre distribution.

In Table 3.4 we show the first few Bragg reflections together with the value of γ for which the best agreement is obtained with the experimentally observed intensity.

With the confidence drawn from these, admittedly limited (we are drawing conclusions for only 4 points in k space, the Bragg reflections, and one point in r space, the bond centre) but nevertheless encouraging, results we shall now move on to discuss the amorphous case. The idea behind our method of modelling the bond charge density distribution should now be evident. Our objective has been to develop a way of including the effects of covalent bonding in a calculation of the X ray and electron diffraction intensities for α-Si. This we have now achieved with the extraction of the bond form factor $f_b(k)$. The important point is that we can retain the assumption contained in equation (2.5 b), namely that we can write the

Table 3.4 : Parameter δ for optimum fit to Bragg reflections in silicon

Reflection	$\lvert S(k) \rvert$	δ
(111)	$4\sqrt{2}(f_c + \sqrt{2}f_b)$	0.2
(220)	$8f_c$	0.1
(311)	$4\sqrt{2}(f_c - \sqrt{2}f_b)$	0.22
(222)	$16f_b$	0.08

total electron density in α-Si as a sum of spherical distributions. The necessary complication, produced by our approach, is that, from the point of view of X-ray and electron diffraction, we must treat α-Si as a two component system; these two components being the spherical charge distribution at each bond centre and the spherical distribution on each nucleus.

3.8 X-ray and Electron Diffraction Formalism for the covalent Bonding Model

The required equations for the calculation of X-ray and electron diffraction intensities from α-Si, as a two component system, can easily be obtained from the formalism of Chapter 2. We need to interpret equations 2.16 and 2.18 in terms of our two components, the charge on the atom and the charge at the bond centre. We thus need to know, in addition to the nuclear-nuclear correlation function g(r), those of the nuclear-bond centre $g_{nb}(r)$, say, and bond centre-bond centre $g_{bb}(r)$. The basic unit for the summations of equation (2.18) contains one Si atom and two bond centres. Thus the X-ray intensity is given by

$$I_x(k) = f_c^2(k)S(k) + 2f_b^2(k)S_{bb}(k) + 2f_c(k)f_b(k)[S_{nb}(k)-1] \qquad 3.52$$

(normalized to one basic unit), where the $S_{ij}(k)$ are related to the correlation functions $g_{ij}(r)$ by equation (2.17a). Clearly, equation (3.52) reduces to equation (2.20) in the limiting case when

a) We have no charge at the bond centre, i.e. $f_b(k) = 0$, and

b) $f_c(k) = f_{atomic}(k)$, the free atom form factor. Similarly, the electron diffraction intensity is given by

$$I_e(k) = K^{-4}\{[Z - f_c(k)]^2 S(k) + 2f_b^2(k)S_{bb}(k) - 2[S_{nb}(k)-1][Z-f_c(k)]f_b(k)\} \qquad 3.53$$

and again putting $f_b(k) = 0$ and $f_c(k) = f_{atomic}(k)$ we regain equations (2.20) and (2.22). Equations (3.52) and (3.53) are our basic formalism for modelling the diffraction intensities from α-Si to allow for the effects of chemical bonding.

Given the coordinates for the structural models described in § 3.2, the same procedure as outlined in § 3.3, for obtaining the nuclear-nuclear correlation function g(r), has been used to determine the other correlation functions and hence the partial structure factors $S_{nb}(k)$ and $S_{bb}(k)$. $S_{nb}(k)$ and $S_{bb}(k)$ (curves 2 and 3 respectively in each case) are shown in figures (3.2), (3.3) and (3.4) for models CT 1, 2, 3 respectively, figure (3.5) for the Steinhardt model and figure (3.6) for the PT model.

Using these model partial structure factors together with the form factors $f_a(k)$ and $f_b(k)$ we have calculated the X-ray and electron diffraction intensities for each model using equations (3.52) and (3.53).

3.9 X-ray diffraction

3.9.1 CRN models

In § 3.3 and § 3.4, we saw in figures 3.2 to 3.6 and 3.8 that the best agreement between model and experimental S(k) functions at, high k ($> 4\,A^{-1}$), was obtained for the CT3 model. Since the scattering at high k arises from the Si core electrons, our interpretation was that the CT3 model provides our best available structural model.

Proceeding on this context we have first calculated the X-ray diffraction intensity for the CT3 model. The three contributions to equation (3.52) from nuclear-nuclear, nuclear-bond centre and bond centre-bond centre correlations, curves 1, 2 and 3 respectively, together with the total intensity, curve 4, and the experimental intensity, (Richter and Breitling, 1958), curve 5, are shown in figure

3.19. It can be seen that now, with the inclusion of the bond charge model, theoretical and experimental intensities are in very good agreement for all k. At the first peak, the nuclear-bond centre correlations contribute about 20% of the peak height but give a small negative contribution at the second peak. The bond centre - bond centre correlations give a much smaller contribution to the first peak ($\sim$ 5%) and a negligible contribution at the second peak.

In figure 3.20 curves 1, 2 and 3 we show the total X-ray intensity for models CT 1, 2 and 3 respectively. This picture shows the effects on the diffraction intensity as the topology of the network is gradually altered. It is evident that the diffraction intensity is quite a sensitive test of the network topology (or more correctly, since the intensity represents average structural information, of the ring statistics). Agreement between theory and experiment at all k is improved as the number of odd membered rings increases. This can clearly be seen by referring to figure 3.19 where agreement between theory and experiment is indeed good. Finally, the CT 1 model predicts a small peak at $k \sim 4.5\ A^{-1}$ which is not seen in experiment. This feature disappears as the number of odd membered rings increases.

For the Steinhardt model, the three contributions from equation (3.52) together with the total intensity and the experimental intensity (Richter and Breitling, 1958) are shown in figure 3.21. The labelling is as in figure 3.19. Agreement with experiment, for all k, is not as good as that given by the CT 3 model. The Steinhardt model does not predict the correct height of either of the first two peaks and gives a peak at $k \sim 7A^{-1}$, where a shoulder is observed experimentally.

3.9.2 PT model

The three contributions from equation (3.52), together with the total intensity and the experimental intensity (Richter and Breitling, 1958) are shown in

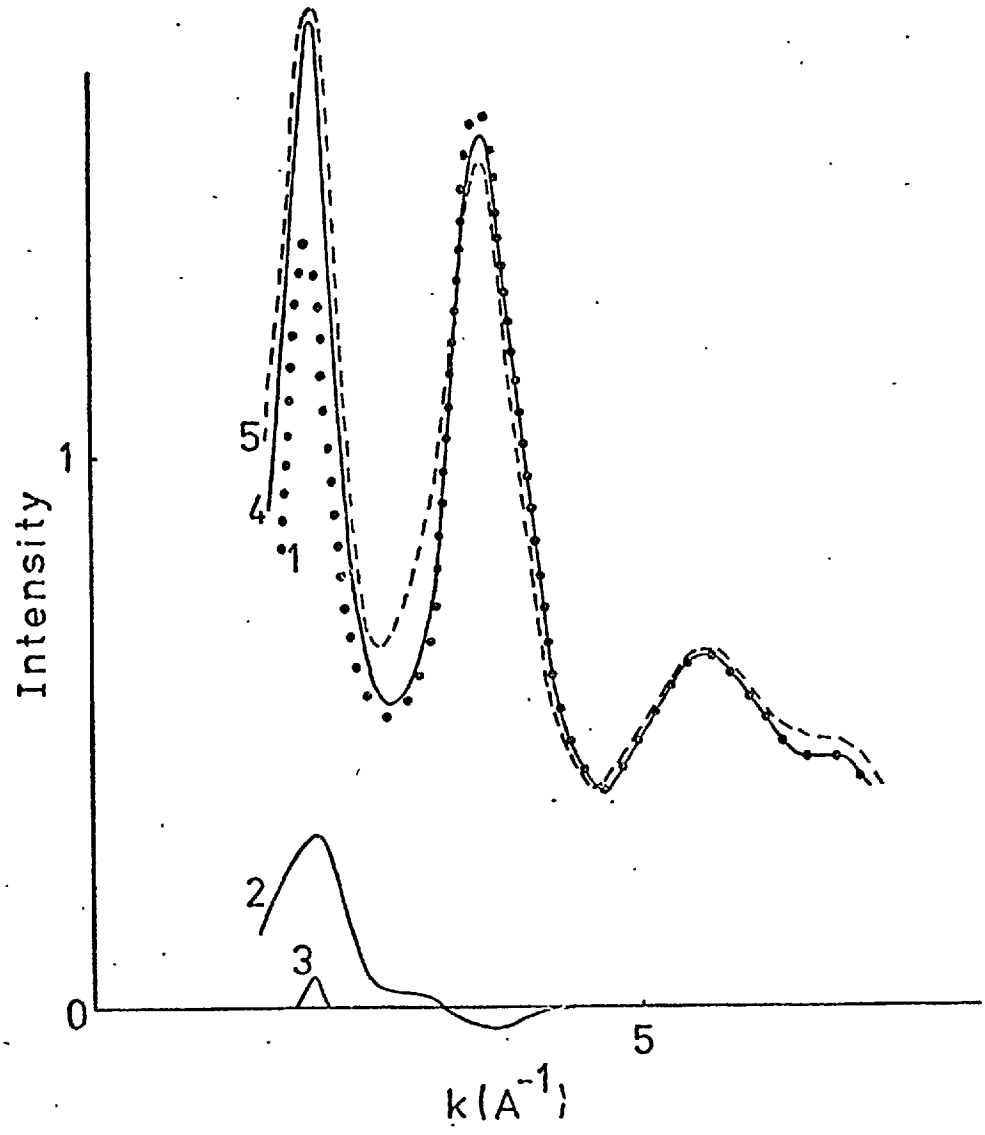

Figure 3.19 : The X-ray scattering intensity for silicon for the CT3 model.

1. Contribution from Si-Si correlations
2. Contribution from Si-bond centre correlations
3. Contribution from bond centre-bond centre correlations
4. Total intensity
5. Experimental intensity

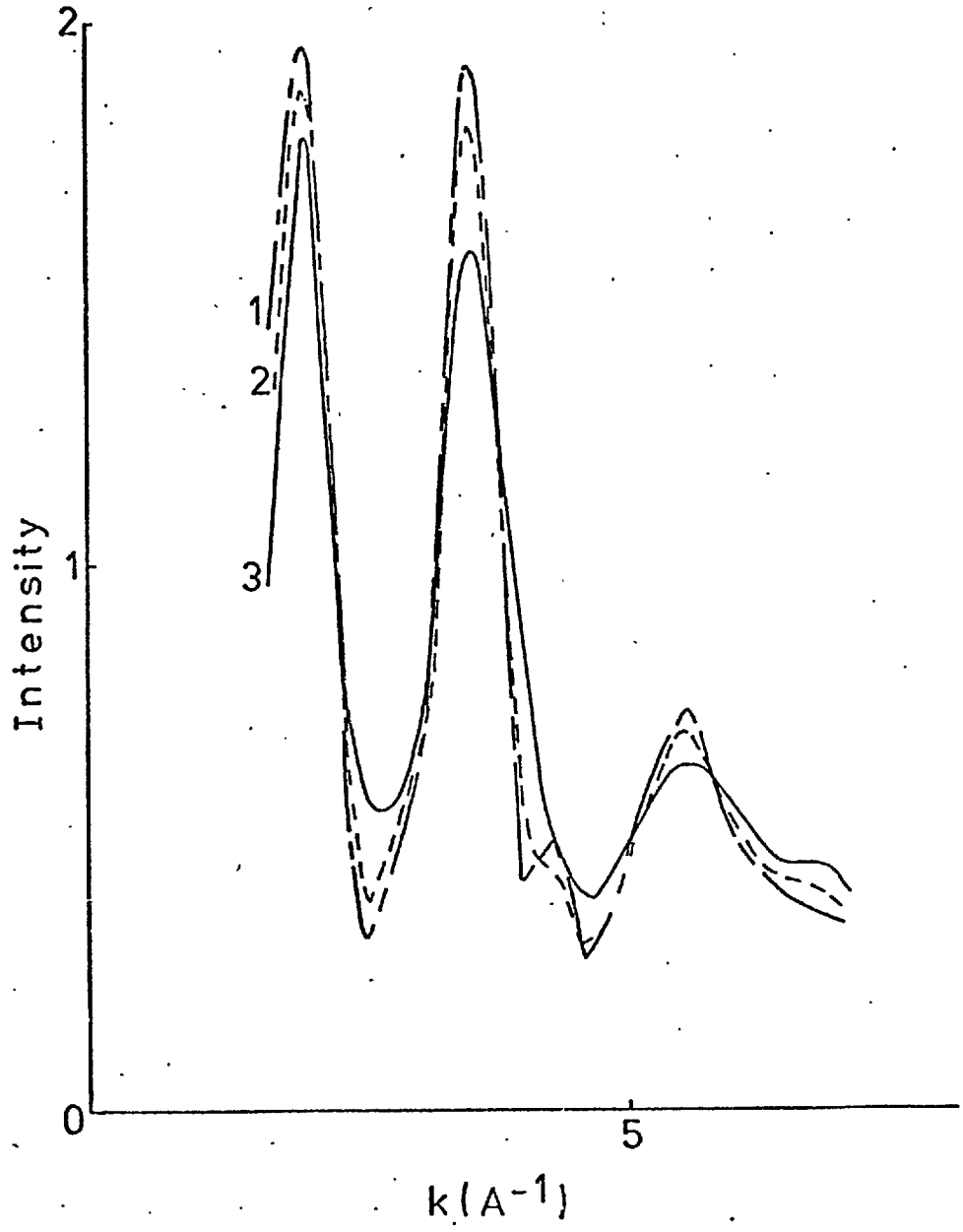

Figure 3.20 : Effect of odd membered rings on the theoretical X-ray intensity.

1. CT1 model
2. CT2 model
3. CT3 model

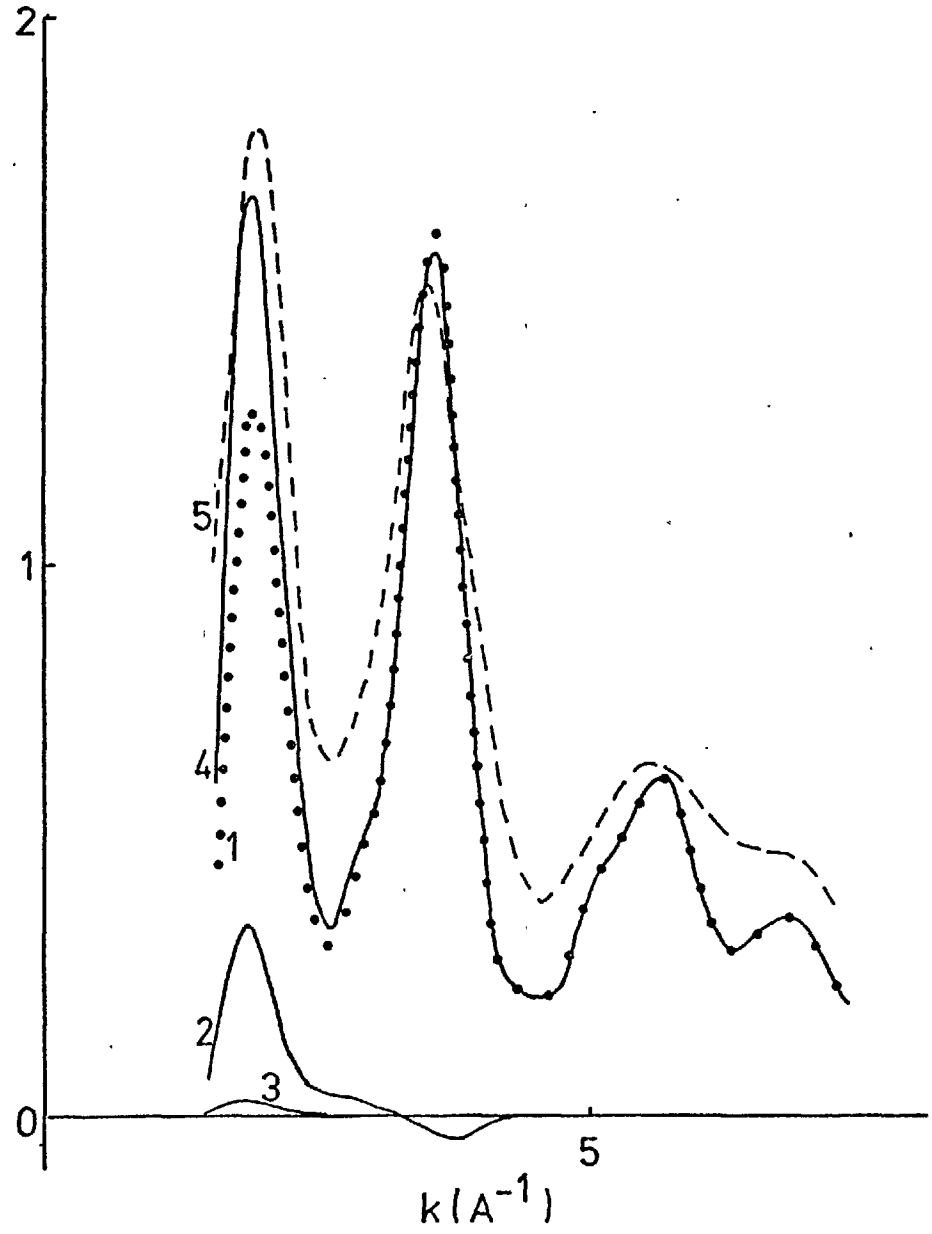

Figure 3.21 : The X-ray scattering intensity for silicon for the Steinhardt model.

1. Contribution from Si-Si correlations
2. Contribution from Si-bond centre correlations
3. Contribution from bond centre-bond centre correlations
4. Total intensity
5. Experimental intensity

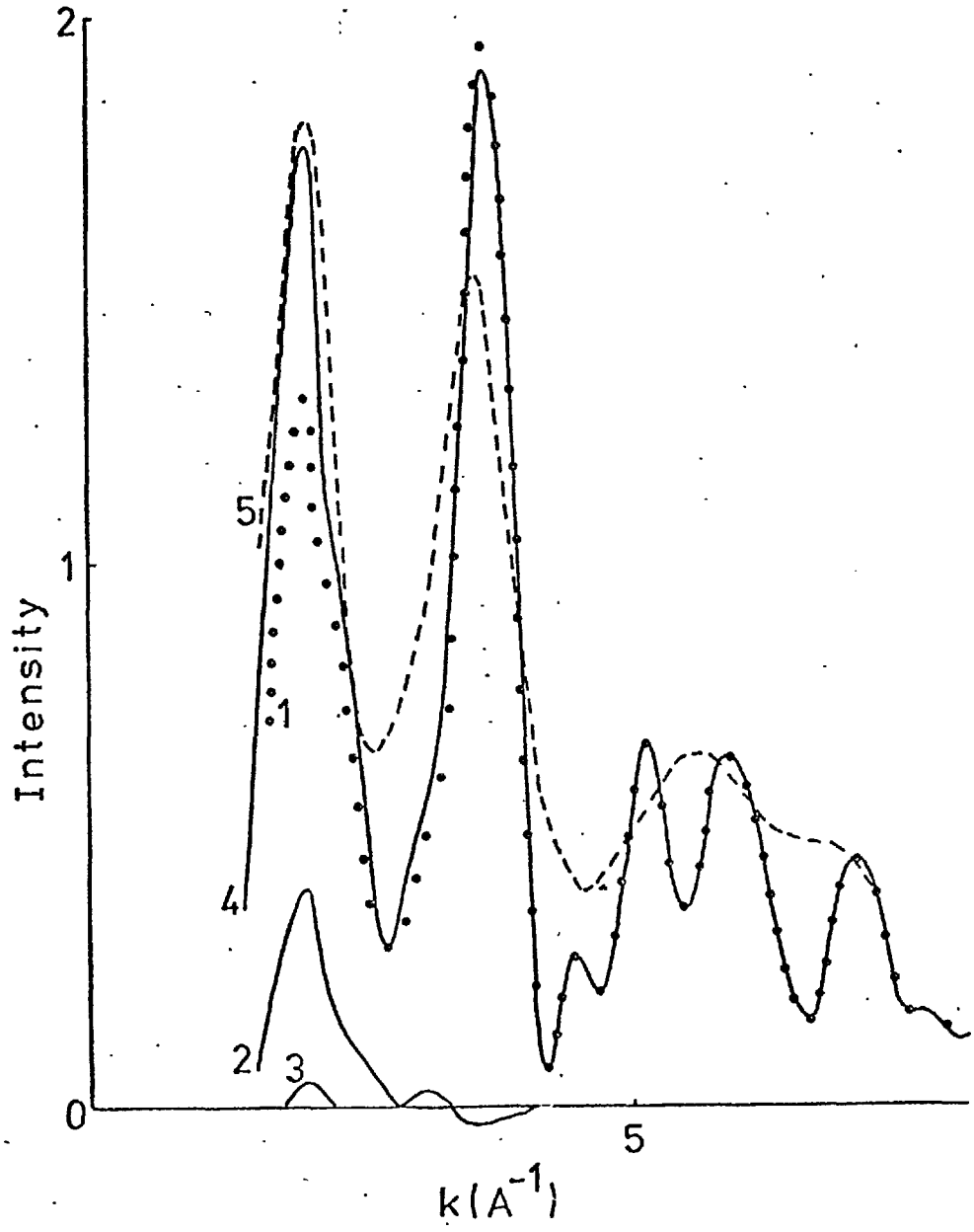

Figure 3.22 : The X-ray scattering intensity for silicon for the PT model.

1. Contribution from Si-Si correlations
2. Contribution from Si-bond centre correlations
3. Contribution from bond centre-bond centre correlations
4. Total intensity
5. Experimental intensity

figure 3.22. The labelling is as in figure 3.19. The PT model correctly predicts the height of the first experimental peak at k = 1.8 A^{-1} and the nuclear - bond centre correlations contribute about 25% of this peak height. At the second peak the model badly overestimates the peak height. This behaviour can clearly be established as a structural effect since the bond charge correlations give only a small negative contribution to this peak. Beyond 4 A^{-1} the PT model shows too much structure, the broad experimental peak at k $\sim$ 5.6 A^{-1}, for example, being split into two peaks corresponding approximately to crystalline Si Bragg reflections (331) and (422). As was similarly found for the CT 1 model, a small peak is observed at k = 4.6 A^{-1} which coincides with the position of the (400) reflection of crystalline Si.

3.10 Electron diffraction

The three contributions from equation (3.53) together with the total intensity and the experimental intensity (Moss and Graczyk, 1969) are shown in figures (3.23), (3.24) and (3.25) for the CT3, Steinhardt and PT models respectively. The labelling is the same as in figure (3.19) with the experimental electron data replacing that of X-rays as curve 5. Generally the remarks made about each model with regard to X-rays also apply in this case.

However, one interesting point is that although both the CT3 and PT models predict the correct height for the first peak of the X-ray intensity, only the CT 3 model does for the same peak in the electron diffraction intensity. The reason for this is that the relative contributions of the nuclear-nuclear and nuclear-bond centre correlations to the total X-ray intensity at the first peak, for the CT3 and PT models, are different. This means (since the bond centre - bond centre correlations give a small contribution) that either the CT3 or the PT model (or both) must predict the wrong intensity for the first peak in the electron case.

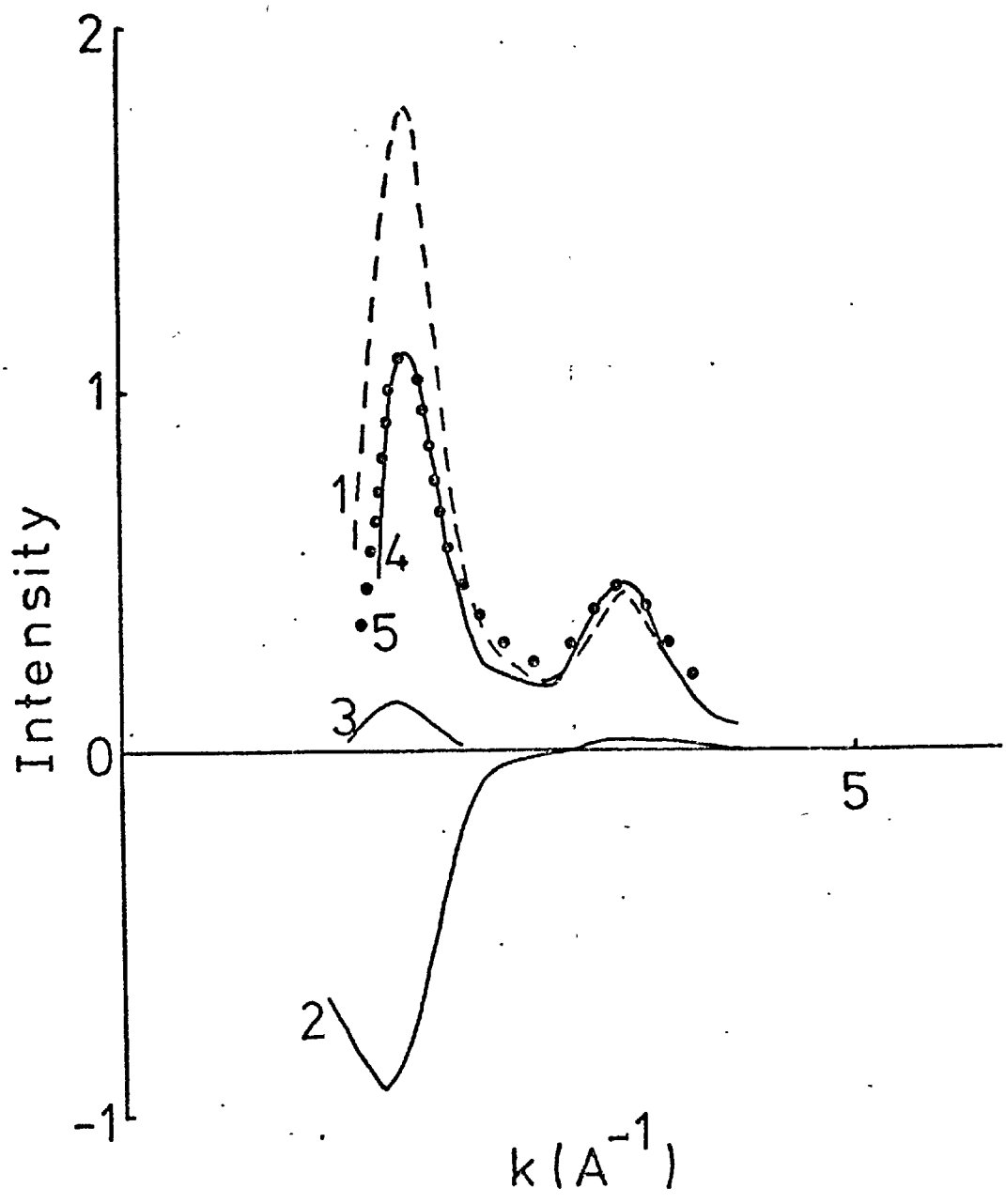

Figure 3.23 : Electron scattering intensity for silicon for the CT3 model.

1. Contribution from Si-Si correlations
2. Contribution from Si-bond centre correlations
3. Contribution from bond centre-bond centre correlations
4. Total intensity
5. Experimental intensity

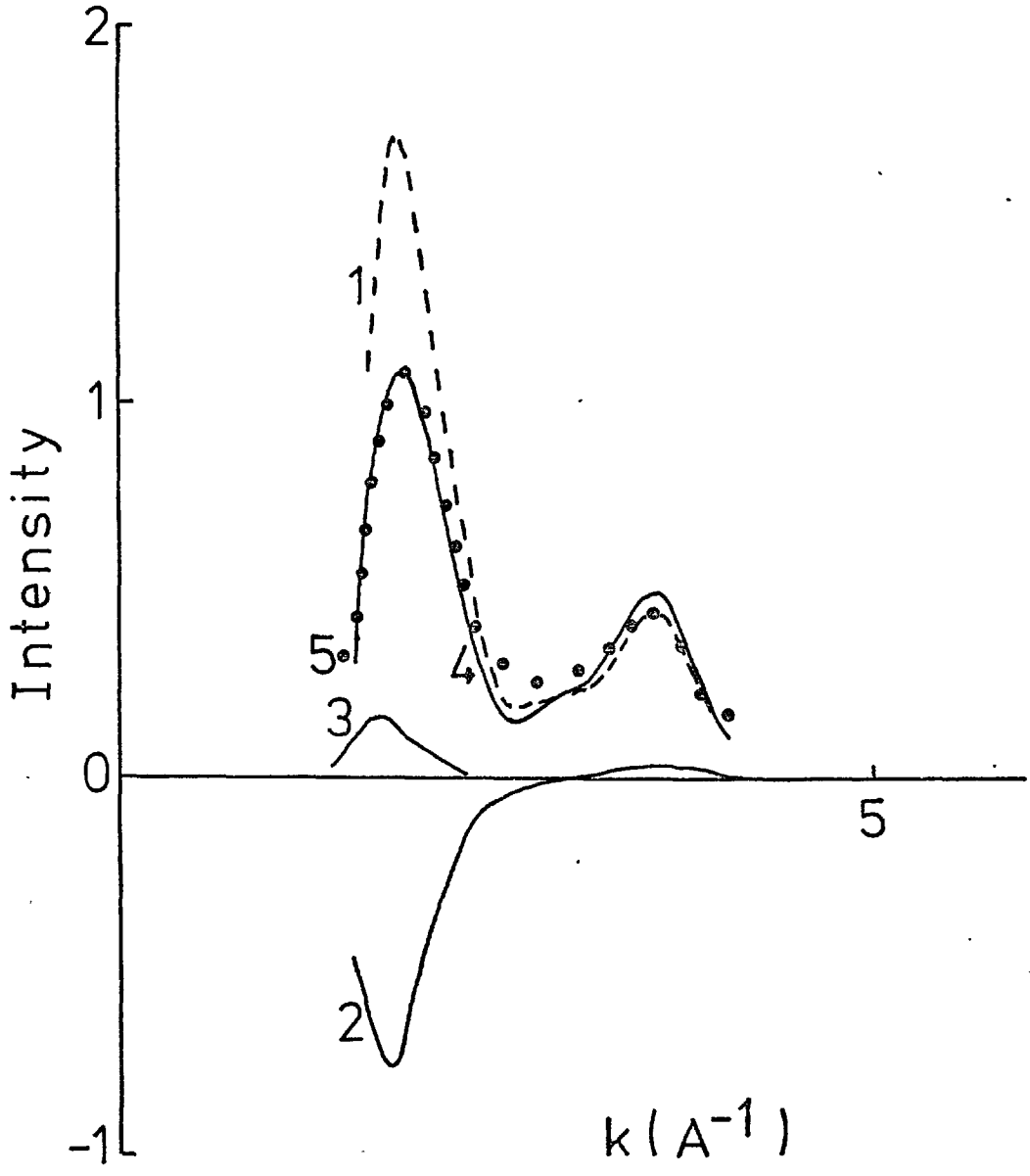

Figure 3.24 : Electron scattering intensity for silicon for the Steinhardt model.

1. Contribution from Si-Si correlations
2. Contribution from Si-bond centre correlations
3. Contribution from bond centre-bond centre correlations
4. Total intensity
5. Experimental intensity

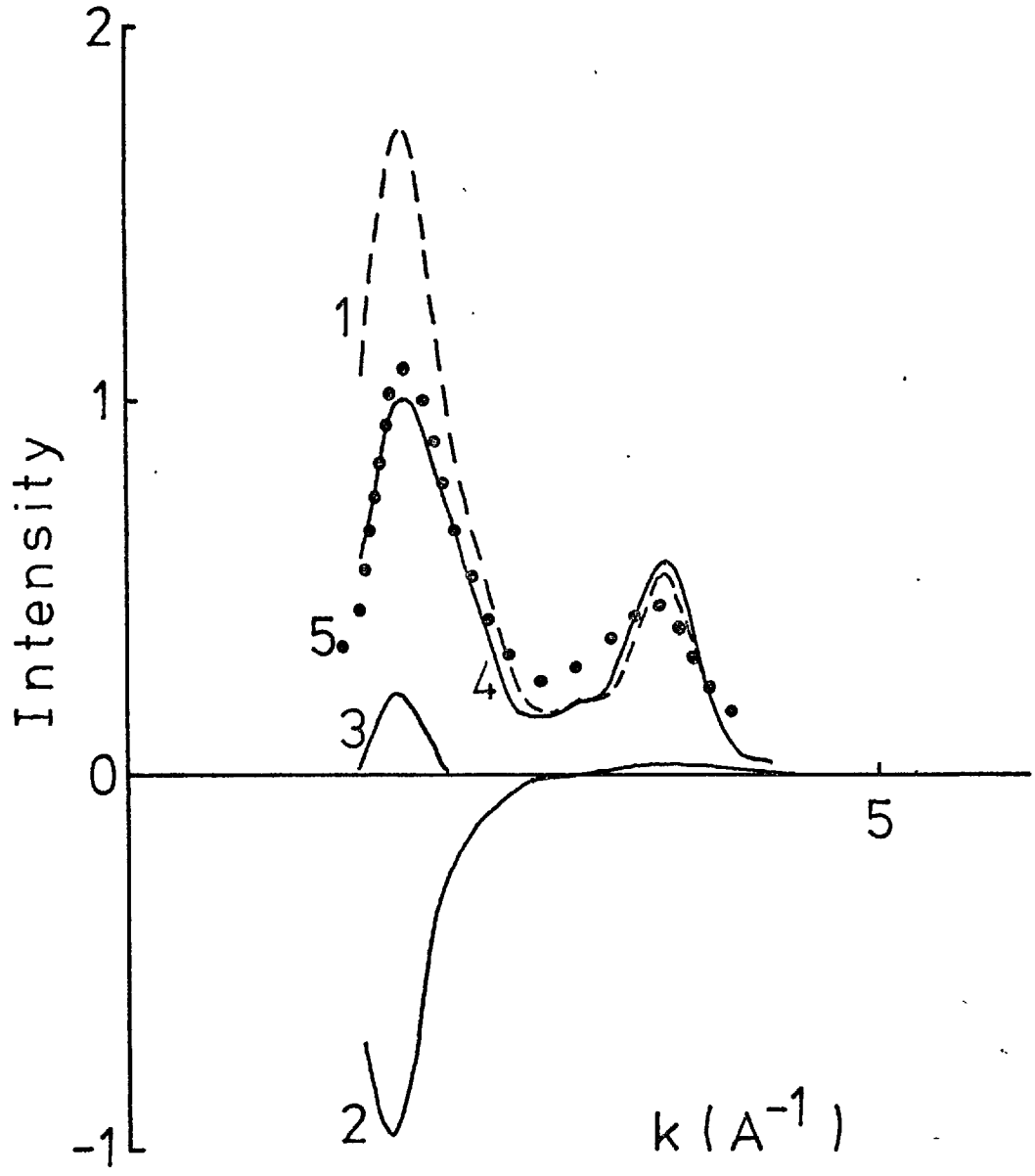

Figure 3.25 : Electron scattering intensity for silicon for the PT model.

1. Coniribution from Si-Si correlations
2. Contribution from Si-bond centre correlations
3. Contribution from bond centre-bond centre correlations
4. Total intensity
5. Experimental intensity

3.11 Discussion

The results of our calculations favour overwhelmingly the CRN model of Connell and Temkin as modified by Beeman and Bobbs to include odd membered rings (the CT3 model). However, the original CRN model containing only even membered rings does not produce significantly better agreement with experiment than was obtained for the PT model . There is thus some scope for improvement of a model based on ordered units, using the same procedure as adopted for the original Connell-Temkin model (Beeman and Bobbs, 1975).

Our work has also demonstrated that chemical bonding effects are important at the first peak in α-Si, the agreement between theory and experiment being now fully qualitative. We would like to reiterate that conclusions about structure can be made based on a comparison of the model and experimental S(k) functions for $k > 4\,A^{-1}$. For low k, however, it is necessary to examine the total intensity. Also, without the neutron experiment, it is necessary to examine both X-ray and electron intensities.

CHAPTER FOUR

AMORPHOUS CARBON

4.1 Introduction

An obvious extension to the work on amorphous silicon, discussed in Chapter 3, is an investigation of the scattering properties of amorphous carbon. Carbon, in the chemist's picture, has an essentially equivalent valence electron structure to silicon and is known to participate in covalent bonding.

Amorphous carbons can be produced by a variety of methods (for a review, see Yamada, 1968) and have many applications, possessing low density and high mechanical strength. However, the properties of a particular sample of amorphous carbon depend on how it was prepared and on its thermal history.

Thus the term amorphous carbon does not define a unique structure as is believed to be the case for α-Si, but rather a class of related structures. The term amorphous is also slightly misleading in the case of carbon because it was established at an early stage (Warren, 1934, Franklin, 1950) that non-crystalline carbons do contain regions (sometimes large) that have a crystalline nature (if only two dimensional). At the outset, then, it is believed that the structure of amorphous carbons can be explained on the basis of the micro-crystallite picture.

Carbon has two crystalline forms, diamond and graphite, the latter being the stable form under normal conditions, and analogues to both are believed to exist in the amorphous state. Thus an amorphous carbon may contain both trigonally and tetrahedrally coordinated carbon atoms, in graphite and diamond-like regions respectively.

Following our work on α-Si, our emphasis here will again be on the

interpretation of X-ray and electron diffraction intensities in terms of the electron density in the amorphous state. We shall need to consider covalent bonds in both diamond and graphite and thus both sp^3 and sp^2 hybridisation of the carbon valence electrons. Clearly, however, both forms of bonding can be treated equally well within the theoretical framework of the bond charge model developed for α-Si.

Finally, the ratio of core/valence electrons in carbon is lower than for silicon. Thus we expect the effects of covalent bonding to be more evident in the X-ray and electron diffraction intensities from amorphous carbons than from α-Si.

4.2 The Structure of Amorphous Carbons

Amorphous carbons have been subjected to extensive investigation by X-ray diffraction and to a lesser extent by electron and neutron diffraction. As long ago as 1934 X-ray investigations and subsequent r space analysis via fourier transform (Warren, 1934) indicated that carbon blacks, the so called 'glassy carbons' formed by the thermal degradation of organic polymers, contained interatomic distances approximately the same as those found in crystalline graphite. However, the diffraction pattern could not be explained simply in terms of microcrystalline graphite.

The theory of random layer lattices was developed (Warren, 1941) and it was demonstrated that the X-ray diffraction patterns from carbon blacks were approximately explainable in terms of such lattices. The structure was envisaged as groups of graphite-like planes arranged parallel to one another at about the graphite inter-plane spacing but with random orientation about the inter plane normal. The diffraction pattern from such a random layer lattice contains two

types of reflection; namely, two dimensional (h k 0) reflections arising from the hexagonal structure within a layer and one dimensional (00 l) reflections arising from the parallel stacking of layers. Due to the random orientation of the layers the diffraction pattern contains no three dimensional (h k l) reflections as would be found in the usual crystalline graphite structure.

We shall refer to the random layer lattices, in this work, as the 'micro-crystallite' domains. Warren's random layer lattice equations were based on these microcrystallites being distributed with random orientation and embedded in a matrix of carbon in a less ordered state. The atoms in this disordered carbon were assumed to scatter independently, giving a gaseous like background to the total observed diffraction intensity.

Subsequent studies of similar non-crystalline carbons were based on the interpretation of the structure in terms of random layer microcrystallites. From Warren's theory the average layer dimension, L_a, could be determined from the profile of the two dimensional reflections. The stacked layer height, L_c, and the interplane spacing could be determined from the profile and position (on the k axis), respectively, of the one dimensional reflections, in particular from the prominent (002) reflection.

It was later found necessary (Franklin, 1951) to distinguish between two types of non crystalline carbon. The random layer type of carbon as studied by Warren was labelled a non-graphitic carbon. Certain of these non-graphitic carbons (referred to as soft-carbons) were found (Franklin, 1951) to show a gradual change from the random layer structure towards the ordered structure of graphite when heated to sufficiently high temperature. This could be recognized

in the diffraction pattern by the appearance of the three dimensional (h k 0) reflections of graphite. The size of the microcrystallite regions was found to depend on the temperature of heat treatment (Franklin, 1951 a) and by varying this temperature Franklin was able to prepare a continous series of structures intermediate between the non-graphitic carbon and crystalline graphite. These intermediate states contained a mixture of orientated and disorientated layers and were, rather confusingly, labelled graphitic carbons. However, certain non-graphitic carbons were also found (Franklin, 1951 a) that could only be graphitized, if at all, by heat treatment to very high temperatures. These so called hard carbons appeared to be those non-graphitic carbons having micro-crystallite regions with a small layer dimension L_a. This agreed with the observation (Franklin, 1951 a) that, for the soft carbons, graphitization would not occur until the layer dimension L_a attained a size of approximately 80 - 100 Å.

It was recognized at an early stage (Franklin, 1950) that the nature and extent of the disorganized carbon was of great significance for understanding the different behaviour of hard and soft carbons upon heat treatment. It was also remarked (Ergun and Tiensuu, 1959) that the hardness, density and non-graphitizability of the soft carbons did not appear to be compatible with an entirely graphite-like structure. The emphasis of Warren's work had been on the interpretation of X-ray diffraction patterns from carbon blacks in terms of the hexagonal layer structure. This was because the diffuse (h k 0) and (0 0 l) reflections observed for the carbon blacks corresponded approximately to the (002), (100) and (110) reflections of graphite. However, it was pointed out (Ergun and Tiensuu, 1959) that for the small layer soft carbons the observed one dimensional reflections were weak (Franklin, 1951 a) and that the diffuse, supposedly two dimensional reflections could be interpreted on the basis of other crystalline forms of carbon. The

calculated intensity (Ergun and Tiensuu, 1959) for a diamond cubic lattice gave diffraction peaks corresponding to the positions of the (100) and (110) peaks of graphite. Of course the presence of the one dimensional (0 0 l) reflections in the experimentally observed intensities indicated that layered structure was definitely present but the question raised by Ergun and Tiensuu's work was, if significant amounts of, say, diamond structure were present would it be detectable in the diffraction intensity. Of course, this picture of amorphous carbons containing two distinct types of structure fitted in with the earlier proposed model (Warren, 1941) if one associated the second structure with the disorganized carbon matrix. The difficulty was to do so without implying too much correlation between atoms in different microcrystallites.

The electron diffraction study of an α-C thin film prepared by vacuum evaporation (Kakinoki et al, 1960 a) gave strong support to the model suggested above (Ergun and Tiensuu, 1959). The radial distribution function, g(r) obtained from the diffraction intensity (equations (2.17 c), (2.20) and (2.22)) had a broad nearest neighbour peak midway between the graphite nearest neighbour distance of 1.42 Å and the diamond distance of 1.54 Å. The existence of two atomic distances in the sample was further demonstrated by a k space comparison between theoretical and experimental intensities (Kakinoki et al, 1960). It was found that if two nearest neighbour and two next nearest neighbour distances, corresponding to those in diamond and graphite, were included in the Debye intensity equation (equation (2.11)) then the calculated and experimental intensities were in phase at high k. If only the graphite or diamond distances were used then theory and experiment were out of phase at large k. Consequently a structural model was proposed (Kakinoki et al, 1960) in which the random

layer microcrystallites were linked together by a tetrahedral random network of carbon atoms of the form that we have used for the modelling of α-Si. The use of a random network as opposed to diamond crystal removed the problem of introducting too much correlation between microcrystals. Clearly though one has to be careful about drawing conclusions for the structure of the carbon blacks based on this study of an amorphous carbon obtained by vacuum evaporation. The layer dimension for the vacuum evaporated carbon was estimated (Kakinoki et al (1960)) to be approximately 10 Å. It was thus surprising in view of the work on the relationship between layer size and graphitization (Franklin, 1951 a), that the vapour deposited sample was subsequently found to graphitize easily at a 'low' temperature ($\sim$ 1000°C) (Kakinoki, 1960 a).

Support for the structural model proposed by Kakinoki came from an X-ray diffraction study of glassy carbons prepared from an organic polymer over a range of temperatures (Noda et al, 1964). The fourier transformed diffraction data was consistent with the presence of two interatomic distances in the amorphous samples. However, no diffraction peaks were detected that corresponded to structures other than the layered microcrystallites. The samples proved very difficult to graphitize even when heat treated to $\sim$ 3000°C.

A more recent study of a glassy carbon heat treated at $\sim$ 2000°C (Mildner and Carpenter, 1974) indicated no evidence for diamond like tetrahedral bonding except perhaps in very thin layers linking large ($L_a \sim$ 50 Å, $L_c \sim$ 40 Å) random layer microcrystallites.

Thus to summarize : amorphous carbons prepared at low temperatures from organic polymers (Franklin, 1950, Noda et al, 1964) and carbons prepared from the vapour at low temperatures (Kakinoki et al, 1960) both show evidence

for diamond-like structure as well as small layer microcrystallites of the sort proposed by Warren. For samples prepared at high temperature (Mildner and Carpenter, 1974) or heat treated samples (Kakinoki et al, 1960 a) evidence for diamond-like structure is small and the hexagonal layers are much more developed. Apparently, similar carbons prepared by different methods (Kakinoki et al, 1960 , Noda et al, 1964) have very different graphitization properties upon heat treatment.

Following the suggestion of Kakinoki, it is clearly of interest to calculate the diffraction intensities from a model amorphous carbon containing random layer microcrystallites linked by a tetrahedral random network. This model can be applied to all the carbons discussed above (except the graphitic carbons) if we allow the amount of random network and the microcrystallite dimensions to be variables of the model. We shall, however, restrict ourselves to considering random layer carbon experiments where there is clear evidence for the two distinct carbon structures. It has been shown for a large layer glassy carbon (Ergun, 1973) that if strain broadening of the diffraction peaks is correctly accounted for, the theory of random layer lattices gives a good description of the experimental intensity.

4.3 The nuclear-nuclear correlation function

In order to study the effects of covalent bonding on the X-ray and electron diffraction intensities of amorphous carbons, we shall, as we did for silicon, describe the covalent bond in terms of two identical spherical charge distributions on the carbon atoms participating in the bond and a different spherical charge distribution at the bond centre. To calculate diffraction intensities using this electron density model, we shall again require the structural characterization

provided by model partial structure factors. From the discussion of § 4.2, it is evident that the structural problems presented by amorphous carbons are much greater than those for α -Si. The construction of a model of α -C of the kind used for α -Si is not a fruitful approach since such a model could only be applied to one α -C sample. We require a more general structural approach that could be used to analyse several sets of experimental data.

We shall begin by obtaining an expression for the nuclear-nuclear correlation function for a model amorphous carbon sample containing two distinct types of amorphous structure. We assume that the two structural regions to be considered, the microcrystallite and random network, are well defined and consequently that the nuclear-nuclear correlation functions $g^m(r)$ and $g^R(r)$ for an infinite extent of the microcrystallite and random network regions, respectively, are known. (Hereinafter we shall use the superscript m to denote quantities associated with the microcrystallite regions and the superscript R to denote those associated with the random network). A schematic representation of the proposed model structure is shown in figure 4.1. The microcrystallite domains are considered as identical perfect rectangular parallelepipeds with dimensions γ, β, δ.

We first of all imagine that we are 'sitting' on an atom in the microcrystallite region. The correlation with another atom in the same microcrystallite will be given simply in terms of $g^m(r)$. The correlation with an atom outside the microcrystallite, however, will be a combination of $g^m(r)$ and $g^R(r)$. We thus need to know, for an atom in a microcrystallite domain, what the probability is that an atom separated from the first by a distance between r and r + dr lies within the same domain. This can be determined in the following way (Bell, 1968). Consider

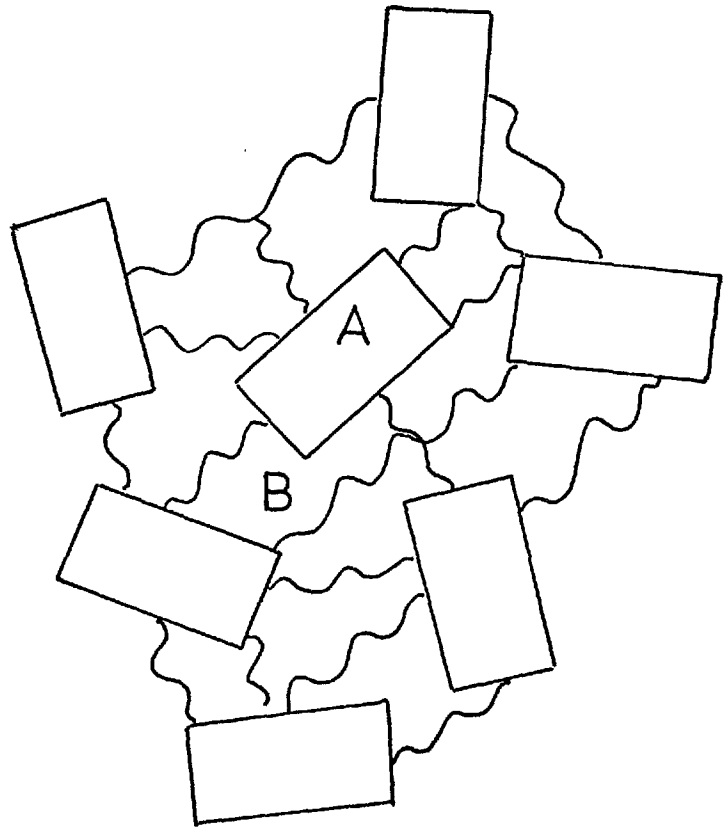

Figure 4.1 : Schematic representation of proposed model structure for amorphous carbons

A. Microcrystallite region

B. Random network region

a rectangular parallelepiped bounded by the pairs of parallel planes

$$\begin{aligned} x &= \pm \gamma/2 \\ y &= \pm \beta/2 \\ z &= \pm \delta/2 \end{aligned} \qquad 4.1$$

and containing particles distributed randomly with unit density. The probability of finding a particle in a volume element d x dy dz containing the point (x, y, z) is

$$f(x,\gamma)\, f(y,\beta)\, f(z,\delta)\, dx\, dy\, dz$$

where

$$\begin{aligned} f(x,\gamma) &= 1 \qquad |x| \leq \gamma/2 \\ &= 0 \qquad |x| > \gamma/2 \end{aligned} \qquad 4.2$$

The probability of finding a second particle separated from the first by a distance in the range r to r + dr is then

$$dx\, dy\, dz\, dr \int_S ds \left[f(x,\gamma) f(y,\beta) f(z,\delta) \times \right.$$

$$\left. \times\ f(x+\lambda,\gamma) f(y+\mu,\beta) f(z+\nu,\delta) \right]$$

where S is the surface

$$\lambda^2 + \mu^2 + \nu^2 = r^2 \qquad 4.3$$

We can now define the average pair distribution function $G_{\gamma\beta\delta}(r)$ by writing the average number of pairs of particles (counting each pair twice) separated by distances in the range r to r + dr as

$$\gamma\beta\delta\, G_{\gamma\beta\delta}(r)\,dr = \int dx\,dy\,dz \Big[\int_S ds\, f(x,\gamma) f(y,\beta) f(z,\delta) \times$$

$$\times\ f(x+\lambda,\gamma) f(y+\mu,\beta) f(z+\nu,\delta)\Big] dr \qquad 4.4$$

Equation (4.4) can be written in terms of $G_{\gamma\beta\delta}(r)$

$$G_{\gamma\beta\delta}(r) = \int_S ds\, \chi(\lambda,\gamma)\chi(\mu,\beta)\chi(\nu,\delta) \qquad 4.5$$

where

$$\chi(\lambda,\gamma) = \frac{1}{\gamma}\int_{-\infty}^{\infty} f(x,\gamma) f(x+\lambda,\gamma)\, dx$$

$$= 1 - |\lambda/\gamma| \qquad |\lambda| \leq \gamma$$

$$= 0 \qquad \text{otherwise} \qquad 4.6$$

For $r \leq \gamma, \beta, \delta$ 4.7

integrating equation (4.5) gives

$$G_{\gamma\beta\delta}(r) = 4\pi r^2 \Big\{ 1 + \frac{1}{\beta\gamma\delta}\Big[-\frac{r}{2}(\gamma\beta + \beta\delta + \delta\gamma)$$

$$+ \frac{2r^2}{3\pi}(\gamma+\beta+\delta) - \frac{r^3}{4\pi}\Big]\Big\} \qquad 4.8$$

and for

$$r \geq \gamma^2 + \beta^2 + \delta^2 \qquad 4.9$$

the integrand of equation (4.5) vanishes over S and $G_{\gamma\beta\delta}(r)$ is zero. This result expresses the fact that no two particles can be further apart than the diagonal of the box. For values of r in between those given by equations (4.7) and (4.9) the evaluation of the integral in equation (4.5) is most easily

achieved by numerical methods. For an infinite rectangle the number of atoms separated by a distance r to r + dr is just

$$G_{\infty}(r) = 4\pi r^2 \qquad 4.10$$

and thus our required probability is just (compare the derivation of $\mathcal{E}(r)$, the spherical model size correction factor in § 3.3)

$$\mathcal{E}_{\gamma\beta\delta}(r) = G_{\gamma\beta\delta}(r) / G_{\infty}(r) \qquad 4.11$$

Thus we write the nuclear-nuclear correlation function $g^1(r)$ for an atom in a microcrystallite region as

$$g^1(r) = \mathcal{E}_{\gamma\beta\delta}(r)\, g^m(r) + \left(1 - \mathcal{E}_{\gamma\beta\delta}(r)\right) g^R(r) \qquad 4.12$$

Obviously $\left(1 - \mathcal{E}_{\gamma\beta\delta}(r)\right)$ is the probability that the atom referred to lies outside the microcrystallite and these essentially large r correlations are assumed to be well described by $g^R(r)$, the random network nuclear-nuclear correlation function.

We next consider that we are sitting on an atom in a random network region of the model amorphous sample. For this case we shall assume that the nuclear-nuclear correlations $g^2(r)$ are well described by $g^R(r)$ for all r

$$g^2(r) = g^R(r) \qquad 4.13$$

We now write the sample averaged correlation function g(r) as the sum of $g^1(r)$ and $g^2(r)$ weighted by the relative amounts of the two structural regions. Thus we have (dropping the subscripts γ, β, δ on $\mathcal{E}_{\gamma\beta\delta}(r)$)

$$g(r) = \frac{N^m \left\{ c(r)\, g^m(r) + (1 - c(r))\, g^R(r) \right\} + N^R g^R(r)}{N^R + N^m}$$

$$= \alpha \{ \varepsilon(r) g^m(r) + (1 - \varepsilon(r)) g^R(r) \} + (1 - \alpha) g^R(r) \qquad 4.14$$

where N^m and N^R are the number of trigonal and tetrahedral carbon atoms, respectively, in the model sample and

$$\alpha = \frac{N^m}{N^m + N^R} \qquad 4.15$$

is a measure of the fraction of layered structure in the model giving an approximate mean density ρ_o for the model amorphous sample of

$$\rho_o = \alpha \rho_o^m + (1 - \alpha) \rho_o^R \qquad 4.16$$

Clearly, if the amount of random network is small, $\alpha \approx 1$, then equation (4.14) reduces to the form of $g^1(r)$ in equation (4.12). This expression has been used previously (Howie et al, 1973) for the modelling of α-Si with microcrystals, based on the wurtzite structure, linked by thin regions of random network. The inclusion by Howie and co-workers of the second term on the right hand side of equation (4.12) improved the agreement with experiment over that obtained by using just a microcrystallite correlation function.

Equation (4.14) is the formalism for the nuclear-nuclear correlation function of our model amorphous sample. It contains the microcrystallite dimensions and the fraction α, of layered material, in a simple form and can thus be easily applied to different amorphous structures. We can now complete the formalism by defining the correlation functions $g^m(r)$ and $g^R(r)$.

Although the basic hexagonal structure of the graphite-like layers has been well established, experimental evidence (Franklin, 1950, Noda et al, 1964) indicates large variations in the inter layer spacing in the ordered domains. It has been suggested (Pauling, 1966) that this variation in the layer spacing is related to two types of layer structure, namely quinoid and turbostatic. The former is a structure in which each carbon atom has associated with it two single and one double bond.

The latter is a fully resonant structure in which all the in plane bonds are equivalent, and the extra, unbonded, electrons are considered as being delocalized. The double bond in the quinoid structure is shorter than the two single bonds and this leads to a distorted hexagonal lattice. Pauling suggested that the double bonded layers were more favourable to close packing. It appears that the quinoid structure and thus the narrower layer spacings are associated with the more ordered glassy carbons (Mildner and Carpenter, 1974). Thus for our study of the highly disordered carbon, where there is evidence for tetrahedral bonding, we shall adopt the fully resonant layer structure. A model of this form containing a stack of perfect hexagonal layers with random orientation about the layer normal was generated by computer.

We shall represent the tetrahedral random network of carbon by the CRN model of Connell and Temkin as modified to include approximately 50% odd membered rings (Beeman and Bobbs, 1975). This was model CT3,in Table 3.1, which was shown to give good agreement with the observed X-ray and electron diffraction intensities for α-Si. In this case, of course, we rescale the CRN model to the nearest neighbour carbon-carbon distance in diamond (see Table 4.1).

The nuclear-nuclear correlation function of equation (4.14) is now completely determined for a given microcrystallite size and value of α. (Of course we are also free to vary the inter layer spacing). The neutron diffraction intensity for the model sample can be calculated from

$$I(k) = b_c^2 S(k) \qquad 4.17$$

where b_c is the neutron scattering length for carbon and S(k) is the nuclear-nuclear structure factor, related to g(r) by equation (2.17 b) for the random network, and given by

$$S(K) = \frac{1}{N^m} \sum_{ij} \frac{\sin kr_{ij}}{kr_{ij}} \exp(-M(r_{ij})) \qquad 4.18$$

with

$$r_{ij} = |\underset{\sim}{r}_i - \underset{\sim}{r}_j|$$

for the layered domain. Equation (4.18) is essentially the discrete form of equation (2.17 a) for a structure having a crystalline nature. In equation (4.18) we have introduced the Debye-Waller factor, $\exp(-M(r_{ij}))$, to take account of the strongly anisotropic thermal vibrations in the layered domains with $M(r_{ij})$ taken from work on crystalline graphite (Bacon, 1952).

Unfortunately, the only available neutron data for an amorphous carbon is that for a glassy carbon heat treated at high temperature (Mildner and Carpenter 1974). The experimental data gave little evidence for tetrahedral bonding and the diffraction intensity was of the form predicted by Warren's random layer equations (Warren, 1941). Analysis of this data is thus outside the spirit of this work, although it should be noted that the essential features of their data, namely the peak positions, shapes and relative heights (of the two dimensional reflections) are well reproduced by S(k) in figure 4.7 for $\alpha = 1$. Consequently, we turn our attention to the X-ray and electron diffraction intensities from amorphous carbons and begin by describing the application of our bond charge model to the covalent bond in carbon.

4.4 Covalent bond density

Since the first calculations of the free atom form factor for carbon (James and Brindley, 1931) there have been many new values presented in the

literature for the atomic form factors appropriate to diamond and graphite (Brill, 1950, McWeeny, 1951, 1952, 1953, 1954, Berghuis et al, 1955). From a study of the X-ray and neutron diffraction patterns from a powder sample of graphite (Bacon, 1952) it was concluded that the X-ray Bragg reflections could be approximately accounted for by an atomic form factor calculated from Slater wavefunctions (McWeeny, 1951) although in the low k region $\sim 3\ \text{Å}^{-1}$ there were quite large discrepancies. However, the McWeeny form factor, which was later shown to be equivalent to that calculated from self-consistent wavefunctions including exchange (Berghuis et al, 1958), gives quite a poor representation of the (111) reflection of diamond (Brill, 1950). Calculations (McWeeny, 1954) of effective spherical atom form factors to account for the inclusion of tetrahedral bonding in diamond have only slightly improved the agreement of the (111) diamond reflection over that shown by the free atom form factor for the carbon atom in its ground state.

For amorphous carbons the failure of the old atomic form factor (James and Brindley, 1931) was first noted (Franklin, 1950) from a comparison of the theoretical and experimental diffraction intensities for a carbon black. However, in more recent calculations (Ergun, 1968) of the X-ray diffraction intensity from a random layer lattice, disagreement at the (100) peak was obtained despite using a spherical atom form factor calculated to include angular distortion of the valence charge cloud due to bonding (Berghuis et al, 1955).

The extension of the atomic form factor to include angular bonding (McWeeny, 1954) generated terms dependent on the orientation of the scattering vector to the bond, and as discussed in Chapter 2 this approach cannot be adopted for an amorphous solid where the bond angles may vary in a random way. Our

method, developed in Chapter 3, for describing the covalent bonding in α-Si, is, however, clearly relevant to α-C. As already mentioned, we need to consider both sp^2 and sp^3 hybridized bonding. We form the sp^3 hybrid, for diamond

$$\phi_{\pm}^{sp^3}(\underset{\sim}{r}) = \frac{1}{2}\{\psi_{2s}(r) \pm \sqrt{3}\,\psi_{3p_x}(\underset{\sim}{r})\} \qquad 4.19$$

and the sp^2 hybrid, for graphite

$$\phi_{\pm}^{sp^2}(\underset{\sim}{r}) = \frac{1}{\sqrt{3}}\{\psi_{2s}(r) + \sqrt{2}\,\psi_{3p_x}(\underset{\sim}{r})\} \qquad 4.20$$

where the hybrids are each normalized to contain one electron and the orthogonalized Slater orbitals (Duncanson and Coulson, 1944) are given by

$$\psi_{2s}(r) = A r \exp(-\mu_1 r) - B\exp(-\mu_2 r) \qquad 4.21$$

$$\psi_{2p_x}(r) = C \times \exp(-\mu_3 r) \qquad 4.22$$

For the sp^3 hybrid the unit of length is taken as $\frac{1}{2}$ the diamond bond length, and for the sp^2 hybrid, $\frac{1}{2}$ the graphite bond length. The values of the constants in equations (4.21) and (4.22) for both types of hybridization, together with diamond and graphite bond lengths, one given in Table 4.1. With the hybrid orbitals defined by equations (4.19) to (4.22) the LCAO bond charge densities for the diamond and graphite bonds are determined from equations (3.15) to (3.18) in terms of ϕ^{sp^3} and ϕ^{sp^2} respectively. Thus in figures 4.2 and 4.3 we show the LCAO charge density contours for sp^3 and sp^2 hybridized bonds respectively. For the sp^3 hybridized bond we have added $\frac{1}{4}$ of the carbon core electrons to each end of the bond to form the basic scattering unit for diamond

Table 4.1 : Constants for the diamond and graphite Slater wavefunctions **

Constant	Diamond Value +	Graphite Value *
μ_1	2.4	2.21
μ_2	7.45	6.87
μ_3	2.27	2.09
A	3.004	2.2
B	2.708	2.62
C	4.36	3.81

+ The unit of length = .77 A, half the diamond C-C bond length

* The unit of length = .71 A, half the graphite C-C bond length

** Duncanson and Coulson (1944)

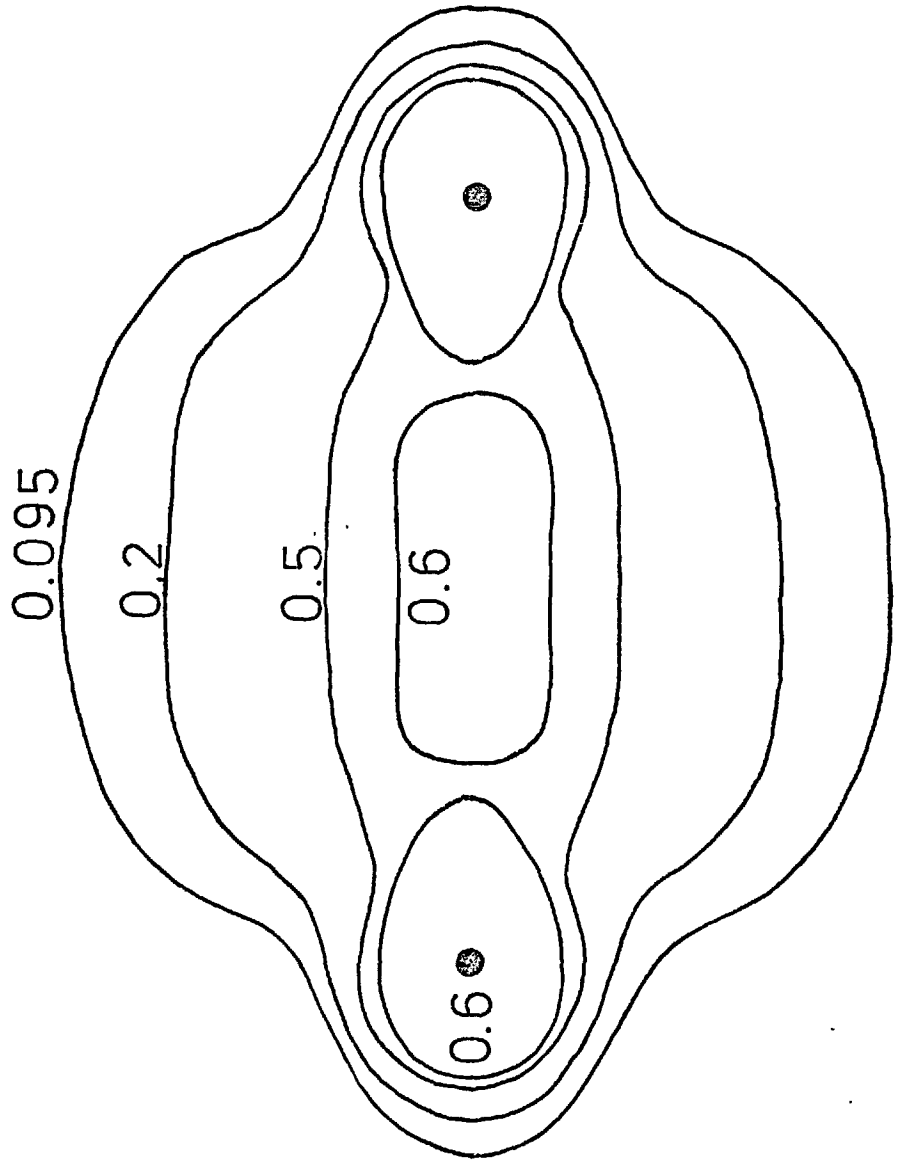

Figure 4.2 : Charge density contours for the LCAO description of the diamond covalent bond.

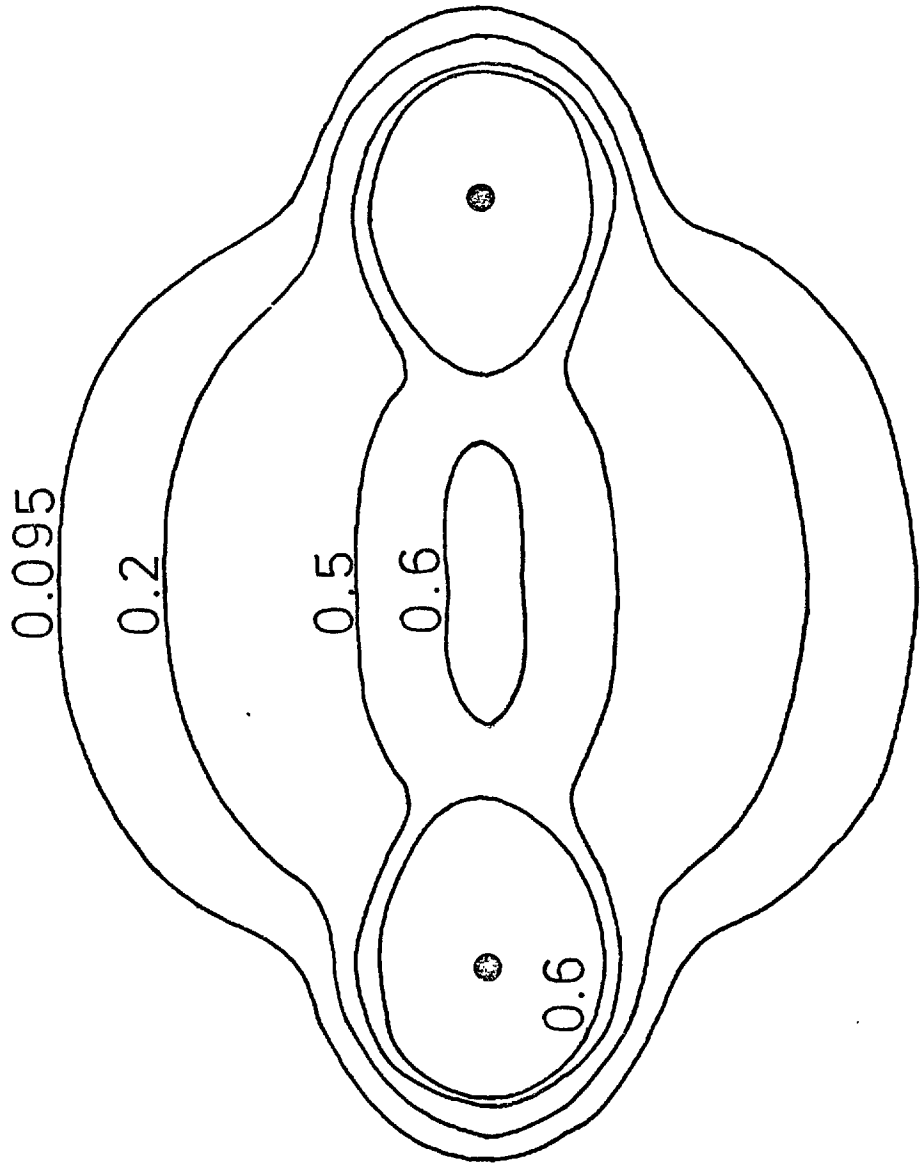

Figure 4.3 : Charge density contours for the LCAO description of the graphite covalent bond.

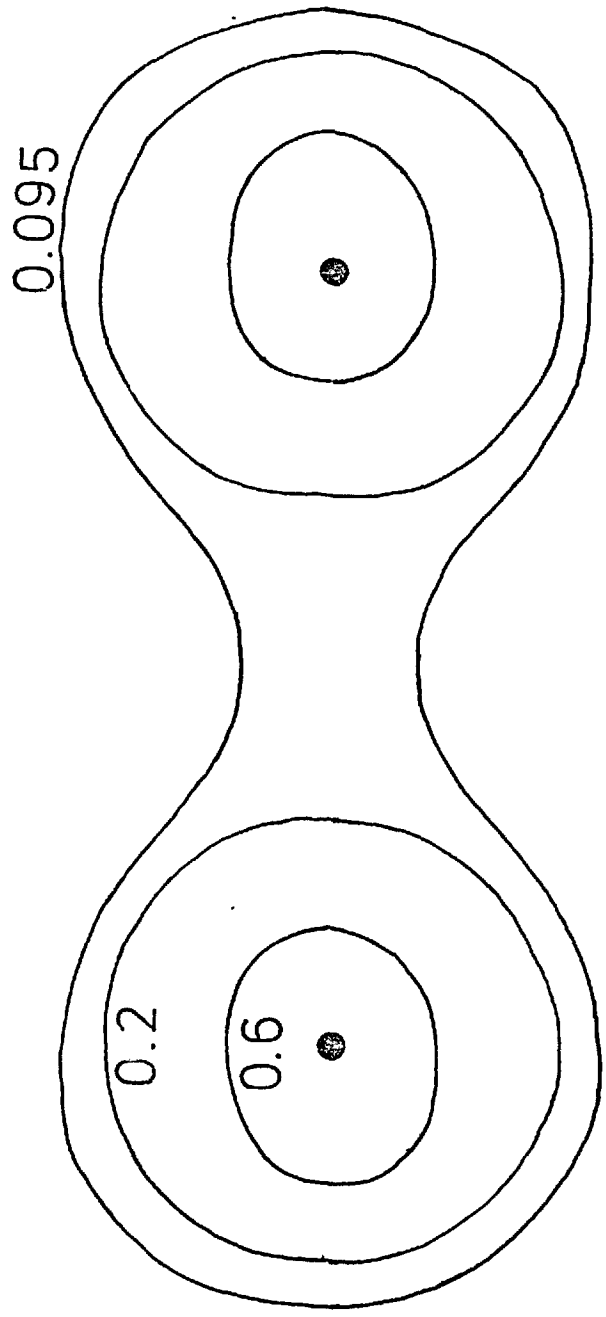

Figure 4.4 : Charge density contours for the superposition of free atom densities model for the diamond covalent bond.

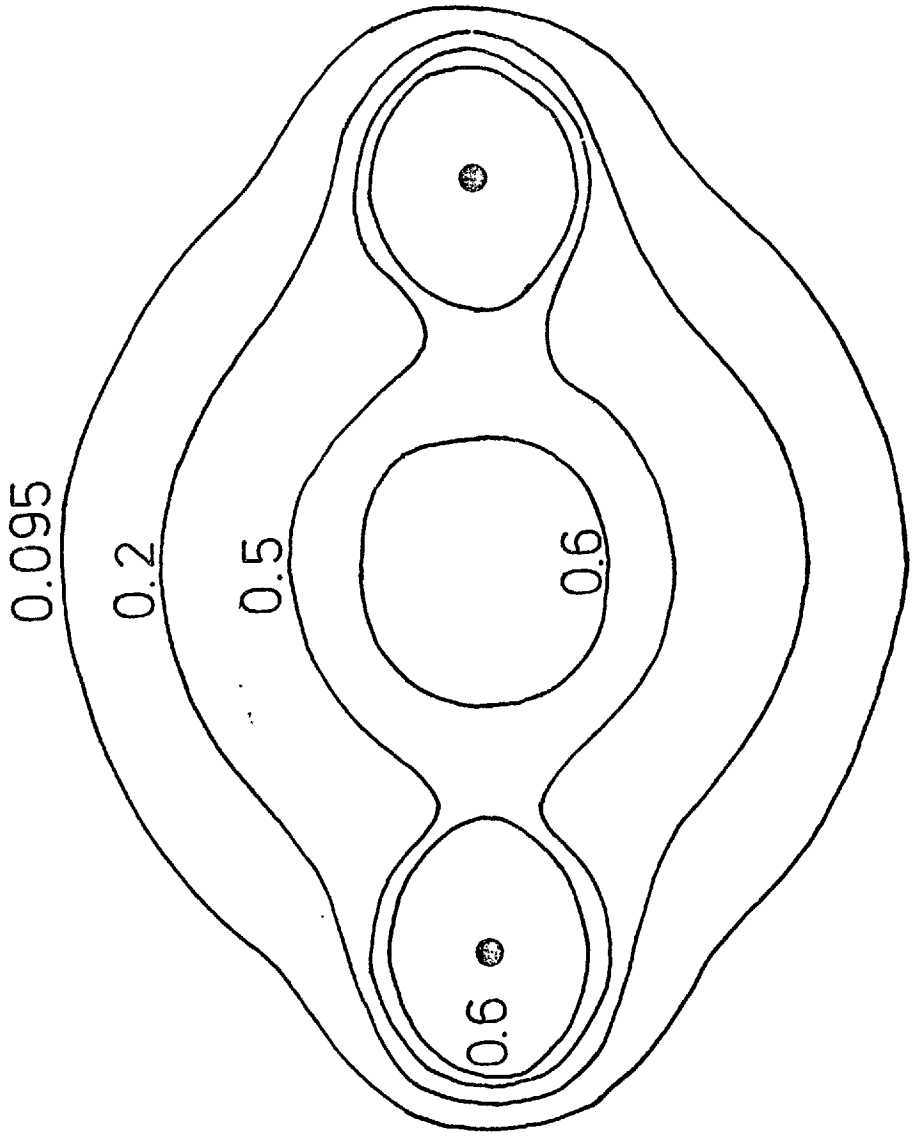

Figure 4.5 : Charge density contours for the superposition of three spherical distributions model for the diamond covalent bond.

containing 3 electrons in all. For the sp^2 hybridized bond we have added $\frac{1}{3}$ of the carbon core electrons (here the unbonded 2p electron wavefunction is spherically averaged and treated in a similar way to the core electrons) to each end of the bond to form the basic scattering unit for graphite of 4 electrons. In figure 4.4 we show the charge density contours for the superposition of free atom densities model. In this picture we have added $\frac{1}{4}$ of the carbon core electrons to each end of the bond and thus the contours are to be compared with those for the diamond bond in figure 4.2. The LCAO bond charge density contours of figures 4.2 and 4.3 can also be compared with the corresponding contours for the silicon bond as shown in figure 3.12.

For carbon both sp^2 and sp^3 bond densities have closed contours around the bond centre although these are not spherical as are those for the silicon bond of figure 3.12. The closed contours around the bond centre are not present in the superposition of free atoms density model in figure 4.4. One important feature of the diamond and graphite bond contours is that if we travel along the bond between two nearest-neighbour carbon atoms the bond density reaches a maximum value twice, once on either side of the bond centre, and has a shallow trough across the bond centre. This is to be contrasted with the silicon bond where the bond density peaks once at the bond centre. Thus the LCAO picture of the covalent bonds in diamond and silicon provides a simple interpretation of their relative insulating and semi conducting properties, the valence electrons in diamond appearing more localized than in silicon. To form the charge density contours for the sp^2 hybridized bond we have essentially localized the unbonded P electron and thus figure 4.3 does not say anything about the conducting properties of graphite. Given the LCAO bond charge densities for diamond and graphite we can now apply the procedure developed

for α -Si in Chapter 3 and extract the form factors $f_a(k)$ and $f_b(k)$ defined by equations (3.27) and (3.36) (with N = 4). Again we restrict the harmonic expansion of equation (3.20) to the carbon valence charge containing 2 electrons. In figure 4.6 we show $f_b^R(k)$ and $f_b^m(k)$, curves 1 and 2 respectively. It can be seen immediately that the bond charge form factors are very similar, with $f_b^R(0) \sim 1.7$ and $f_b^m(0) \sim 1.6$. This means that $\sim .15$ valence electrons are left around each atom in diamond and $\sim .2$ electrons in graphite (not including the delocalized p electron). The overlap integral S, equation (3.16), has the value 0.65 for diamond and 0.81 for graphite. As for silicon, the expression for the bond charge density $\varrho(\underset{\sim}{r})$, for diamond and graphite, contains two one-centre terms and one two-centre term. For diamond the amount of charge in the spherical $\psi_{2S}^2(r)$ part of the one-centre term is $1/4\,(1 + S) \approx .15$ electrons and for graphite $1/3\,(1 + S) \approx .18$ electrons. It can be seen that these values are in good agreement with $f_a^R(0)$ and $f_a^m(0)$ obtained from the harmonic expansion procedure. It is not surprising that the bond form factors are very similar when one considers the similarity between the diamond and graphite bond charge density contours of figures 4.2 and 4.3.

However, as was the case for Si, our bond charge division is not a unique procedure, and it is important to examine the charge contours formed from the superposition of three spherical distributions model. Since the LCAO bond charge density contours for diamond and graphite are very similar, we shall do this only for diamond. Thus for the atom form factor we write

$$f_e^R(k) = f_{core}(k)/4 + f_a^R(k) \qquad 4.23$$

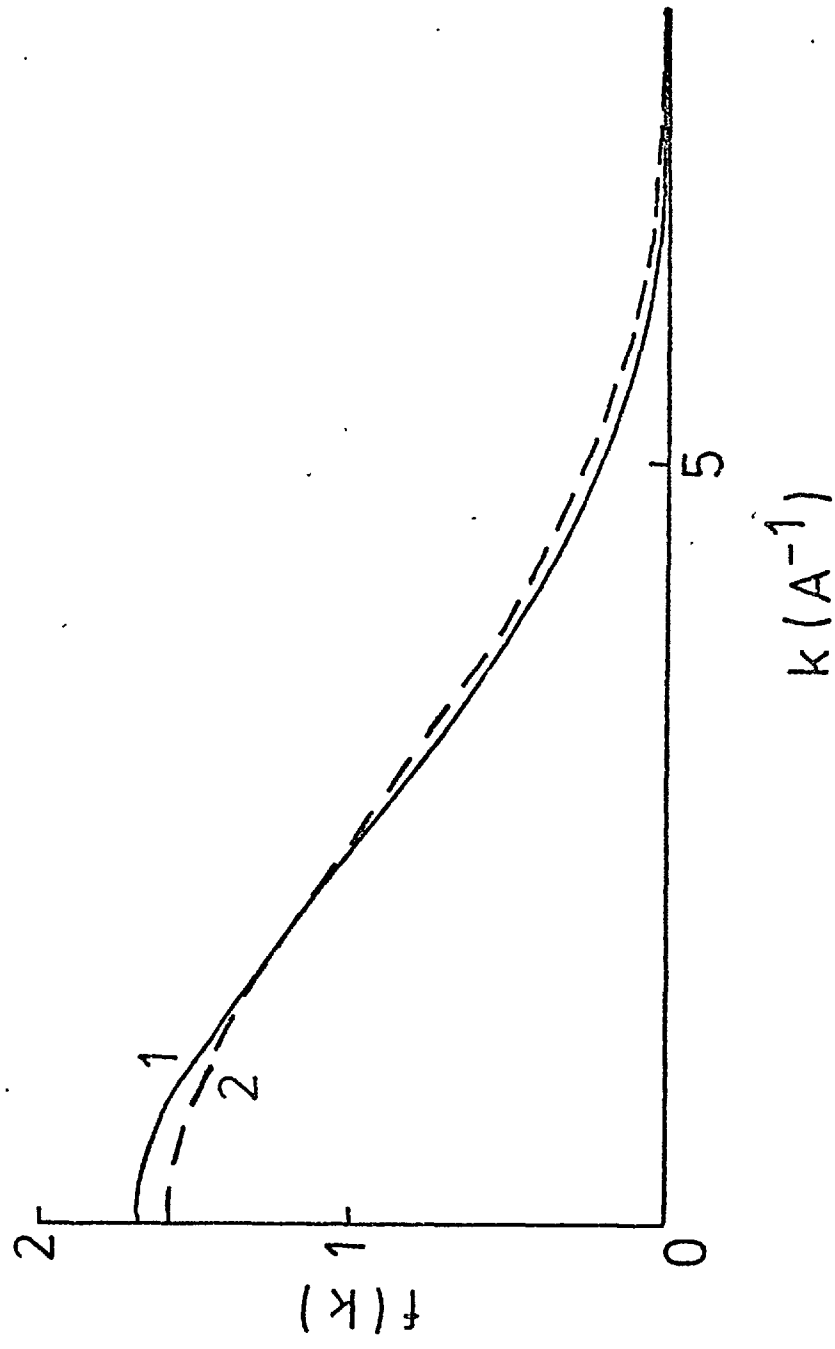

Figure 4.6 : The bond charge form factors for carbon.

1. $f_b^R(k)$
2. $f_b^m(k)$

where $f_{core}(k)$ is the form factor for the carbon core electrons. We then combine $f_b^R(k)$ and $f_e^R(k)$ to define our basic scattering unit containing 3 electrons. The charge density contours for this scattering unit are shown in figure 4.5. It can be seen by comparing the LCAO contours for the diamond bond in figure 4.2 with those from the three spherical distributions model that the model density is notas successful in its description of the LCAO density as it was for silicon, although the bonding is still usefully simulated.

4.5 Crystal intensities for diamond

The many modifications to the spherical atom form factor for carbon, that have appeared in the literature (McWeeny, 1951, Berghuis et al, 1955) have in general given a poor representation of the crystalline diamond Bragg reflections, particularly the (111) reflection. We shall now examine the Bragg reflections for diamond predicted by the three spherical distributions model of a covalent bond. $|S(k)|$ is defined exactly as for silicon in § 3.7. We define the form factor $f_c^R(k)$ by

$$f_c^R(k) = 4 f_e^R(k) \qquad 4.24$$

where $f_e^R(k)$ is given by equation (4.23). The relationship between $f_c^R(k)$ and $f_b^R(k)$ at a few Bragg reflections, together with the calculated and observed values are shown in Table 4.2. It can be seen that the choice of $f_c^R(k)$ and $f_b^R(k)$ adopted here give a good representation of the Bragg reflections, including the (111) reflection.

We can now use the Bragg reflections to give a further indication of the values of $f_b^R(k)$ and $f_c^R(k)$ for $k \to 0$. In a similar way to that adopted in § 3.7 we divide the atomic form factor into core and valence parts and introduce the parameter δ representing the fraction of the four carbon atom valence electrons not participating in the bonding. The form factor $f_c^R(k)$ is now defined in the same

Table 4.2 : Some observed and calculated Bragg intensities for diamond

Reflection	$\lvert S(k) \rvert$	Calculated intensity	Observed intensity *
(111)	$4\sqrt{2}(f_c + \sqrt{2}f_b)$	18.52	18.6
(220)	$8f_c$	15.2	15.3
(311)	$4\sqrt{2}(f_c - \sqrt{2}f_b)$	9.1	9.0
(222)	$16f_b$	1.12	1.15

* McConnell and Sanger (1970)

Note : the (222) reflection is the so-called forbidden reflection.

way as equation (3.43). The bond form factor is represented by a gaussian in terms of γ and ρ_o the value of the diamond LCAO bond charge density at the centre of the bond (equation (3.47)). In table 4.3 we give the relationship between $f_c^R(k)$ and $f_b^R(k)$ for the first few Bragg reflections together with the value of γ for which the best agreement with experiment is obtained. It can be seen that the values of γ agree well with the value $f_a^R(0)$ obtained from the harmonic expansion. With the encouragement from these results we turn to consider the amorphous state. We shall assume, as we did for Si, that the localized bond densities for the crystal can be carried over into the amorphous state.

4.6 X-ray and electron diffraction formalism

The model as formulated above contains four components, namely (in K-space) $f_c^R(k)$ and $f_b^R(k)$ in the random network and $f_c^m(k)$ and $f_b^m(k)$ in the random layer microcrystallites where

$$f_c^m(k) = f_{core}(k) + f_{2p}(k) + 3f_a^m(k) \qquad 4.25$$

and $f_{2p}(k)$ is the form factor for the spherically averaged, unbonded P electron. We now make two plausible simplifying assumptions :

(i) We can model both the diamond and graphite bonds with the same three spherical charge distributions

(ii) We can define an average atom form factor given by

$$f_c(k) = \alpha f_c^m(k) + (1-\alpha) f_c^R(k) \qquad 4.26$$

which, of course, gives the *correct* form factor in either limiting case $\alpha = 1$ or 0. The first assumption can be clearly justified by the similarity between the charge density contours for the two types of bonding shown in figures 4.2 and

Table 4.3 : Parameter γ for optimum fit to Bragg reflections in diamond

Reflection	$\lvert S(k) \rvert$	γ
(111)	$4\sqrt{2}(f_c + \sqrt{2}f_b)$	0.15
(220)	$8f_c$	0.0
(311)	$4\sqrt{2}(f_c - \sqrt{2}f_b)$	0.1
(222)	$16f_b$	0.1

4.3 and by the similarity of the bond charge form factors. The second assumption whilst having no firm theoretical basis is made in the spirit of the rest of this work and in order to make progress.

With assumptions (i) and (ii) we have a two component system of spherical distributions (we take the diamond bond charge form factor $f_b^R(k)$). To calculate the X-ray and electron diffraction intensities from equation (2.18) we thus require, in addition to the nuclear-nuclear correlation function $g(r)$ those of the nuclear - bond centre $g_{nb}(r)$ and bond centre - bond centre $g_{bb}(r)$. These are defined in terms of the random layer and tetrahedral regions in exactly the same way as $g(r)$ in equation (4.14). The associated partial structure factors $S_{nb}(k)$ and $S_{bb}(k)$ are then given by equations (2.17 b) and (4.18) in terms of $g_{nb}(r)$ and $g_{bb}(r)$. Of course, our model sample is inhomogeneous and strictly we cannot simply relate the cross correlations $g_{nb}(r)$ and $g_{bn}(r)$. For the diamond structure we have

$$g^R_{nb}(r) = 2 g^R_{bn}(r) \qquad 4.27$$

and for graphite

$$g^m_{nb}(r) = \frac{3}{2} g^m_{bn}(r) \qquad 4.28$$

However, if we define an average unit for the model sample containing $(4 - \alpha)/2$ bond centres per carbon atom and write

$$S_{nb}(k) = \frac{4-\alpha}{2} S_{bn}(k) \qquad 4.29$$

then we obtain for the X-ray diffraction intensity, from equation (2.18)

$$I_x(k) = S(k) f_c^2(k) + 2[S_{nb}(k)-1] f_c(k) f_b(k) + \frac{4-\alpha}{2} S_{bb}(k) f_b^2(k) \qquad 4.30$$

and for the electron diffraction intensity

$$I_e(k) = k^{-4} \{ S(k)(z-f_c(k))^2 - 2[S_{nb}(k)-1](z-f_c(k)) f_b(k) + \frac{4-\alpha}{2} S_{bb}(k) f_b^2(k) \} \qquad 4.31$$

where the intensities are in terms of the scattering from the basic structural unit. We can now proceed to apply equations (4.30) and (4.31) to some experimental data for amorphous carbons. We shall discuss each experiment separately.

4.7 Results

4.7.1 Electron Diffraction

The electron diffraction study of a vacuum deposited amorphous carbon thin film (Kakinoki et al, 1960) indicated a random layer microcrystallite size of approximately 10 Å and a ratio of diamond-like to graphite-like carbon atoms of about one. We can interpret the microcrystallite dimension, in terms of our hexagonal lattice, as three randomly orientated layers with dimensions 10 Å x 10 Å. This gives the microcrystallite a stack height of 3×3.44 Å $\sim$ 10 Å. The ratio of diamond to graphitic type atoms obviously corresponds to a value of $\alpha = 0.5$. The data presented by Kakinoki is in the form of the structure factor $S^e(k)$ as derived from experiment using the atomic form factor (equations (2.20) and (2.22)). In figure 4.7 we show the structure factor $S^e(k)$ as derived from the experimental intensity (curve 5) together with S(k) for our model with the above mentioned microcrystallite dimensions and for increasing proportions of random network : α = 1.0,

.75, .5, .25 (curves 1 to 4). The origins have been displaced for clarity. We would not expect agreement between S(k) and $S^e(k)$ at small k (the first two peaks) because of (a) the neglect of chemical bonding in the extraction of $S^e(k)$ from the experimental intensity, and (b) the experimentally observed peak at $k \sim 1.2\ \mathring{A}^{-1}$ which (if it is associated with the (002) reflection) corresponds to an interplane spacing of $\sim$ 5A. Such a peak position has not been observed in any other experimental work on amorphous carbon and does not correspond to any graphitic or diamond peak. For $k \sim 4\mathring{A}^{-1}$ the agreement between $S^e(k)$ and S(k) is good for $\alpha = 0.25$. Increasing the value of α, decreasing the amount of random network in the model structure, leads overall to too much structure in S(k), a very significant effect of which is the appearance of a shoulder at $k \sim 6.1\ \mathring{A}^{-1}$ which develops into a well defined peak for $\alpha = 1.0$. Thus the k space comparisons given here indicate rather more tetrahedrally bonded carbon than was deduced by Kakinoki. Their conclusions were based upon fitting gaussian distributions, at the diamond and graphite nearest and next nearest neighbour distances, to the radial distribution function g(r). For our model sample with $\alpha = 0.25$ the calculated S(k) function is not very sensitive to the microcrystallite dimensions. Thus the structural trends evident in figure 4.7 would still be evident for a range of microcrystallite sizes. Consequently, we believe the main conclusion to be drawn from these structure factor calculations is that the experimental data indicates a highly disordered carbon. This conclusion has been reached previously (Stenhouse et al, 1977) where the full experimental diffraction intensity (Kakinoki et al, 1960) was shown to be fairly well described, for $k > 2\mathring{A}^{-1}$ when covalent bonding effects were included, by the theoretical intensity for a tetrahedral random network. For $\alpha = 0.25$ the calculated peak that is most sensitive to the microcrystallite dimensions is the one dimensional (002) reflection at $k \sim 1.8\ \mathring{A}^{-1}$.

However, this is the very peak that appears wrongly placed in the experimental curve.

In figure 4.8 we show the total electron diffraction intensity calculated using equation (4.31) for the same microcrystallite size as above and for α = 1.0, .75, .5, .25 (curves 1 to 4). The experimental intensity (Kakinoki et al, 1960) is given as curve 5. Here the effect of the k^{-4} factor in equation (4.31) is to dampen the structure at large k, and these figures provide a comparison between theory and experiment at low k and show the effects of covalent bonding. The experimental and theoretical peaks below k = 2 $\mathring{A}^{-1}$ are not shown since theory and experiment will obviously be in disagreement in this region. For $k > 2\ \mathring{A}^{-1}$ agreement between theory and experiment is good for $\alpha = 0.25$. For this value of α we show in figure 4.9 the contributions to equation (4.31) from the nuclear - nuclear, nuclear - bond centre and bond centre - bond centre correlations (curves 1, 2 and 3 respectively) together with the total intensity $I_e(k)$ (curve 4). We also show in figure 4.9 the height of the (100) peak (graphite notation) as calculated using two different atomic form factors, namely those of James and Brindley (1931) and McWeeny (1951). It can be seen that, at the (100) peak the covalent bonding has a significant effect on the electron diffraction intensity and that the intensities predicted by the atomic form factors are on either side of the experimental peak height.

4.7.2 X-ray diffraction

The X-ray diffraction study of an amorphous carbon prepared by pyrolysis of polyvinylidene chloride at 1000°C (Franklin 1950) indicated that 65% of the carbon was in the form of perfect graphite-like layers of mean diameter $\sim$ 15 - 20 $\mathring{A}$ and that 35% was in a much less organized state. Franklin adopted two approaches to analyzing the experimental data. First, a comparison of the radial

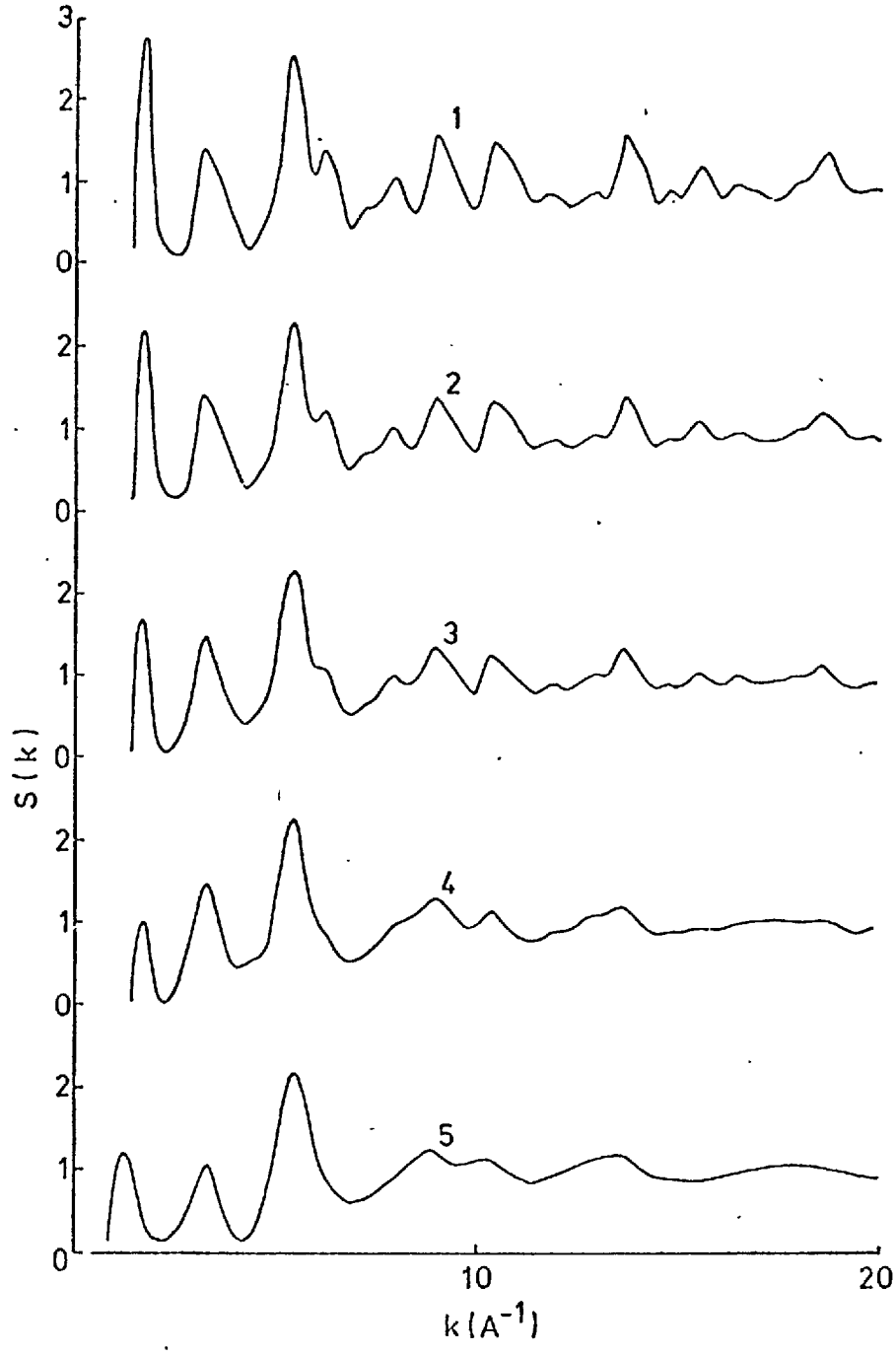

Figure 4.7 : Structure factors for the 10 x 10 x 10 A^3 model.

1. For $\alpha = 1.0$
2. For $\alpha = 0.75$
3. For $\alpha = 0.5$
4. For $\alpha = 0.25$
5. Derived from experiment

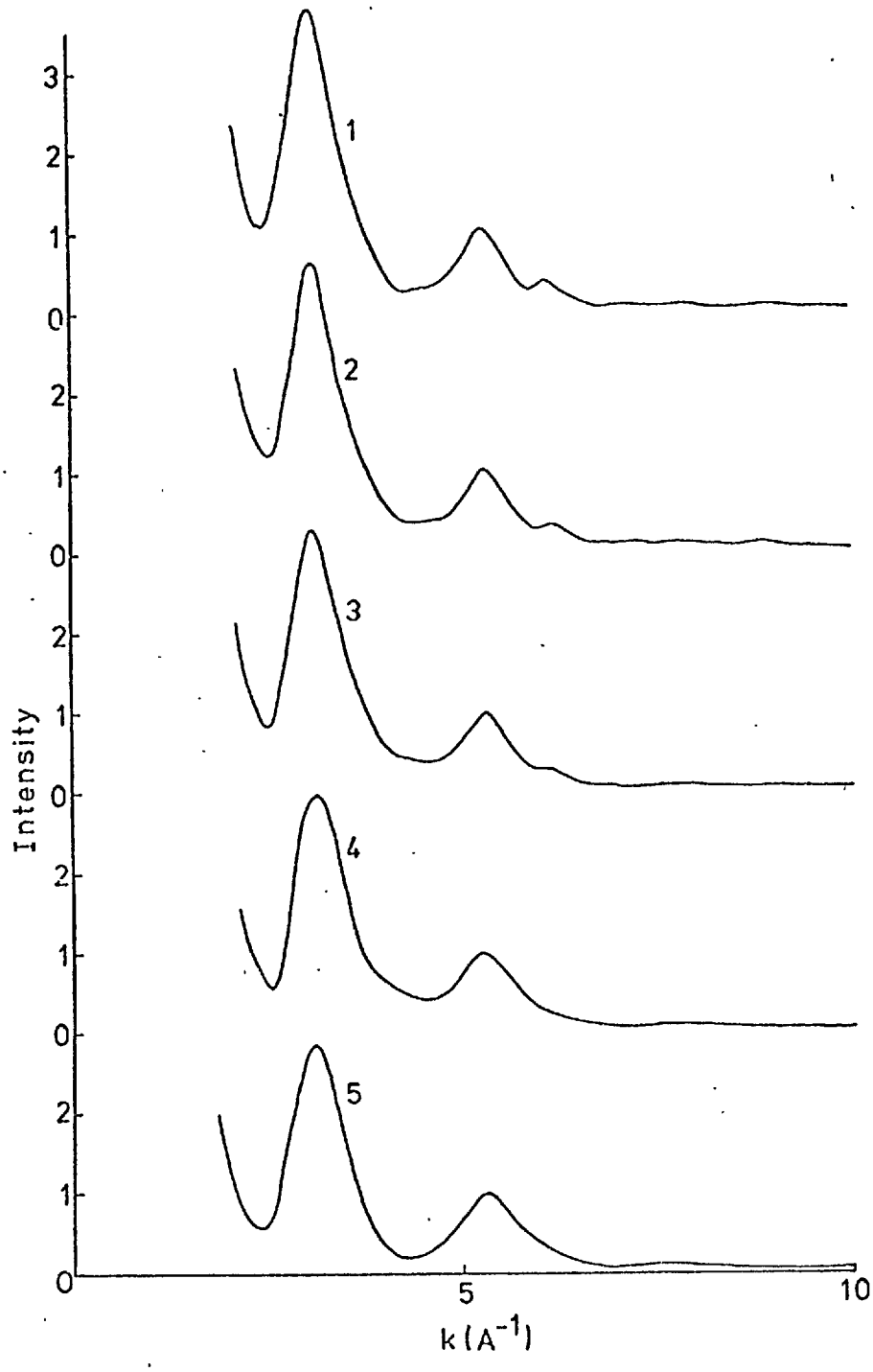

Figure 4.8 : Electron scattering intensities for the 10 x 10 x 10 A^3 model.

1. For $\alpha = 1.0$
2. For $\alpha = 0.75$
3. For $\alpha = 0.5$
4. For $\alpha = 0.25$
5. Experimental intensity

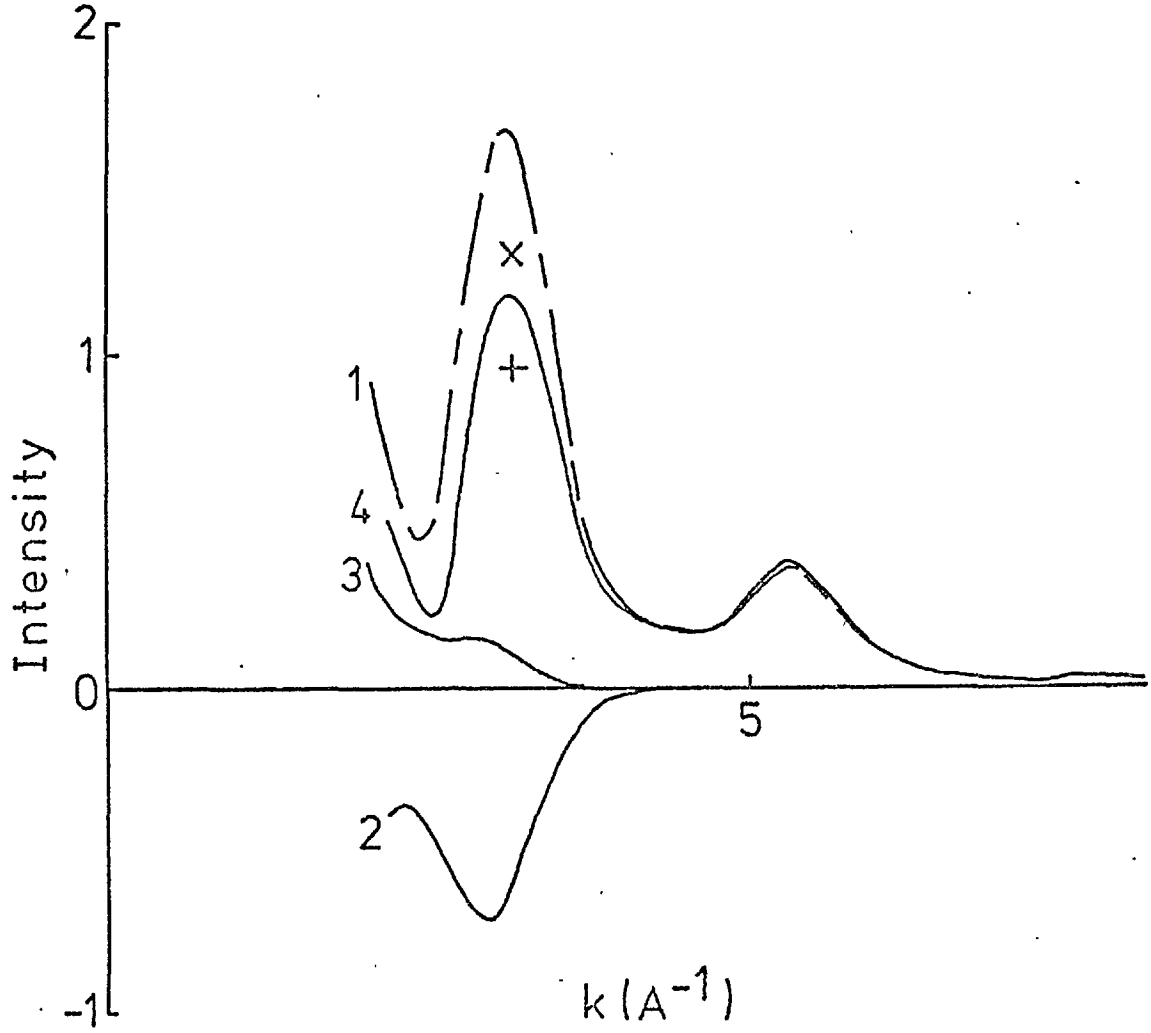

Figure 4.9 : Electron scattering intensity for the 10 x 10 x 10 A^3 model with $\alpha_C = 0.25$.

1. Contribution from carbon-carbon correlations
2. Contribution from carbon-bond centre correlations
3. Contribution from bond centre-bond centre correlations
4. Total intensity

x The intensity maximum using the atomic form factor of James and Brindley (1931).

+ The intensity maximum using the atomic form factor of McWeeny (1951).

distribution function, obtained from experiment using equations (2.17 c) and (2.20),with that for a single infinite graphite layer. Second, a comparison between the experimental reduced intensity function F(k) (see equation (3.1)) obtained using an atomic form factor (James and Brindley 1931) and that calculated for a random layer lattice with layer dimension $L_a = 16$ Å.

Both of these approaches clearly demonstrated the presence of graphite-like distances in the amorphous sample. However, the nearest neighbour peak in the experimental radial distribution function was broad enough to allow the possibility of their being diamond-like distances present in the sample and the agreement between theoretical and experimental intensity functions was not good.

The value of 35% for the disorganized carbon content was estimated by Franklin from the intensity difference between the calculated and observed two dimensional (h k o) reflections where it was assumed that the atoms in the disorganized carbon scattered independently. This method would obviously lead to error, where there diamond-like structure present in the amorphous sample, since, as discussed above, both graphite and diamond structures give rise to diffraction peaks at similar positions in k-space.

In figure 4.10 we show the X-ray scattering intensity calculated from equation (4.30) for Franklin's estimated domain size ($\sim 20 \times 20 \times 10$ Å^3) and for $\alpha = 1.0, 0.75, 0.5, 0.25$ (curves 1 to 4) together with her observed X-ray scattering intensity (curve 5). As was the case for electron diffraction, a significant feature in the model intensity patterns is the appearance at $k \sim 6.1$ Å^{-1} of a shoulder for $\alpha = 0.5$ which as α increases develops into a well defined peak. This feature is observed experimentally as a shoulder and overall for $\alpha = 0.5$ good

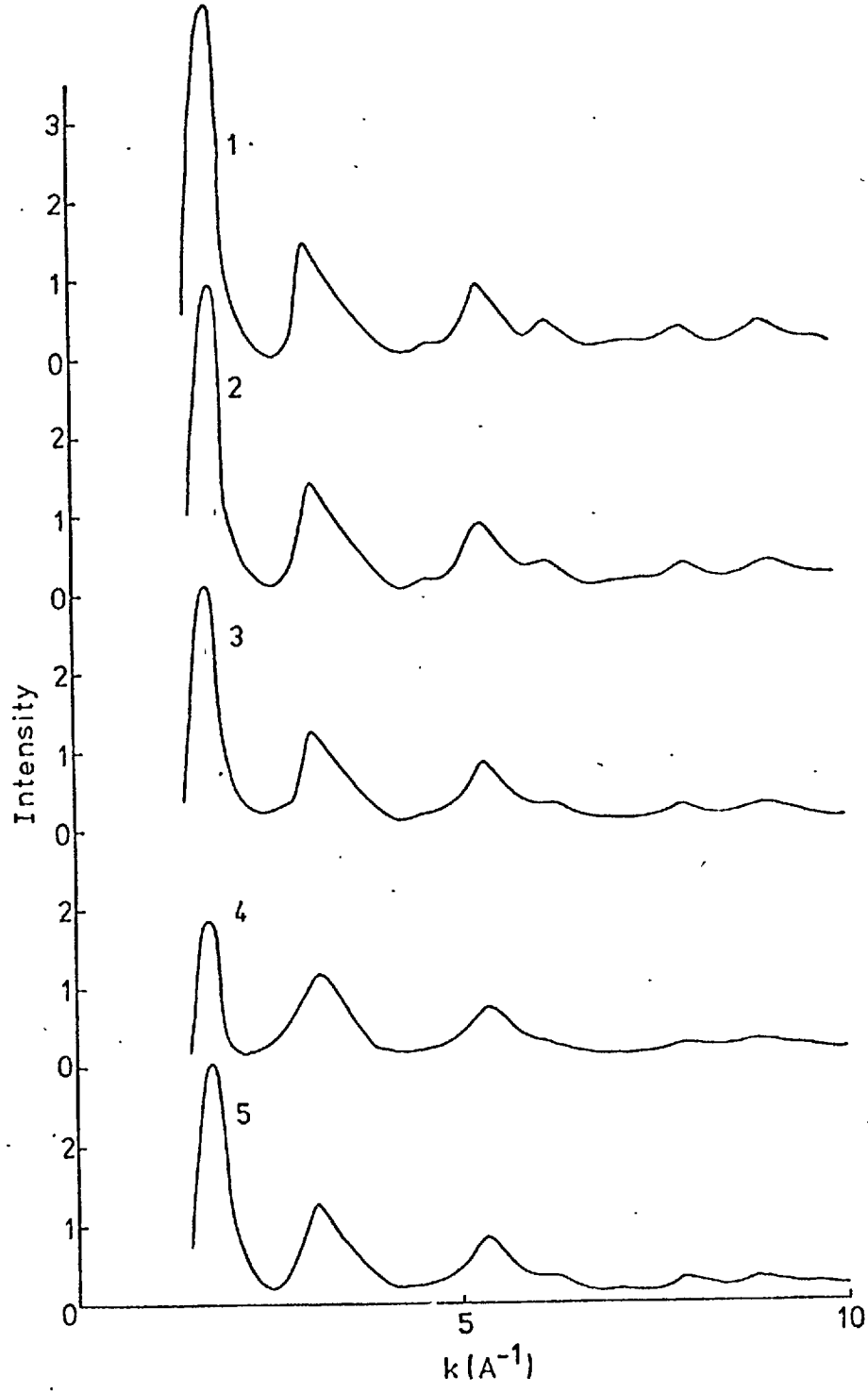

Figure 4.10 : X-ray scattering intensities for 20 x 20 x 10 A model.

1. For $\alpha = 1.0$
2. For $\alpha = 0.75$
3. For $\alpha = 0.5$
4. For $\alpha = 0.25$
5. Experimental intensity

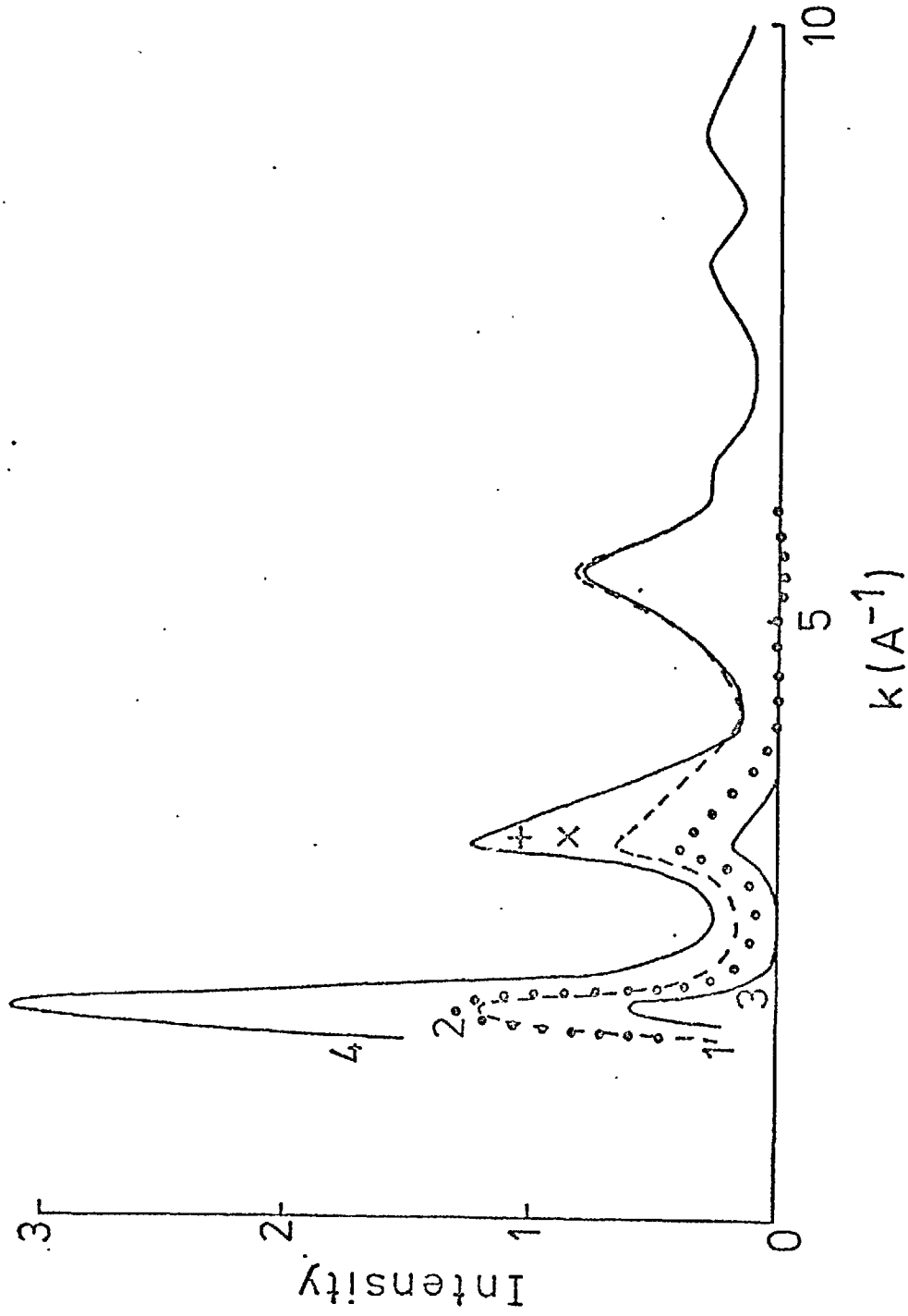

Figure 4.11 : X-ray scattering intensity for 20 x 20 x 10 A^3 model with $\alpha = 0.5$.

1. Contribution from C-C correlations
2. Contribution from C-bond centre correlations
3. Contribution from bond centre-bond centre correlations
4. Total intensity

× The intensity maximum using the atomic form factor of James and Brindley (1931).

+ The intensity maximum using the atomic form factor of McWeeny (1951).

agreement is obtained between the calculated and observed intensities.

In figure 4.11 we show for $\alpha = 0.5$ the effects of the three components in equation (4.30) on the diffraction intensity together with that calculated at the (100) peak (graphite notation) for the same atomic form factors as used in 4.7.1 (James and Brindley, 1931, McWeeny, 1951). The same remarks apply here as for the electron scattering curve in figure 4.9. It is also worth noting that if one attempts to describe the X-ray and electron scattering purely by means of atomic form factors then using McWeeny's form factor gives better agreement between the theoretical and experimental X-ray scattering intensity at the (100) peak than by using that of James and Brindley. However, in the electron case using the McWeeny form factor gives too small a maximum whereas using that of James and Brindley gives too large a one. It is, therefore, clear that it is possible to fit this peak in only one experiment by a suitable modification of the atomic form factor.

4.8 Discussion

Amorphous carbon has presented us with a difficult problem with regard to modelling both structure and electron density. Consequently we have made some rather broad assumptions in order to simplify and make progress. The large number of parameters involved in a treatment of diffraction from a single α-C sample makes the effects at low k, due to bonding and to structure, harder to separate.

However, the resemblance of the electron diffraction pattern for the evaporated carbon film (Kakinoki et al, 1960) to that given by a random network structure is clearly shown in figure 4.7. The ease of graphitization of this sample is thus rather remarkable and remains to be explained.

For both α-C samples considered our results indicate that the effects of covalent bonding are significant in the region of the (100), graphite, (111), diamond, peak in X-ray and electron diffraction intensities. These effects cannot be accounted for solely by the use of a spherical atom form factor.

CHAPTER FIVE

VITREOUS SILICA

5.1 Introduction

Silicon dioxide is of great technological importance in both the crystalline state, for use in semiconductor electronics, and the vitreous state, for glass manufacture. Consequently, the structure and electronic properties of crystalline and amorphous SiO_2 have been extensively investigated. (For a recent review see Griscom, 1977). Vitreous silica, α-SiO_2, is the only true glass (that is, formed from the melt) that we shall study in this thesis.

Silicon dioxide is polymorphic, its various allotropes including quartz, cristobalite, tridymite, coesite, stishovite and vitreous silica. It has been suggested (Goodman, 1975) that polymorphism could be a necessary condition for a material to be a glass former; for example BeF_2, PbO and As_2O_3 are all polymorphic and glass formers. With the exception of stishovite all of the SiO_2 allotropes are known to be constructed from the same fundamental structural unit, the SiO_4 tetrahedron. In quartz, silica glass, cristobalite and tridymite most of the experimental evidence indicates that the tetrahedron is regular (contrast this with the 'tetrahedral' angle variation in α-Si). Consequently the structural differences between the various polymorphs arise from variations in the Si-O-Si angle, β (figure 5.1). For example in quartz this angle is 144° (Wyckoff, 1963) whilst in α-SiO_2 experimental evidence (Mozzi and Warren, 1969) indicates that it can vary considerably, with a mean value of approximately 150° (Da Silva et al, 1975).

The perfect SiO_4 tetrahedron in α-SiO_2 indicates the presence of sp^3 hybridization of the silicon valence electrons. It is therefore probable that the electron density in vitreous silica can be interpreted in terms of our

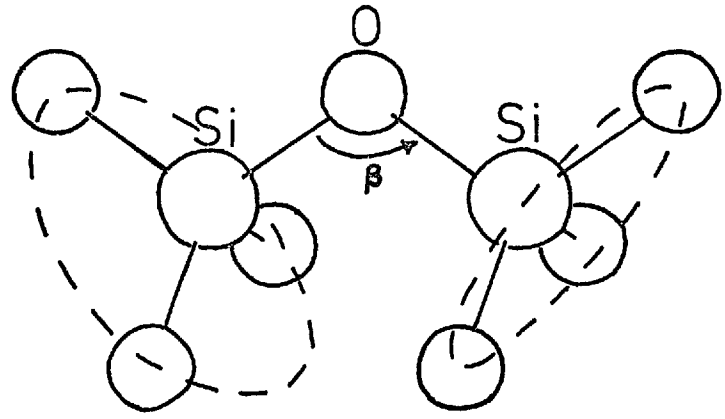

Figure 5.1 : Two SiO_4 tetrahedra joined by a common oxygen atom.

model of covalent bonding. However the Si-O bond will contain charge density contributions from silicon and oxygen atoms and will clearly have different characteristics from the covalent bond in α-Si and α- C ; for example one no longer has inversion symmetry about the bond centre.

Vitreous silica has been extensively studied by neutron and X-ray diffraction (Konnert et al, 1973, Mozzi and Warren, 1969). A description of the diffraction intensities for neutrons, and for X-rays and electrons in the spherical atom densities model (equation 2.5b), requires three correlation functions, namely those of silicon-silicon, silicon-oxygen and oxygen-oxygen, $g_{Si-Si}(r)$, $g_{Si-O}(r)$ and $g_{O-O}(r)$ respectively. These functions can only be extracted from experiment by combining three sets of data, for example from neutron, X-ray and electron diffraction. However, electron diffraction can only be used to study surface layers and for α-SiO_2 due to surface crystallization, these usually have very different properties to the bulk sample, as is studied by neutrons and X-rays. Consequently, conclusions about the structure of α-SiO_2 are usually drawn from a comparison of the total correlation function (or radial distribution function, RDF) as derived from X-rays with that derived from neutrons. The total correlation function is obtained from the fourier transform of the diffracted intensity using equation (2.20) where $f_i(k)$ is some average atomic form factor. The RDF contains contributions from all three correlation functions $g_{Si-Si}(r)$, $g_{Si-O}(r)$ and $g_{O-O}(r)$ and the problem becomes one of assigning particular peaks to the correct correlation function. One is helped in this respect by the different relative scattering powers for X-rays and neutrons of the Si and O atoms. The neutron scattering lengths are $b_{Si} = 0.42$ and $b_O = 0.58$ and the atomic form factors $f_{Si}(k)$ and $f_O(k)$ (International Tables for X-ray and crystallography, 1965) are shown in figure 5.2. Thus the peaks

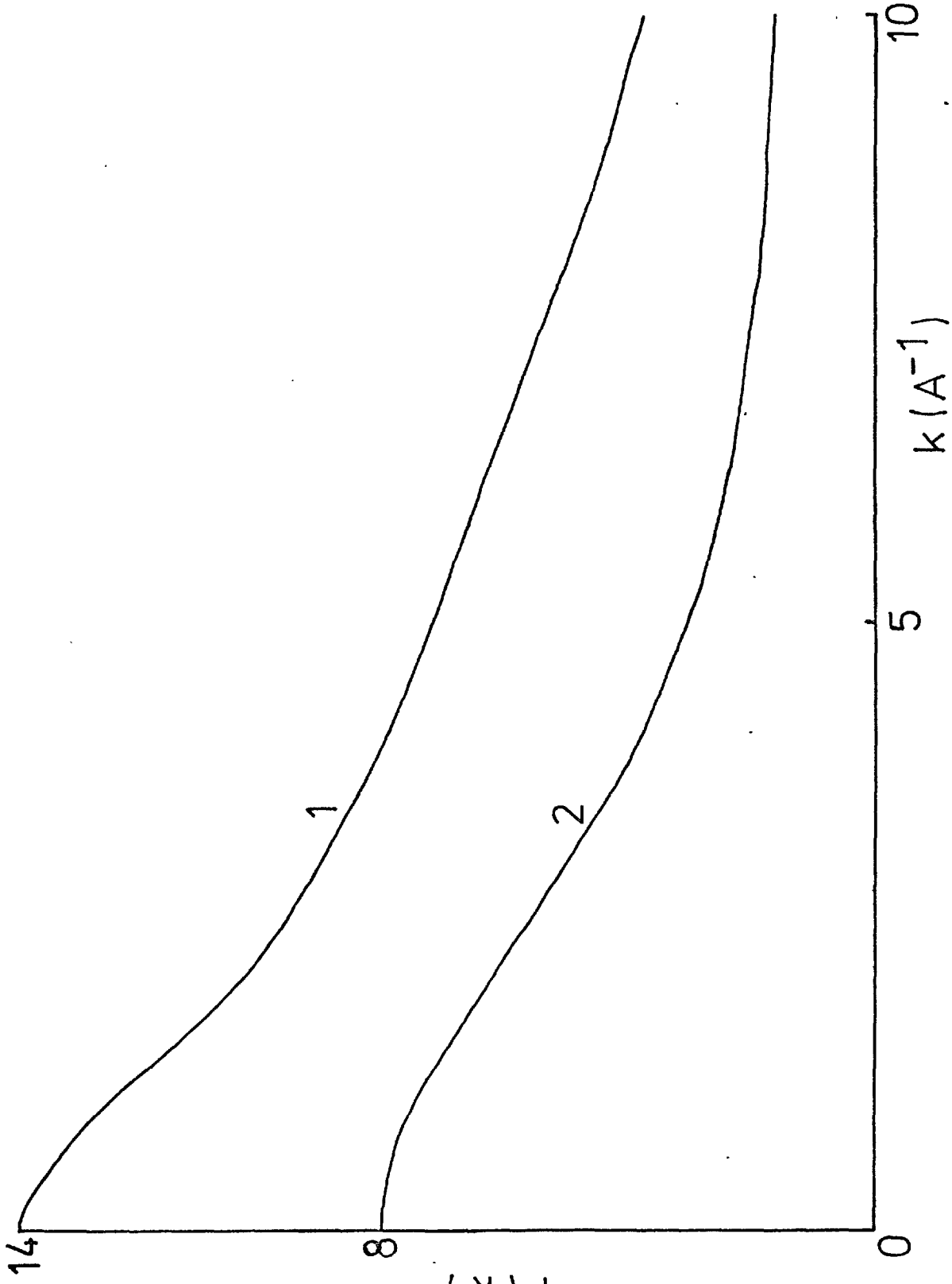

Figure 5.2 : Atomic form factors for silica.

1. For silicon
2. For oxygen

arising, for example, from the O-O correlations may be more evident in the RDF derived from neutron diffraction than in that derived from X-ray diffraction and conversely for the Si-Si correlations. However, from two experiments it is clearly not possible to uniquely extract three correlation functions. For a two component system, such as α-SiO_2, where only limited experimental data is available the approach of model building becomes very useful. Not only can a model RDF or diffraction intensity be compared with experiment but also effects arising from individual correlations (for example long range order) can be investigated.

Before considering the X-ray and neutron diffraction intensities from such a model it is convenient to begin by reviewing the present state of our knowledge of the structure of α-SiO_2

5.2 The structure of vitreous silica

The structure of α-SiO_2 has been interpreted in terms of both the continuous random network (CRN) model (Zachariasen, 1932, 1935 - these papers were the origin of the term random network) and the microcrystallite model (Warren, 1934, Valenkov, 1936). The sharpness of the first two peaks in the RDF, arising from Si-O and O-O distances, allowed early workers to deduce that the SiO_4 unit in α-SiO_2 was a perfect tetrahedron. Thus in the CRN interpretation of the structure of α-SiO_2 the principle randomizing factors are the Si-O-Si bond angle β (see figure 5.1) the value of which may lie anywhere between 120° and 180° (Mozzi and Warren, 1969) and the orientation of neighbouring tetrahedral units about the bonds which join their central Si atoms via a common oxygen atom. Thus, again referring to figure 5.1, for a particular value of β, the oxygen atoms can assume any position given by the dotted lines.

The microcrystallite picture is essentially the same as that for α-Si as discussed in Chapter 3 except that here one clearly has a much wider choice of possible crystalline structures to employ in an ordered units model of the amorphous state.

After the initial suggestions of Zachariasen and Warren, evidence in support of either picture was slow to accumulate. However the majority of the early evidence was in support of the CRN picture. Hand built CRN models (Evans and King, 1966, Bell and Dean, 1966) were shown to give RDFs in quite good agreement with the RDFs derived from both neutron and X-ray diffraction experiments. However, the Bell and Dean model with a mean value for the bond angle β of 140° had a density $\sim$ 20-25% above the experimental value. The correct density is obviously an important requirement for any model and Bell and Dean estimated that a value of $\beta \sim 150^{\circ}$ would give a model density in agreement with experiment.

The RDF for α-SiO_2 obtained by X-ray diffraction (Mozzi and Warren, 1969) showed no structural detail beyond 7Å whereas for a microcrystallite with cristobalite structure the calculated RDF (Mozzi and Warren, 1969) continued to show structure for $r \lesssim 12$Å (the limit of the calculation). Mozzi and Warren also considered a model consisting of three linked SiO_4 tetrahedral units. Allowing complete freedom for adjacent units to rotate about their linking Si-O bonds, the calculated RDF for various values of the Si-O-Si angle β (see figure 5.1) was compared with that from experiment. With $\beta = 144^{\circ}$ good agreement was obtained with the experimental RDF for $r \lesssim 4$A. However, as remarked above, this value for β leads to too high a model density. Recently Da Silva et al (1975) have reanalysed the data of Mozzi and Warren and have concluded that the best fit to the experimental RDF is obtained with $\beta \sim 150^{\circ}$.

Another CRN model was built soon afterwards (Bell and Dean, 1972) containing 188 tetrahedral units. The Si-O-Si angle was preset at 160°. As more tetrahedral units were added to the model the existing structure became slightly distorted so that the completed model contained a wide range of β values. For the final structure the value of β was found to be 153°, in good agreement with the analysis by Da Silva et al of Mozzi and Warren's data. Bell and Dean showed that the RDF for the model, for X-rays, was in good agreement with a composite of three sets of experimental data (Mozzi and Warren, 1969, Henninger et al, 1967, Kitchens, 1963) and that the RDF for neutrons was in good agreement with a composite of two experimental results (Carraro and Domenici, 1963, Henninger et al, 1967). The model RDFs reproduced both the major and minor features of the experimental curves for $r \lesssim 8\text{Å}$. By analyzing the model ring statistics Bell and Dean were able to show that an experimentally observed shoulder, for both the neutron and X-ray RDFs, was due to the presence of 4-fold rings in the network, a feature not found in earlier models (for example, that of Evans and King, containing hardly any). The model also had the correct density.

In view of the success obtained by Bell and Dean , and the lack of structure observed in the experimental RDF for $r \gtrsim 7\text{Å}$, it was surprising to have crystallite models of α-SiO_2 proposed, based on interpretations of diffraction data (Konnert and Karle, 1972, Konnert et al, 1973). Their approach was stimulated by an examination of the densities of the various allotropes of SiO_2 and germania, GeO_2. These are shown in Table 5.1 (Konnert et al, 1973). It can be seen that the densities of tridymite and cristobalite are very close to the density of α-SiO_2. Consequently, Konnert and coworkers

Table 5.1 : Densities of SiO_2 and GeO_2 Polymorphs

SiO_2

Structure	Density ($g\ cm^{-3}$)
Silica Glass	2.20
Tridymite	2.31
Cristobalite	2.32
Keatite	2.49
Quartz	2.65
Coesite	3.01
Stishovite	4.28

GeO_2

Germania Glass	3.65
Quartz	4.2
Rutile	6.2

suggested that tridymite and cristobalite could be related to the glassy structure. They further pointed out that the ratio of the densities of germania glass to quartz - like germania is approximately that of tridymite to quartz.

Konnert and coworkers found that the experimental RDFs as derived from both neutrons and X-rays, for α-SiO_2 and α-GeO_2, were consistent with those calculated for a tridymite microcrystal with dimensions $\sim 20\text{Å}$. Clearly this study indicated much more order than had been observed previously (Mozzi and Warren, 1969). It was, however, recognised (Konnert et al, 1973) that, for a microcrystallite structure, the crystallite regions would need to be bonded together with a large number of random orientations to give the bulk sample its isotropic properties. Thus Konnert and coworkers explained the small differences between the RDFs for α-SiO_2 and tridymite as being due to junctions between tridymite-like regions. They predicted that these junctions would introduce strain into the structure, so distorting the ordered regions. Their proposed model was thus strictly not a microcrystallite but rather similar to the ordered units PT model (Gaskell, 1975) discussed in Chapter 3.

The work of Konnert and coworkers has been the subject of much controversy (Evans et al, 1973, Konnert et al, 1973a, 1974, Sayers et al, 1975, Karle and Konnert, 1976). One major criticism was that they treated the first few neighbour correlations in the glass as variable parameters used in fitting the high k theoretical and experimental intensity curves. It is these small r distances that form a crucial part of the building procedure for a CRN model. Thus it was, perhaps, not surprising that the conclusions drawn from the two approaches differed at low r. For $4 < r < 8$A both CRN and microcrystallite models gave agreement with experiment. For $8 < r < 20$A the experimental RDF was fitted quite well by the tridymite curve; however this region was not considered

at all by Bell and Dean.

The presence of long range crystal-like correlations in the glass is of interest and it has been suggested (Moss, 1974) that in an AB_2 network such as α-SiO_2 there are important long range correlations associated with A-A and A-B distances (but not B-B); this being a consequence of the way in which AB_4 tetrahedra link together.

However, one important point about the microcrystallite study was that the RDF was presented in a form which amplified the curve at large r (a factor of r^2). It was thus not surprising that more structure was detected in this region than had been observed by Mozzi and Warren. Thus, perhaps the most important conclusion to be drawn from the work is that the network topology in the glassy state is probably very similar to that found in tridymite. We shall present X-ray and neutron diffraction calculations for the model that gave the best agreement with the experimental RDFs, namely that of Bell and Dean.

Finally it should be mentioned that in dark field configuration electron microscopy experiments for sputtered SiO_2 bright spots $\sim 10\text{Å}$ across have been observed (Chaudhari et al, 1972). However the interpretation of these results in terms of models of the vitreous state is subject to the same difficulties as were discussed for α-Si in Chapter 3 and we shall not dwell further on them here.

5.3 Partial structure factors and neutron diffraction

We define the pair distribution histograms $R_{Si-Si}(r)$ and $R_{O-O}(r)$ using equations (3.2) and (3.3). The Bell and Dean model is approximately rectangular and represents a region of α-SiO_2 having dimensions of $\gamma \approx 30\text{Å}$, $\beta \approx 20.5\text{Å}$, $\delta \approx 18.9\text{Å}$. Hence the factor $\mathcal{E}_{\gamma\beta\delta}(r)$ of equation (4.8) is used to correct the pair distribution histograms for finite model size. The pair correlation function

$g_{A-B}(r)$, where A and B stand for Si or O, is then defined by

$$g_{A-B}(r) = R_{A-B}(r) / 4\pi r^2 \rho_{oB} \qquad 5.1$$

and the partial structure factor, $S_{AB}(k)$ is obtained from equation (2.17a). $S_{Si-O}(k)$, $S_{Si-Si}(k)$ and $S_{O-O}(k)$ are shown in figure 5.3, curves 3, 4 and 5 respectively. The scale is on the left hand axis.

The neutron diffraction intensity for the model can now be calculated using equation (2.18). Thus for the composition unit consisting of one Si atom and two O atoms we have

$$I_{neutron}(k) = S_{Si-Si}(k) b_{Si}^2 + 2[S_{Si-O}(k) - 1] b_{Si} b_O + 2 S_{O-O}(k) b_O^2 \qquad 5.2$$

where b_{Si} and b_O, the neutron scattering lengths for the silicon and oxygen atoms, are given in §5.1.

The calculated intensity for the model is shown in figure 5.3, curve 2, together with the experimental intensity (Carraro et al, 1965), curve 1. For clarity the origin for the neutron intensities has been displaced from that for the partial structure factors. The scale for the neutron intensities is on the right hand axis. It can be seen that the general agreement between theory and experiment is good, the main differences being in the intensity in the vicinity of 3Å^{-1} and the shoulder in the theoretical curve at approximately 2Å^{-1} which is apparent in all the structure factors and is not seen in experiment.

5.4 X-ray diffraction using atomic form factors

Using the neutral atom form factors shown in figure 5.2, we have calculated the X-ray diffraction intensity for the model in the spherical atom densities approximation. For the basic composition unit equation (2.18) takes the form

$$I_x(k) = f_{Si}^2(k) S_{Si-Si}(k) + 2 f_{Si}(k) f_O(k) [S_{Si-O}(k) - 1] + 2 S_{O-O}(k) f_O^2(k) \qquad 5.3$$

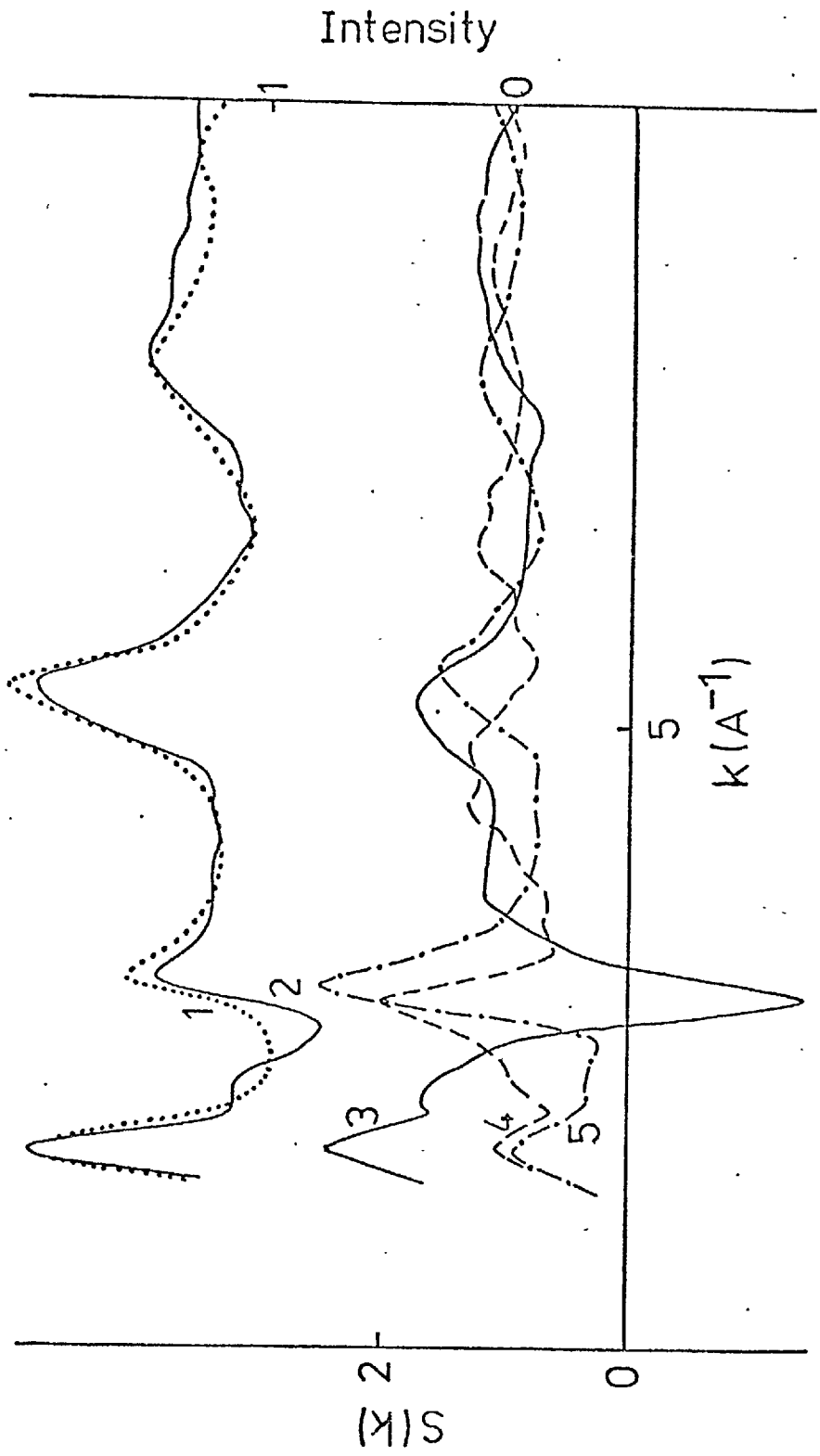

Figure 5.3 : Neutron intensity and structure factors for vitreous silica.

1. Experimental intensity
2. Theoretical intensity
3. S_{Si-O} (k)
4. S_{Si-Si} (k)
5. S_{O-O} (k)

The calculated X-ray intensity is shown in figure 5.4, curve 1, together with the experimental results of Mozzi and Warren (1969). Overall agreement between theory and experiment is quite good, the essential differences being at $k \sim 2\text{Å}^{-1}$ where the theoretical curve has a small peak, and experiment a broad shoulder, and in the region of $k \sim 3\text{Å}^{-1}$ where the theoretical curve underestimates the experimental intensity.

In view of our work on α-Si and α-C the agreement at the first peak between theory and experiment is surprising when one considers that we have used atomic form factors and neglected bonding effects. King (1967) has also calculated X-ray diffraction intensities for a random network model of α-SiO_2. In her calculations, using atomic form factors, the theoretical curve badly overestimated the experimentally observed intensity at the first peak. Better agreement was obtained using ionic Si^{4+} and O^{2-} form factors. For the Bell and Dean model we also show in figure 5.4 (marked X) the height of the first peak as calculated using ionic form factors (International Tables of Crystallography, 1965). As can be seen, the agreement with experiment is now much worse than was obtained by using atomic form factors.

From the values of the electronegativity of silicon and oxygen atoms, Pauling (1960) estimated that the Si-O bond is 50% ionic - 50% covalent. Current, non-empirical, molecular orbital calculations (Gilbert et al, 1973, Yip and Fowler, 1974) are in general agreement with Paulings classification. Thus the agreement shown by our calculations, using atomic form factors, and King's work, using ionic form factors, is possibly fortuitous. Following our work in Chapters 3 and 4 we are in a position to study the effects on X-ray diffraction intensities of a partially ionic - partially covalent bond. We shall begin by examining the LCAO charge density contours for a covalent Si-O

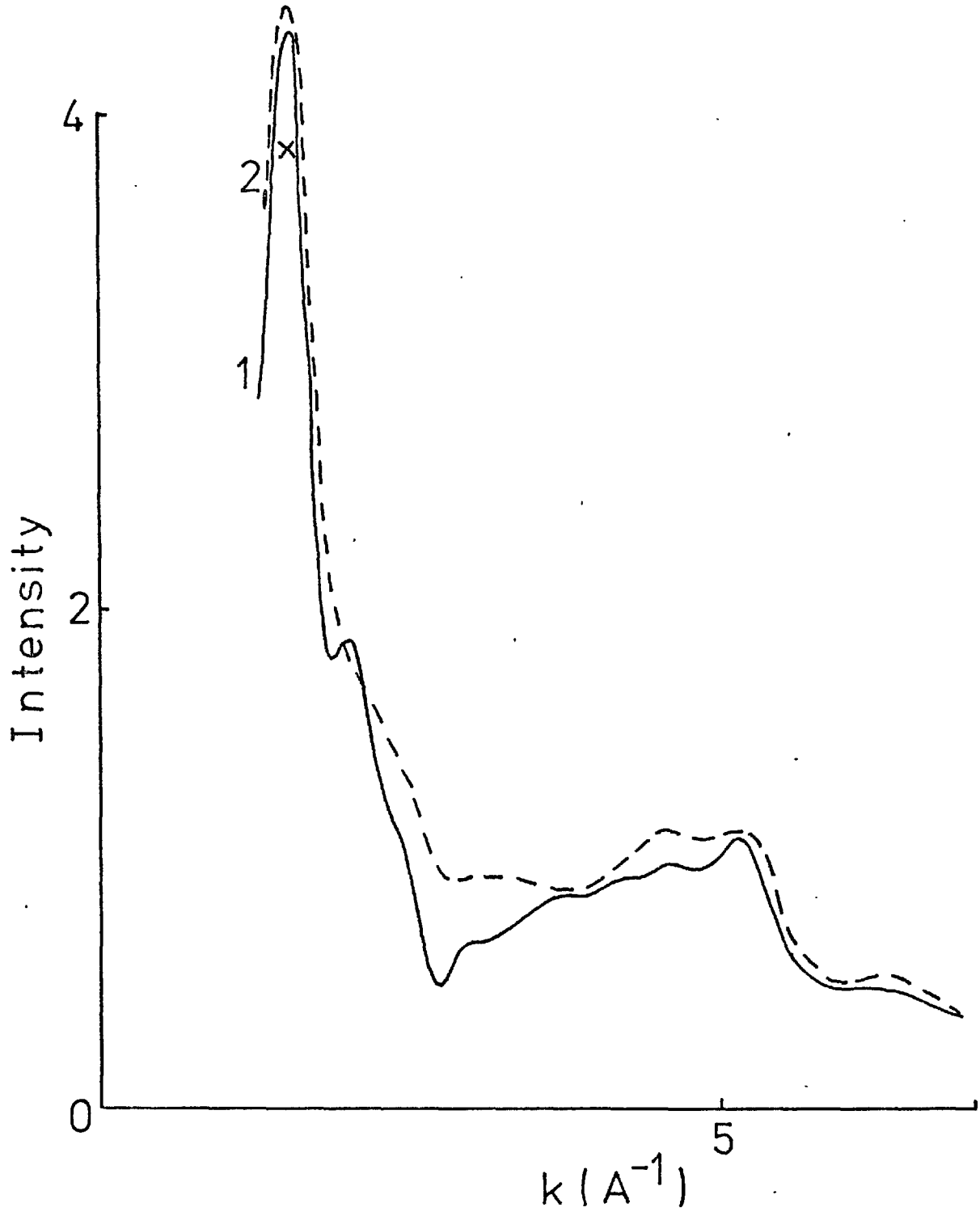

Figure 5.4 : X-ray intensity for vitreous silica using atomic form factors.

1. Theoretical intensity
2. Experimental intensity

× Intensity maximum using ionic Si^{4+} and O^{2-} form factors.

bond containing two electrons.

5.5 The Si-O bond

We shall take the covalent bond to be formed from a linear combination of a silicon sp^3 hybrid and an oxygen 2p orbital. It should be noted that the work of Gilbert et al (1975) indicates that the two lobes of a single 2p orbital may be used for bonding to two silicon atoms. The bond charge density is given by (referring to figure 3.11)

$$\rho(\underset{\sim}{r}) = 1 \phi^{sp^3}_{Si\,+}(\underset{\sim}{r}_1) + \psi_{O\,2p_x}(\underset{\sim}{r}_2)\,|^2/(1+S) \qquad 5.4$$

where S is the overlap integral given by

$$S = \int_{\underset{\sim}{r}} \phi^{sp^3}_{Si\,+}(\underset{\sim}{r}_1)\,\psi_{O\,2p_x}(\underset{\sim}{r}_2)\,d\underset{\sim}{r} \qquad 5.5$$

and $\phi^{sp^3}_{Si\,+}(\underset{\sim}{r})$ and $\psi_{O\,2p_x}(\underset{\sim}{r})$ are defined by equations (3.13), (3.14) and (4.22). The values for the constants in these equations are given in Table 5.2 where the wavefunctions are normalised with the unit of length now being half the Si-O bond length, which is also given in Table 5.2.

The LCAO charge density contours defined by equation(5.4) are shown in figure 5.5 and those for the superposition of free atoms model in figure 5.6. In both figures we have included $\frac{1}{2}$ of the oxygen and $\frac{1}{4}$ of the silicon core electrons to give a basic scattering unit containing 7.5 electrons. The main difference between the contours of figures 5.5 and 5.6 is that in figure 5.5 the charge density is, to an extent, concentrated around a point, X say, approximately three-quarters of the way along the Si-O bond. In the context of our bond charge model this can be interpreted in terms of a spherical charge distribution at that point on the bond. We shall now proceed to extract such a distribution. However we shall adopt a slightly different approach to that used for Si and C; based on physically reasonable arguments, we shall divide up the bond density in r-space.

Table 5.2 : Constants for the Slater wavefunctions for Silicon and Oxygen in the Si-O bond

Constant	Value[+]	
	Silicon[*]	Oxygen[**]
μ_1	2.09	
μ_2	7.45	
μ_3	21.1	3.36
A	1.6	
B	8.1	
C	2.56	11.68
D	2.75	
E	13.41	

[+] The unit of length = 0.81A, half the Si-O bond length.

[*] See equation (3.14)

[**] See equation (4.22)

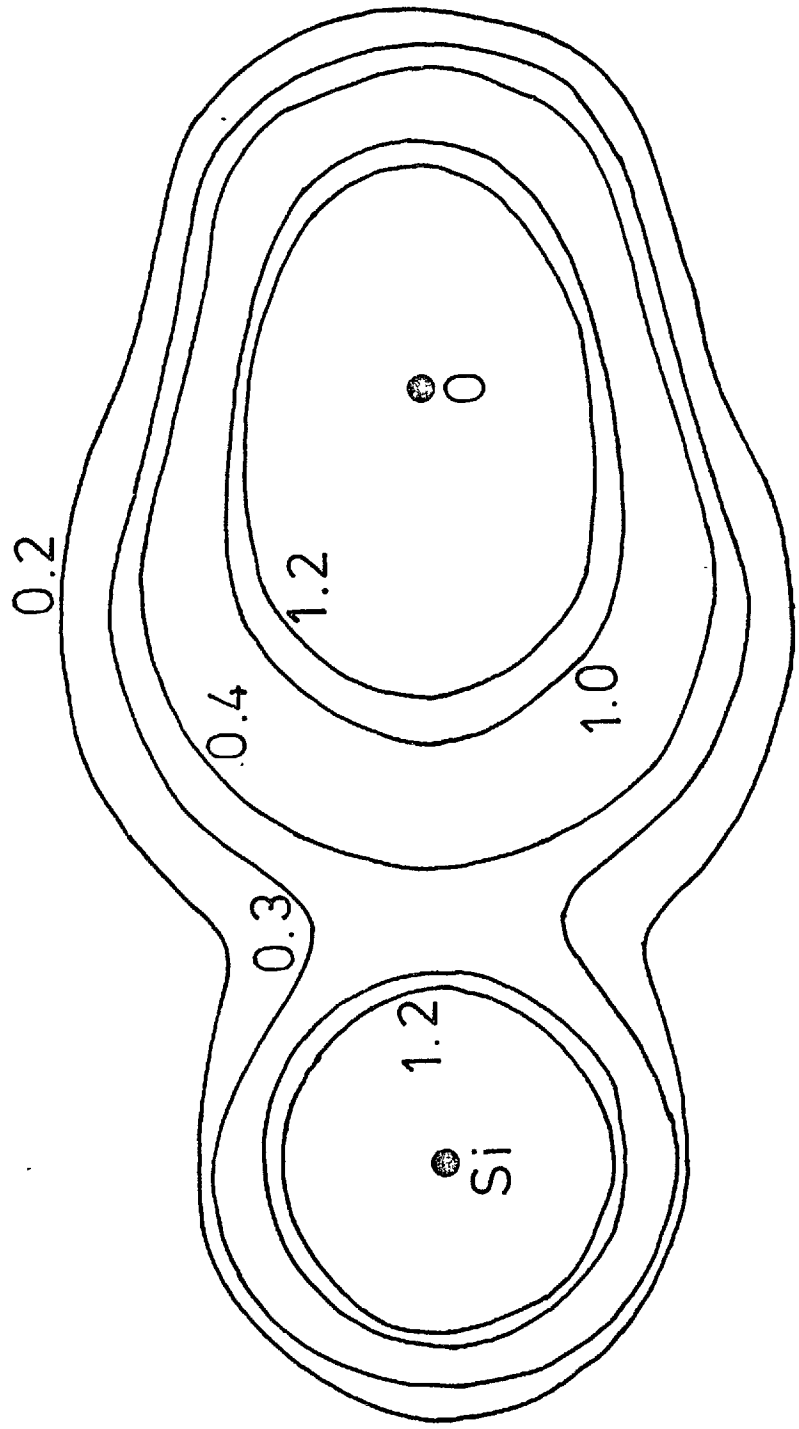

Figure 5.5 : Charge density contours for the LCAO covalent Si-O bond.

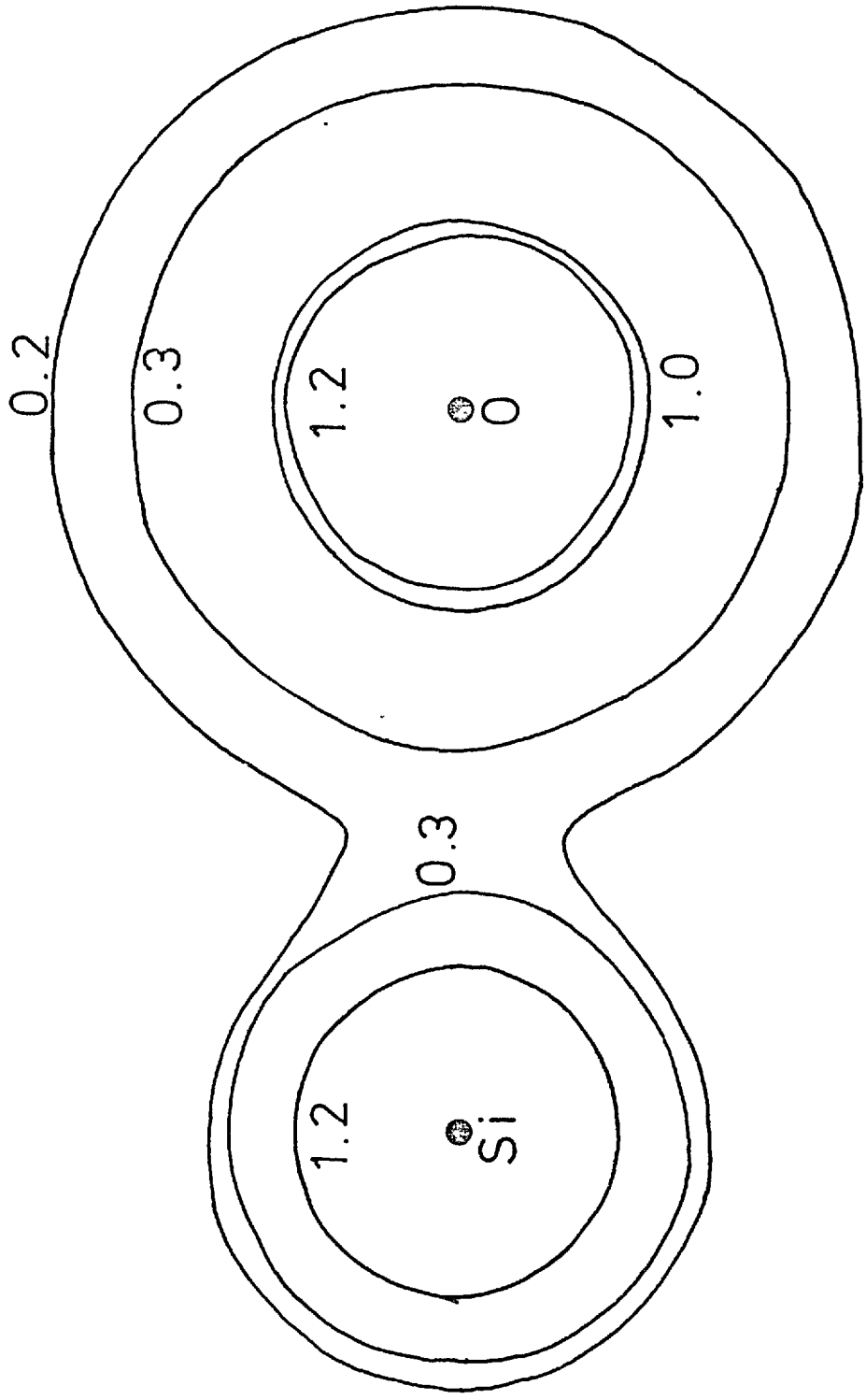

Figure 5.6 : Charge density contours for the superposition of free atoms model of the Si-O bond.

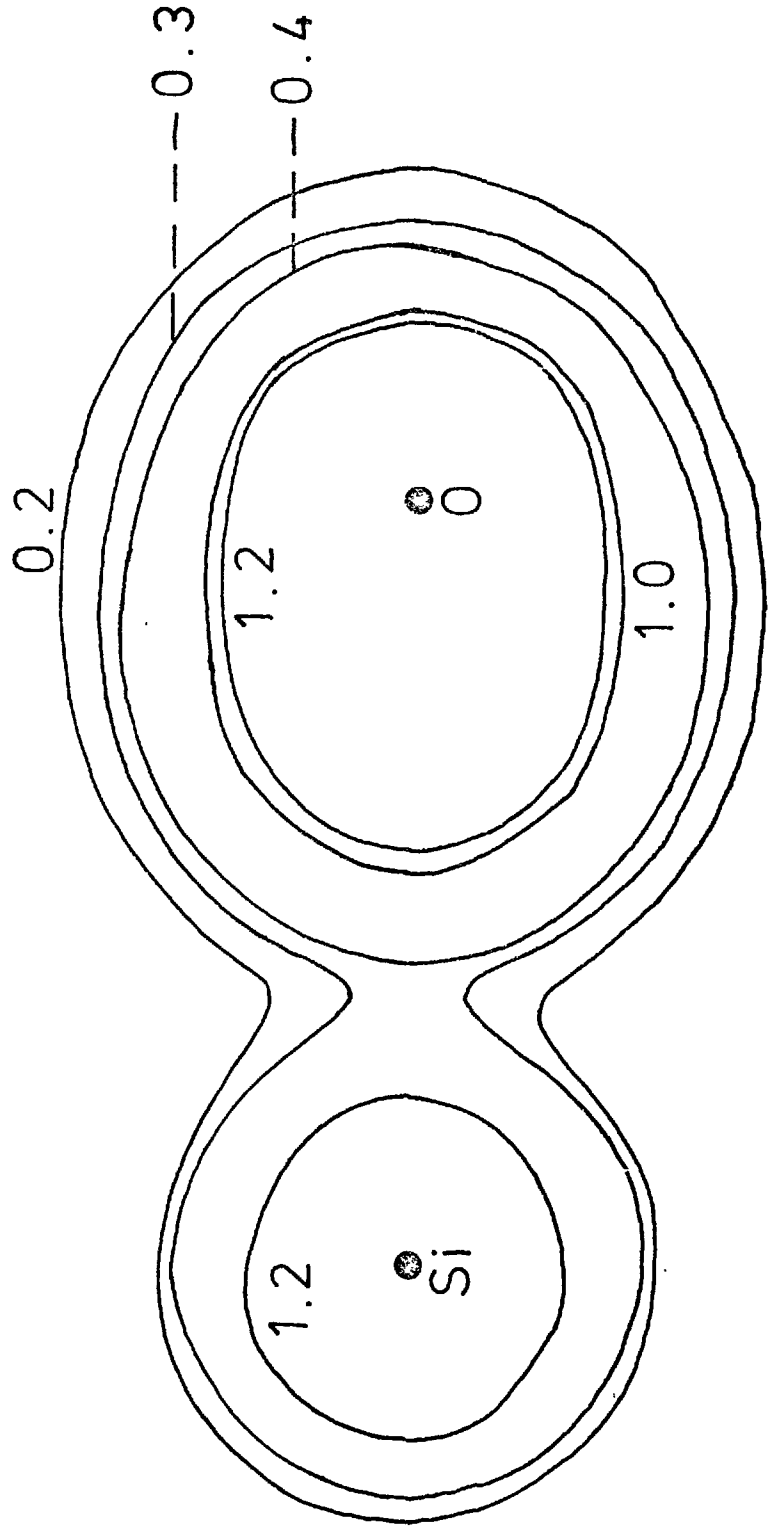

Figure 5.7 : Charge density contours for the three spherical distributions model of a covalent Si-O bond.

We wish to represent the Si-O covalent bond, containing two electrons, approximately as the superposition of 3 different spherical distributions, $\rho_A(r)$ and $\rho_C(r)$ on the silicon and oxygen atoms, respectively, and $\rho_B(r)$ at the point X. Thus referring to figure 3.11 we shall write the bond density $\rho(\underset{\sim}{r})$ as

$$\rho(\underset{\sim}{r}_1) = \rho_A(r_1) + \rho_B(|\underset{\sim}{r}_1 - 3\underset{\sim}{R}/2|) + \rho_c(|\underset{\sim}{r}_1 - 2\underset{\sim}{R}|) \qquad 5.6$$

Now, prompted by the results for the covalent bonds in silicon and carbon, we choose $\rho_A(r)$ to be the spherical charge distribution due to the $\psi^2_{3S}(r)$ term in equation (3.39). The overlap integral, S of equation (5.5), has the value 0.275. Thus the amount of charge in the distribution $\rho_A(r)$ is $0.25/(1+S) \approx 0.2$ electrons. Strictly, of course, there is no term in equation (5.4) spherical about the oxygen atom site. However, the charge lobe of $\psi^2_{2p_x}(r)$ that points away from the bond clearly does not contribute to the bonding region. We thus spherically average this lobe about the oxygen atom. This distribution, $\rho_C(r)$, contains $0.5 \times 1/(1+S) \approx 0.4$ electrons. From equations (3.21) and (5.6) we have

$$f(\underset{\sim}{k}) = f_A(k) + f_B(k)\, e^{i3\underset{\sim}{k}\cdot\underset{\sim}{R}/2} + f_C(k)\, e^{i2\underset{\sim}{k}\cdot\underset{\sim}{R}} \qquad 5.7$$

Expanding $f(\underset{\sim}{k})$ in terms of Legendre polynomials and using Bauer's expansion (equation (3.26)) we obtain, for the spherically average bond form factor, $f_0(k)$,

$$f_o(k) = f_A(k) + f_B(k)\frac{\sin 3kR/2}{3kR/2} + f_c(k)\frac{\sin 2kR}{2kR} \qquad 5.8$$

Thus given $f_A(k)$ and $f_C(k)$, as described above, equation (5.8) can be used to extract $f_B(k)$, the bond charge form factor.

We shall now examine the bond charge density contours for the three spherical distributions model of the Si-O covalent bond. These are shown in

figure 5.7 where again we have included the oxygen and silicon core electrons, as described above for figures 5.5 and 5.6. It can be seen that the three spherical distributions model in figure 5.7 gives a better representation of the LCAO covalent bond density in figure 5.5 than the free atom densities model in figure 5.6.

5.6 Effects of the Si-O bond on X-ray diffraction intensities

Having established our modelling of the Si-O covalent bond we can now proceed to calculate the X-ray diffraction intensity for a 50% ionic - 50% covalent system. We write the form factor associated with the silicon atom, $f_{Si}(k)$, as

$$f_{Si}(k) = [f_{Si^{4+}}(k) + 4f_A(k) + f_{Si^{4+}}(k)]/2$$
$$= f_{Si^{4+}}(k) + 2f_A(k) \qquad 5.9$$

where $f_{Si^{4+}}(k)$ is the silicon core electron form factor and $f_A(k)$, as described above, is that portion of the covalent bond that lies around the silicon atom. For the oxygen atom form factor, $f_O(k)$, we write

$$f_O(k) = [f_{O^{2+}}(k) + 2f_C(k) + f_{O^{2-}}(k)]/2 \qquad 5.10$$

where $f_{O^{2+}}(k)$ and $f_{O^{2-}}(k)$ are the O^{2+} and O^{2-} ion form factors, respectively and $f_C(k)$ is determined from the covalent bond density as described above. The form factor associated with the point X is just

$$f_b(k) = f_B(k)/2 \qquad 5.11$$

where $f_b(k)$ is determined from equation (5.8). The three components $f_{Si}(k)$, $f_O(k)$ and $f_b(k)$ are shown in figure 5.8. To calculate the X-ray diffraction intensity we require, in addition to $g_{Si-Si}(r)$, $g_{Si-O}(r)$ and $g_{O-O}(r)$, the correlations $g_{Si-x}(r)$, $g_{O-x}(r)$ and $g_{x-x}(r)$. These are obtained using equations

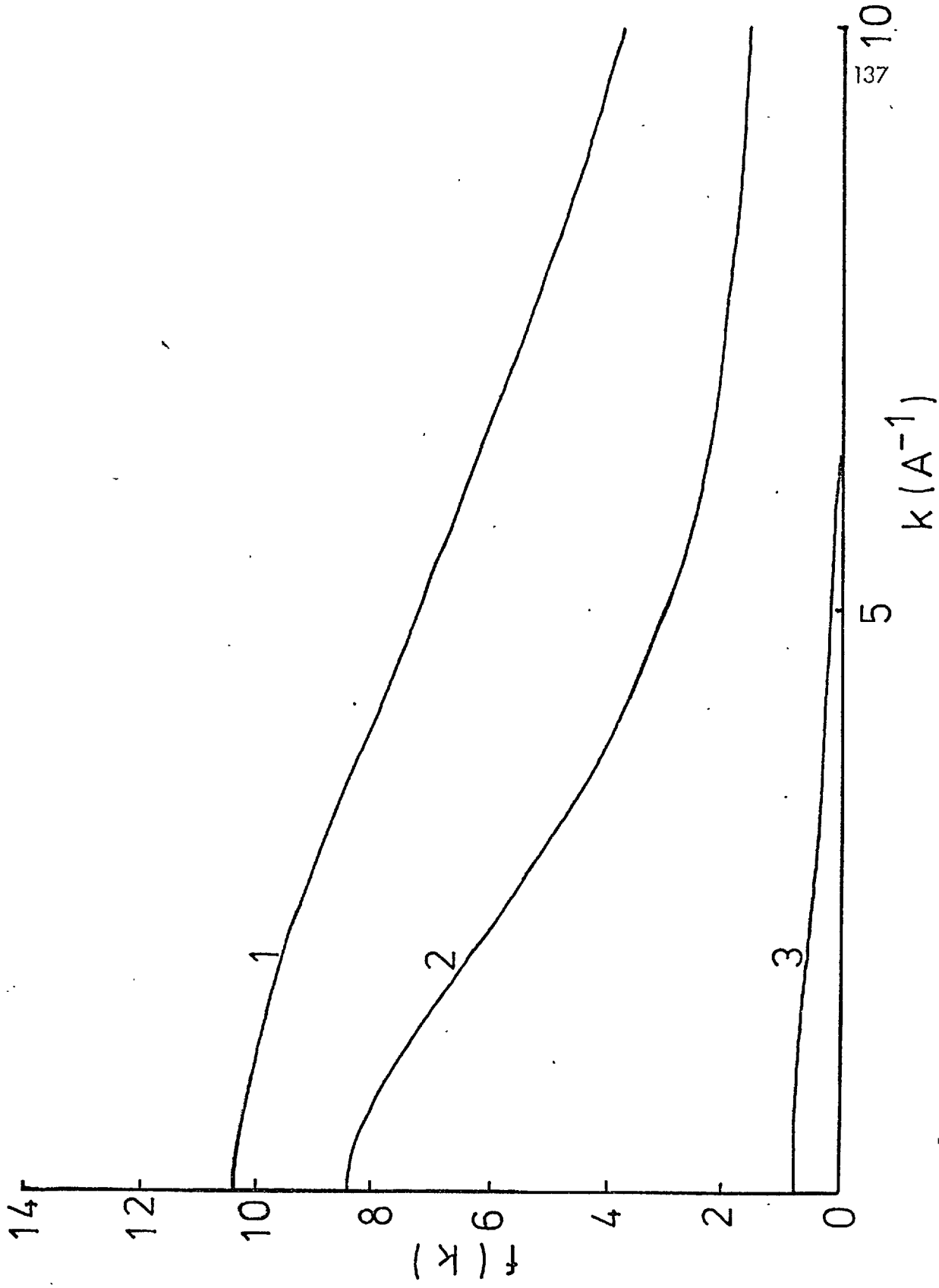

Figure 5.8 : Scattering factors for 50% ionic - 50% covalent model of the electron density in α-SiO_2.

1. f_{Si} (k)
2. f_O (k)
3. f_b (k)

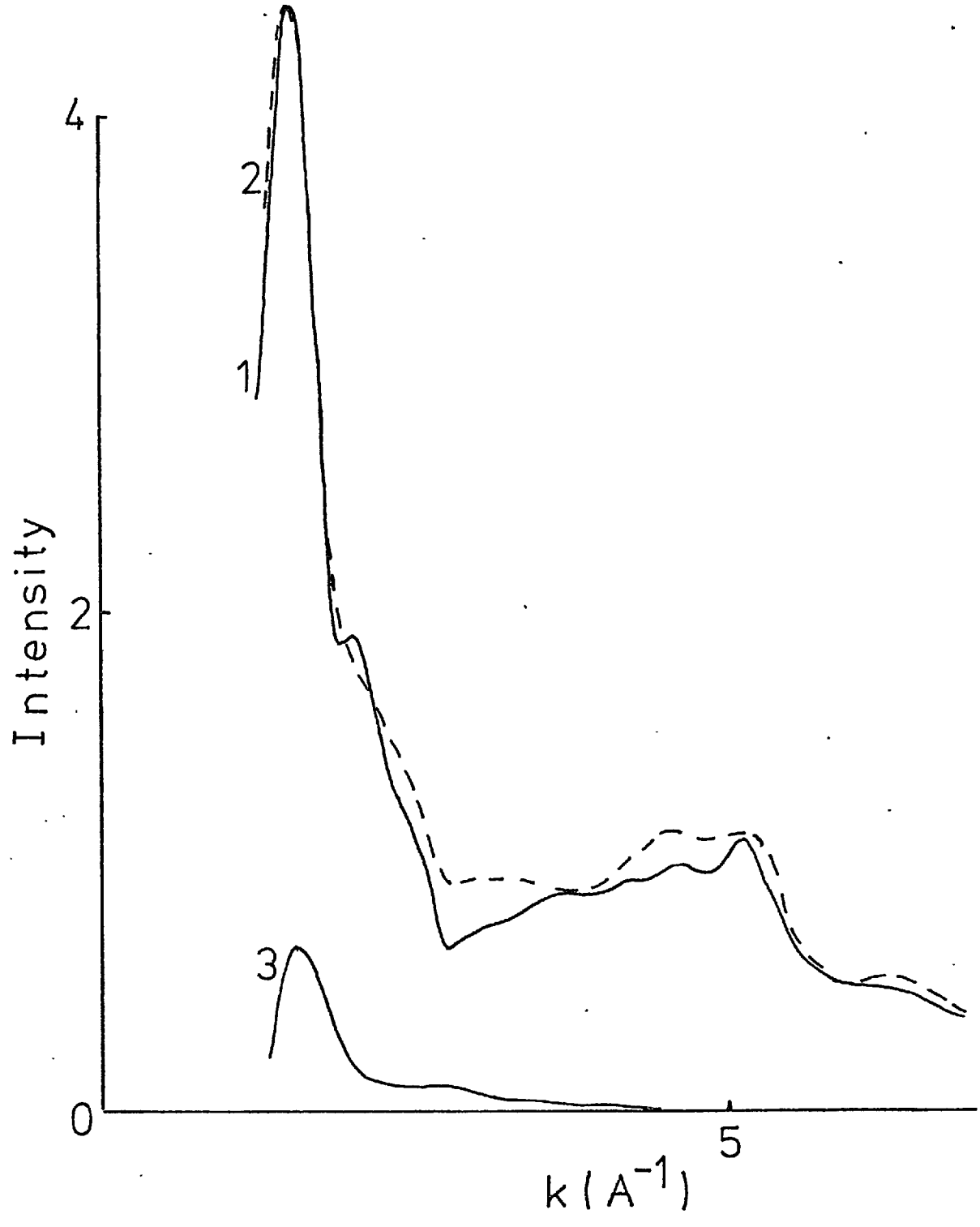

Figure 5.9 : X-ray intensity for α -SiO_2.

1. Theoretical intensity
2. Experimental intensity
3. Contribution from the bond charge correlations

(3.2), (3.3) and (5.1) and the partial structure factors $S_{Si-x}(k)$, $S_{O-x}(k)$ and $S_{x-x}(k)$ are then given by equation (2.17a). Our basic composition unit now contains one silicon atom, two oxygen atoms and two bond charges. From equation (2.18) we have

$$I_x(k) = S_{Si-Si}(k) f_{Si}^2(k) + 2[S_{Si-O}(k) - 1] f_{Si}(k) f_O(k) + 2 S_{O-O}(k) f_O^2(k) \quad 5.12$$

$$+ 2[S_{Si-x}(k) f_{Si}(k) f_b(k) + 2 S_{O-x}(k) f_O(k) f_b(k) + 2 S_{x-x}(k) f_b^2(k)]$$

The intensity calculated from equation (5.12) is shown in figure 5.9, curve 1, together with the experimental data (Mozzi and Warren, 1969), curve 2. The contribution from the last term on the right hand side of equation (5.12) (the bond charge correlations) is also shown as curve 3. It can be seen that the agreement between theory and experiment is good and in particular at the first peak. Referring to figure 5.4, and the agreement obtained using atomic form factors, it can be concluded that the effects of covalent and ionic bonding have tended to cancel out. It would thus be interesting to perform a similar calculation for the CRN model of Evans and King (1966) wher good agreement was obtained by using ionic form factors (King, 1967).

5.7 Discussion

The Bell and Dean CRN model has been shown to give a good representation of the X-ray and neutron diffraction intensities for α-SiO_2. However, the theoretical X-ray intensity at the first diffraction peak depends, to a certain extent, upon the adopted electron density model for the Si-O chemical bond. The correct peak height is predicted both by using atomic form factors and by including a simple model for the partially ionic - partially covalent bond, but

not by using ionic Si^{4+}, O^{2-} form factors. This can be explained by the fact that ionic and covalent bonding in α-SiO_2 have opposite effects upon the X-ray diffraction intensity at the first peak.

REFERENCES

Aldred, P.J.E. and Hart, M., 1973, Proc. Roy. Soc. A 332, 223 and 239

Anderson, P.W., 1968, Phys. Rev. Lett., 21, 13

Anderson, P.W., 1969, Phys. Rev., 181, 25

Bacon, G.E., 1952, Acta. Cryst., 5, 492

Bacon, G.E., 1962, "Neutron Diffraction", Clarendon Press, Oxford

Beeman, D. and Bobbs, B.L., 1975, Phys. Rev. B 12, 1399

Bell, R.J. and Dean, P., 1966, Nature, 212, 1354

Bell, R.J., Nature, 1968, 218, 985

Bell, R.J. and Dean, P., 1972, Phil. Mag., 25, 1381

Berghuis, J., Haanappel, I.M., Potters, M., Loopstra, B.O., MacGillavry, C.H. and Veenendaal, A.L., 1955, Acta. Cryst., 8, 478

Brill, R., 1950, Acta. Cryst., 3, 333

Bullett, D.W., 1974, AIP Conference Proceedings, Tetrahedrally Bonded Amorphous Semi-conductors, page 139

Bullett, D.W., 1975, J. Phys. C. 8, 2695

Bullett, D.W., 1976, Phil. Mag., 32, 1063

Carraro, G. and Domenici, M., 1963, Vetro Silic, 7, 5

Carraro, G., Domenici, M. and Zucca, T., 1965, Physics of non-crystalline solids, ed. J. Prinns (North-Holland, Amsterdam) 152

Chaudhari, P., Graczyk, J.F. and Herd, S.R., 1972, Phys. Stat. Sol. B 51, 801

Chaudhari, P., Graczyk, J.F. and Charbnau, H.P., 1972 a, Phys. Rev. Lett. 29, 425

Chaudhari, P., Graczyk, J.F. and Herd, S.R., 1972 b, Phys. Stat. Sol. B 51, 1068

Chaudhari, P., Graczyk, J.F. and Herd, S.R., 1973, IBM Research Report RC 4491

Chaudhari, P. and Graczyk, J.F., 1974, Amorphous and Liquid Semiconductors, ed. J. Stuke and W. Brenig (London : Taylor and Francis Ltd) page 54

Cochran, W., 1974, AIP Conference Proceedings, Tetrahedrally Bonded Amorphous Semiconductors, 177

Connell, G.A.N. and Temkin, R.J., 1974, Phys. Rev. , B 9, 5323

Da Silva, J.R.G., Pinatti, D.G., Anderson, C.E. and Rudee, M.L., 1975, Phil. Mag. 31, 713

Donovan, T.M., Spicer, W.E. and Bennett, J.M., 1969, Phys. Rev. Lett., 22, 1058

Duncannon, W.E. and Coulson, C.A., 1944, Proc. Roy. Soc. Edinb. A., 62, 37

Ergun, S. and Tiensuu, V.H., Acta. Cryst., 1959, 12, 1050

Ergun, S., 1968, Carbon, 6, 141

Ergun, S., 1973, Acta. Cryst. A 29, 605

Evans, D.L. and King, S.V., 1966, Nature 212, 1353

Evans, D.L., Borrelli, N.F. and Teter, M.P., 1973, Science 181, 774

Franklin, R.E., 1950, Acta. Cryst., 3, 107

Franklin, R.E., 1951, Acta. Cryst., 4, 253

Franklin, R.E., 1951 a, Proc. Roy. Soc. A 209, 196

Gaskell, P.H., 1975, Phil. Mag., 32, 2111

Germer, L. and White, A.H., 1941, Phys. Rev., 60, 447

Gilbert, T.L., Stevens, W.J., Schrenk, H., Yoshimine, M. and Bagus, P.S., 1973, Phys. Rev. B8, 5977

Goodman, C.H.L., 1975, Nature, 257, 370

Griscom, D.L., 1977, J. Non-Cryst. Solids, 24, 155

Henderson, D. and Herman, F., 1972, J. Non-Cryst. Solids, 8-10, 359

Henninger, E.H., Bunchert, R.C. and Heaton, L., 1967, J. Phys. Chem. Solids, 28, 423

Herbert, D.C., 1974, J. Phys. C., 7, 669

Hohenberg, P.C. and Kohn , W., 1964, Phys. Rev., 136 B, 864

Howie, A., Krivanek, O.L. and Rudee, M.L., 1973, Phil. Mag., 27, 235

"International Tables for X-ray Crystallography", 2nd edn., 1965, Vol. 1, Kynoch Press : Birmingham

James, R.W. and Brindley, G.W., 1931, Phil. Mag., 12, 104

Kakinoki, J., Katada, K., Hanawa, T. and Ino, T., 1960, Acta. Cryst. 13, 171

Kakinoki, J., Katada, K. and Hanaw, T., 1960 a, Acta. Cryst., 13, 448

Karle, J. and Konnert, J.H., 1976, Phys. Rev. Lett., 36, 823

King, S.V., 1967, Nature, 215, 615

Kitchens, T.A., 1963, Ph.D. Thesis, Rice University, 1972 (quoted in Bell and Dean (1972))

Konnert, J.H. and Karle, J., 1972, Nature Phys. Sci., 236, 92

Konnert, J.H., Karle, J. and Ferguson, G.A., 1973, Science, 179, 177

Konnert, J.H., Karle, J. and Ferguson, G.A., 1973 a, Science 181, 774

Konnert, J.H., Ferguson, G.A. and Karle, J., 1974, Science, 184, 93

Leadbetter, A.J. and Wright, A.C., 1972, J. Non-Cryst. Solids, 7, 23

Lewis, G.N., 1916, J.A.C.S., 38, 762

McConnell, J.F. and Sanger, P.L., 1970, Acta. Cryst., A 26, 83

McWeeny, R., 1951, Acta. Cryst., 4, 513

McWeeny, R., 1952, Acta. Cryst., 5, 463

McWeeny, R., 1953, Acta. Cryst., 6, 631

McWeeny, R., 1954, Acta. Cryst., 7, 180

Meek, P.E., 1977, Private Communication

Mildner, D.F.R. and Carpenter, J.M., 1975, Proceedings of the International Conference on Amorphous and Liquid Semiconductors, North-Holland Publishing Co., Amsterdam, 463

Moss, S.C. and Graczyk, J.F., 1969, Phys. Rev. Lett., 23, 1167

Moss, S.C., Flynn, P and Luc-O Baver, 1971, Bull. Amer. Phys. Soc. 16, 1392

Moss, S.C. and Adler, D., 1973, Comments on Solid State Physics, 5, 47

Moss, S.C., 1975, Proceedings of the International Conference on Amorphous and Liquid Semiconductors, North Holland Publishing Co., Amsterdam, 463

Mozzi, R.L. and Warren, B.E., 1969, J. Appl. Cryst. 2, 164

Noda, T. and Inagaki, M., 1964, Bull. Chem. Soc. Japan, 37, 1534

Pauling, L., 1960, "The Nature of the Chemical Bond", Cornell University Press

Pauling, L., 1960 a, Ibid, page 6

Pauling, L., 1966, Proc. Nat. Acad. Sci., U.S.A., 56, 1646

Phillips, J.C., 1968, Phys. Rev., 166, 832

Polk, D.E., 1972, J. Non-Cryst. Solids, 8, 359

Polk, D.E. and Bourdeaux, D.S., 1973, Phys. Rev. Lett., 31, 92

Richter, H. and Breitling, G., 1958, Z. Naturforsch., 13 a, 988

Rudee, M.L., 1972, Phys. Stat. Sol (B) 46, K 1

Rudee, M.L. and Howie, A., 1972, Phil. Mag., 25, 1001

Sayers, D.E., Stern, E.A. and Lytle, F.W., 1975, Phys. Rev. Lett., 35, 584

Smith, J.E. Jr., Brodsky, M.H., Crowder, B.L., Nathan, M.I. and Pinczuk, A., 1971, Phys. Rev. Lett., 26, 642

Steinhardt, P., Alben, R. and Weaire, D., 1974, J. Non-Cryst. Solids, 15, 199

Stenhouse, B., Grout, P.J., March, N.H, and Wenzel, J., 1977, Phil. Mag., 36, 129

Temkin, R.J., Paul, W. and Connell, C.A.N., 1973, Adv. Phys., 22, 581

Valenkov, N. and Porai-Koshits, E., 1936, Z. Kristallogr., 91, 195

Warren, B.E., 1934, J. Chem. Phys., 2, 551

Warren, B.E., 1934 a, J. Amer. Ceram. Soc., 17, 249

Warren, B.E., 1937, Appl. Phys., 8, 645

Warren, B.E., 1941, Phys. Rev., 9, 693

Weinstein, F.C. and Davis, E.A., 1973/74, J. Non-Cryst. Solids, 13, 153

Wright, A.C., 1974, Adv. Struct. Res. Diffr. Meth., 5, 1

Wyckoff, R.W.G., 1963, Crystal Structures, Interscience, New York, 1, 1

Yamada, S., 1968, DCIC Report 68-2, Defense Ceramic Information Centre

Yip, K.L. and Fowler, W.B., 1974, Phys. Rev., B 10, 1391 and 1400

Zachanasen, W.H., 1932, J. Amer. Chem. Soc., 54, 3841

Zachanasen, W.H., 1935, J. Chem. Phys., 3, 162